Development of Reactivity Scales via 3-D Grid Modeling of California Ozone Episodes

Final Report

Contract No. 98-309

Prepared for:

California Air Resources Board

Prepared by:

Philip Martien and Robert Harley
Department of Civil and Environmental Engineering
University of California
Berkeley, CA 94720-1710

Jana Milford
Department of Mechanical Engineering
University of Colorado
Boulder, CO 80309-0427

Amir Hakami and Armistead Russell
School of Civil and Environmental Engineering
Georgia Institute of Technology
Atlanta, GA 30332-0512

May 2002

Disclaimer

The statements and conclusions in this Report are those of the contractors and not necessarily those of the California Air Resources Board. The mention of commercial products, their source, or their use in connection with material reported herein is not to be construed as actual or implied endorsement of such products.

Acknowledgments

We thank Dr. William Carter of UC Riverside for technical assistance and helpful discussions. We thank Greg Noblet of UC Berkeley for assistance with developing trajectory model input data files. This report was submitted in fulfillment of ARB contract 98-309, Development of Reactivity Scales via 3-D Grid Modeling of California Ozone Episodes. Work was completed as of May 31, 2002.

Table of Contents

List of Tables

List of Figures

Abstract

The reactivity of carbon monoxide and 30 individual organic compounds was assessed using a 3-D photochemical air quality model with online sensitivity analysis based on the direct decoupled method (DDM-3D). Reactivity was assessed using an extended version of the SAPRC99 chemical mechanism in the South Coast Air Basin and in Central California (including San Francisco Bay Area, Sacramento, and the San Joaquin Valley). Reactivity scales developed using 3-D modeling resulted in similar rankings to those developed by Carter using a box model. Relative measures varied less than absolute measures of reactivity as a function of location. Different measures of reactivity including MIR, MOIR, population exposure, and 1-hour vs. 8-hour average ozone all gave similar results. Isoprene and α-pinene in the South Coast Air Basin were found to be less reactive than previous calculations have suggested, because of a different spatial distribution vs. anthropogenic emissions. Alkenes and carbonyls were found to vary in their relative reactivity as a function of location, due to special features of their atmospheric chemistry. Uncertainties in relative reactivity of individual VOC were dominated by uncertainties in the rate parameters of their primary oxidation reactions.

Executive Summary

In regulating some emission sources, California considers not only the mass, but also the reactivity of volatile organic compound (VOC) emissions. Reactivity scales have been derived in prior work by Carter using a 0-D box model to study the influence of small incremental additions of individual VOC to pre-existing mixtures of VOC and nitrogen oxides (NO_x). The goal of the present research is to use more detailed photochemical modeling tools to assess reactivity, thereby capturing complex spatial and temporal relationships between emissions and photochemical air pollution that cannot be represented using a box model.

Hot summertime conditions that were conducive to high levels of photochemical smog formation were considered in the modeling, for both the South Coast Air Basin and Central California (including the San Francisco Bay Area, Sacramento and the San Joaquin Valley). The most important chemical and emissions uncertainties that affect ozone formation have been propagated through the analysis to quantify the magnitude of their contribution to uncertainties in reactivity.

An extended version of the SAPRC99 chemical mechanism was developed in this research. In most photochemical modeling studies, VOC are aggregated or lumped into a relatively small number of compound classes to reduce the number of different species that must be tracked in the air quality model. In contrast, we represent the chemistry of 30 individual organic compounds explicitly, with remaining VOC assigned to lumped species groups. The individual emitted species for which reactivity metrics are calculated in this study include alkanes, alkenes, aromatics, carbonyls, acetylene, n-butyl acetate, ethanol, isopropanol, MTBE, and carbon monoxide. In our assessment, perturbations to the emissions of each compound follow the underlying, spatial and temporal distribution of the pre-existing emissions.

We have used a 3-D implementation of the direct decoupled method (DDM-3D) to compute sensitivity coefficients of ozone with respect to incremental additions of each emitted organic compound. DDM is not prone to numerical noise for small perturbations to model inputs, and sensitivity coefficients to many different model input parameters can be calculated at the same

1. Introduction

Volatile organic compounds (VOC), together with nitrogen oxides (NO_x), are the main reactants in the photochemistry that produces ozone in the troposphere. VOC species are known to differ significantly in their effects on ozone formation (Carter, 1994). Both the rate at which VOC are oxidized and the products of their oxidation reactions contribute to these reactivity differences. The relative ozone-forming potentials of individual VOC can differ greatly from one compound to another. For example, in a typical urban atmosphere, 1 kg of ethane will form about two orders of magnitude less ozone than 1 kg of formaldehyde. Ignoring the reactivity of emissions when regulations are developed may lead to ineffective, inefficient control strategies, and possibly even lead to measures that worsen air quality. Consideration of reactivity focuses control efforts on those VOC emissions with the greatest impacts on urban ozone.

1.1 Research Objectives

The objectives of this research are to

(1) use state-of-science grid-based photochemical air quality models with online sensitivity analysis capabilities to assess the reactivity of individual VOC with respect to ozone formation in airsheds of interest throughout California;
(2) compare incremental reactivities computed using 3D models with Carter's reactivity scales computed using a box model; and
(3) conduct formal sensitivity and uncertainty analysis of incremental reactivity.

1.2 Technical Background

1.2.1 Incremental Reactivity

Carter (1994) used a chemically detailed box model to quantify the ozone formed from 180 different VOC in 39 cities across the United States. Eighteen different reactivity scales were developed from those model calculations. The scales differ in the assumptions about the levels of NO_x and the measure of ozone impact (such as impact on the peak ozone versus integrated impact over time). One scale, the Maximum Incremental Reactivity (MIR) scale, was chosen for regulatory application in California. MIR values for individual VOCs are calculated in 10-hour box model simulations and are

defined as the maximum sensitivity of the peak ozone concentration ($[O3]_p$) to a small increase in the initial conditions and emissions of the VOC (E_i). MIR is determined for the input ratio of VOC to NO_x that leads to the maximum sensitivity to VOC:

$$MIR_i = \max(\Delta([O3]_p)/\Delta E_i) \text{ over all VOC/NO}_x \qquad (1.1)$$

Example MIRs are given in Table 1.1, which shows both their averages and standard deviations across 39 sets of simulation conditions representing different cities. The MIRs have been normalized by dividing the city-specific value of MIR_i by the geometric mean reactivity of all the compound reactivities for that city, and multiplying by the geometric mean reactivity of the 39-city average MIRs. Normalized in this manner, the variability across cities ranges from about 10 - 20% of the mean MIR value for each compound.

Table 1.1. Examples of Maximum Incremental Reactivity or MIR (mean±1 standard deviation) across 39 cities (Russell et al., 1995).

Compound	MIR (g O_3/g VOC)
HCHO	7.1 ± 0.58
Methanol	0.55 ± 0.064
Ethane	0.24 ± 0.045
Toluene	2.7 ± 0.28
Pentene	6.1 ± 0.64

In California, the MIR scale has been used to quantify the reactivity of the exhaust emissions from alternatively-fueled vehicles, scaled to the reactivity of exhaust emissions from a vehicle using conventional gasoline. The ratio of the reactivity of the alternative fuel to that of the base fuel is called the reactivity adjustment factor (RAF):

$$RAF_j = \sum_{i=1}^{N} f_{ji} MIR_i / \sum_{i=1}^{N} f_{bi} MIR_i \quad (1.2)$$

where f_{ji} is the mass fraction of compound i in alternative fuel j, and f_{bi} is the mass fraction of compound i in the base fuel (conventional gasoline). If RAF<1, a higher mass rate of VOC emissions is allowed. For example, an RAF of 0.37 for M85-fueled vehicle emissions indicates that on a mass-weighted basis, those emissions should produce 37% as much ozone as the same mass of VOC emitted from a gasoline-fueled vehicle under urban conditions. Under California's regulations, M85-fueled vehicles would therefore be allowed to emit 2.7 times as much VOC mass, leading to an equivalent ozone impact.

Typically, MIR is computed at relatively low VOC/NO_x ratios (4-6 ppmC : 1 ppm NO_x), as might be found in dense source regions. This indicates that the MIR scale will be more applicable to urban core conditions where VOC control is most effective, than to rural conditions where ratios are usually higher (and NO_x controls may be more effective). At lower NO_x levels, the absolute incremental reactivity of any individual VOC is expected to be less than under MIR conditions. To investigate this effect, Carter (1994) developed several alternative scales, including the maximum ozone incremental reactivity (MOIR) scale. MOIR is evaluated for VOC/NO_x conditions leading to the maximum ozone (instead of conditions leading to the maximum reactivity):

$$MOIR_i = (\Delta \max ([O3]_p)/\Delta E_i) \quad (1.3)$$

The MOIR is calculated at higher VOC/NO_x levels (about 7 to 8:1) than those associated with the MIR scale. Nevertheless, reactivity adjustment factors calculated using the MOIR scale are similar to those calculated using MIR values.

1.2.2 Uncertainties in Incremental Reactivity

A question that is frequently raised with the use of reactivity weighting is the effects of uncertainties and level of detail in the physical and chemical representation in the models

used for quantifying reactivity. A specific concern regarding the physical level of detail arises because the MIR scale has been developed using a box or 0-D model. Moreover, the MIR scale has been developed based on 10-hour simulations, whereas some organic compounds may remain in an urban airshed for 2 to 3 days.

Another concern often raised is that the quantification of compound reactivities is limited by uncertainties in our knowledge of atmospheric chemistry and its representation through chemical mechanisms. Measurement errors in laboratory kinetic and product studies contribute to uncertainty in the chemical mechanisms used to calculate incremental reactivities. Moreover, the reactions of many of the organic compounds emitted into urban atmospheres have never been studied in controlled experiments. Their representation in chemical mechanisms is based on analogy to compounds of similar structure, creating added uncertainty. At issue is whether the uncertainties in the chemistry significantly impact the calculation of the reactivities for organic compounds. Previous studies using a box model (Yang et al., 1995; 1996) and an airshed model (Bergin et al., 1995; 1998) have explored to what degree uncertainties in chemical rate parameters impact the calculated reactivities.

Uncertainties in calculated reactivities have been estimated from box model simulations using Monte Carlo analysis with Latin Hypercube Sampling. To reduce computational requirements, the simulations were conducted for a single set of trajectory conditions, which was designed by Carter (1994) to give results close to the average MIRs from the 39 cities. Uncertainty estimates were compiled for all of the rate parameters of the SAPRC90 mechanism, largely from concurrent reviews of kinetic data (Atkinson et al., 1989; DeMore et al., 1990). Rate parameters are treated as lognormally distributed, independent random variables. Uncertainty estimates (1σ) range from 30 to 50% of the mean MIR values, for most compounds. In general, the most influential uncertainties are those in rate parameters that control the availability of NO_x and radicals (Yang et al., 1995). For MIR, uncertainties in the rate parameters of primary oxidation reactions, or reactions of stable intermediates, are also influential. Uncertainties in many rate parameters have similar effects on the reactivities of various compounds, so the resulting

MIR are strongly correlated. For example, an increase in the photolysis rate for NO_2 increases the reactivity of most species by about the same proportion. Thus the relative reactivity of one species compared to another is not affected as much as the absolute MIR by uncertainties in rate coefficients.

For exhaust emissions from selected fuel/vehicle combinations tested in the Auto/Oil Air Quality Improvement Research Program (AQIRP) uncertainties in RAF were also calculated using Monte Carlo simulations with Latin Hypercube Sampling (Yang and Milford, 1996). Both chemical rate parameters and exhaust compositions were treated as random variables. Uncertainties in the exhaust compositions were estimated from the variance and covariance of emissions of each compound across the vehicles that were tested on a given fuel. Emissions of each compound were then treated as correlated, normally distributed random variables. As an example, the mass-based RAF for the M85 exhaust composition had a mean value of 0.49 with an uncertainty of 17% (1σ relative to the mean). Compared to the degree of uncertainty in the MIR for HCHO (32%) and methanol (48%), the RAF uncertainty is significantly reduced due to inter-species correlation. This reduction in uncertainty is even more pronounced for RAF of fuels such as reformulated gasoline that have exhaust compositions closer to that associated with conventional gasoline.

After the most influential rate parameters were identified through Monte Carlo simulations, their values were varied, one-at-a-time, in 3-D airshed model simulations (Bergin et al., 1998). Incremental reactivities were found based on a variety of metrics, and normalized by the composite reactivity of a mixture of compounds similar to exhaust emissions from vehicles operated using standard gasoline. The response to chemical parameter uncertainties calculated with the airshed model was similar to that found with the box model, and confirmed the low sensitivity of normalized reactivities to uncertainties in rate constants.

1.2.3 Online Sensitivity Analysis in 3D Models

Yang et al. (1997) demonstrated the application of the direct decoupled method (DDM; Dunker, 1984) as a sensitivity analysis tool for three-dimensional models. In direct sensitivity analysis methods, sensitivity equations as well as the governing equations for species concentrations are integrated through time. The decoupled direct method has the advantage of relative stability and ease of implementation compared to the coupled direct and Green's function methods for evaluating the sensitivity coefficients (Dunker, 1984). In DDM-3D, the sensitivity equations are derived from the atmospheric diffusion equation:

$$\frac{\partial C_i}{\partial t} + \nabla \cdot (\vec{u} C_i) = \nabla \cdot (K \nabla C_i) + R_i (C_1, C_2, \ldots, C_N) + S_i \qquad (1.4)$$

In equation (1.4), C_i is the concentration of species i, $\vec{u}$ is the wind velocity vector, K is the diffusivity tensor, R_i is the net rate of formation of compound i due to chemical reactions, S_i is the source term for compound i due to emissions, and N is the number of species being tracked in the model. The coupled system of equations (4) is solved numerically subject to initial and boundary conditions (see McRae et al., 1982 for details). To obtain the sensitivity coefficients, the governing equation and boundary conditions are differentiated with respect to model parameters (either input parameters such as emissions or parameters used in the model such as reaction rate constants). For example, for the jth model parameter:

$$\frac{\partial s_{ij}^*}{\partial t} = -\nabla \cdot (\vec{u} s_{ij}^*) + \nabla \cdot (K \nabla s_{ij}^*) + J_{ik} s_{kj}^* + \frac{\partial R_i}{\partial \varepsilon_j} + \frac{\partial S_i}{\partial \varepsilon_j} - \nabla \cdot (\vec{u} C_i) \delta_{ij} + \nabla \cdot (K \nabla C_i) \delta_{ij} \qquad (1.5)$$

In equation (1.5), $s_{ij}^* = \frac{\partial C_i}{\partial \varepsilon_j}$ is the semi-normalized sensitivity coefficient, which is the partial derivative of C_i with respect to a scaling factor ε_j applied to parameter j (ε_j has a nominal value of 1 and is interpreted as a uniform multiplicative factor applied to parameter j throughout the spatial domain and time period of an air quality model

simulation). For the purposes of the present study, C_i is ozone concentration and the e_j are scaling factors applied to the emission rates of individual VOC. Incremental reactivities for each VOC are obtained as a function of location and time directly from s_{ij}.

DDM-3D is a computationally efficient method for sensitivity analysis of multidimensional models. In the decoupled direct method, sensitivity coefficients are calculated by alternating the solution of equation (1.4) with the solution to equation (1.5).

1.3 Approach and Overview

The SAPRC99 chemical mechanism is extended to include reactions that represent explicitly the chemistry of CO and 30 VOC that were the focus of the current research to quantify incremental reactivity. The augmented chemical mechanism used here is described in Chapter 2. The augmented SAPRC99 chemical mechanism is installed in two photochemical air quality models that include online sensitivity analysis capabilities (DDM-3D) as described above. The air quality models are applied to intensive field measurement episodes where development and evaluation of models and input data have already been performed. Reactivities derived from 3D modeling are compared on a relative basis to Carter's MIR and MOIR scales.

In the South Coast Air Basin (SoCAB) that surrounds the Los Angeles area, the CIT airshed model is used to model ozone formation and VOC reactivity for the period 23-25 June 1987, which was one of the high-ozone summer intensive study periods of the Southern California Air Quality Study (SCAQS). Model application and results for the SoCAB are described in Chapter 3.

In Chapter 4, estimates of uncertainties in 33 relevant model input parameters including chemical reaction rate coefficients, product yields, emission rates, and deposition parameters are propagated through a vertically-resolved (1-D) Lagrangian photochemical trajectory model using Latin Hypercube Sampling. The trajectory model is applied to the same June 1987 period to which the CIT airshed model is applied. LHS is similar in concept to a Monte Carlo analysis, but provides more efficient sampling of the parameter space. The LHS analysis provides uncertainty bounds on model predictions of

incremental reactivity for each VOC under study. Multivariate linear regression analysis is used to identify which uncertain input parameters are responsible for most of the uncertainty in incremental reactivities.

Chapter 5 describes the application of the MAQSIP air quality model to Central California for the 3-6 August 1990 intensive monitoring period of the San Joaquin Valley Air Quality Study (SJVAQS). The Central California modeling domain includes the San Francisco Bay Area, Sacramento, and much of the San Joaquin Valley.

Chapter 6 presents a summary and synthesis of findings, and major conclusions of this research. Recommendations for future research also are provided.

time. In contrast, brute-force methods require a separate model run for each input parameter under study, and are susceptible to round-off errors in calculating differences between base case and perturbed model runs.

VOC Reactivity in the South Coast Air Basin

Photochemical modeling was conducted for the South Coast Air Basin (SoCAB) during the period 23-25 June 1987, one of the intensive periods of the Southern California Air Quality Study (SCAQS). For this period, a three-dimensional version of the California Institute of Technology (CIT) airshed model was applied to produce both predictions of ozone and estimates of incremental reactivity. DDM-3D provided sensitivities from which normalized, or relative, values of incremental reactivity (RIR) were determined for each of 8 sites in the SoCAB at the time of maximum observed ozone. These results were analyzed and compared to similarly normalized reactivities generated via the standard, box-model approach for calculating maximum incremental reactivity.

This analysis and comparison led to the following main findings. For most species, the average RIR values (over the 8 sites) and relative rankings based on average RIR were consistent with similar information derived using a box-model approach. However there were cases where emissions and transport patterns did affect incremental reactivity. At coastal and central sites in the SoCAB, VOC such as formaldehyde and alkenes that initiate radical formation have higher reactivity than at inland sites on both absolute and relative bases. A consistent finding for all 8 sites examined was that biogenic VOC, while ranked high in box model determinations of MIR, have low RIR at South Coast urban monitoring sites. This is because most of the biogenic emissions were downwind of the urban sites that were examined. Finally, the differences in relative reactivity were often magnified when the absolute reactivities were low, such as at coastal sites.

Uncertainty Analysis

Monte Carlo analysis with Latin Hypercube Sampling was applied to the vertically-resolved trajectory version of the CIT model with the SAPRC99 chemical mechanism, to estimate uncertainties in incremental reactivity values for representative VOCs. Uncertainties in chemical and deposition parameters and emissions rates were considered. Incremental reactivities and corresponding uncertainties were calculated for trajectories ending at Anaheim, Azusa, Claremont and Riverside at the time that peak ozone concentrations were observed on 25 June 1987.

Coefficients of variation (one standard deviation relative to the mean) quantifying the uncertainty in absolute incremental reactivities range from 0.16 for XYLM at Anaheim to 0.63 for HCHO at Riverside. For most of the compounds and receptor endpoints studied, the uncertainties in the absolute incremental reactivities range from 0.3 to 0.4. Normalizing the reactivity values by the incremental reactivity of a base mixture generally reduces the estimated uncertainties. Coefficients of variation in relative incremental reactivities range from 0.08 for propene at Anaheim and Azusa to 0.49 for CO at Riverside, with uncertainty values for most of the compounds studied ranging from 0.2 to 0.35.

The major sources of uncertainty in the absolute incremental reactivity of the base mixture are relatively consistent across trajectories. The most influential parameters are those that control the amount of NO_x and radicals in the air parcel, and include the rate constants for NO_2, HCHO and O_3 photolysis, HO + NO_2 and PAN decomposition, and the rate of non-mobile NO_x emissions.

The largest contributors to relative incremental reactivities of individual compounds generally include the rate parameters for the primary oxidation pathways of the compound. For relatively slowly reacting compounds that react primarily with OH, parameters that control its abundance are influential. The RIRs of the more reactive compounds such as m-xylene and propene show negative sensitivity to uncertain parameters that increase the reactivity of other compounds in the base mixture.

Reactivity Assessment for Central California

We quantified organic compound reactivities over the central portion of California using the three dimensional air quality model MAQSIP (the Multi-scale Air Quality SImulation Platform). The chemical mechanism was upgraded to SAPRC-99, with about 40 explicitly described organic species. Simulations were done for SARMAP's 5-day August 1990 episode. Spatially and temporally resolved absolute and relative reactivities of 31 organic compounds and CO were calculated. In order to be able to compare different species, the emissions of all the targeted organic compounds were perturbed equally. This perturbation followed the same spatial distribution as the total anthropogenic VOC emissions, so that a more realistic representation of the reactivities is produced.

A great deal of variability (both spatial and temporal) was observed in the absolute reactivities. On the other hand, and on a relative basis (compared to a base mixture), Relative Incremental Reactivities (RIRs) were fairly constant. Three different types of domain-wide metrics, i.e. MIR-3D, MOIR-3D, and exposure were calculated. MIR and MOIR metrics were calculated for two different averaging times (1-hour and 8-hour), while the exposure was estimated as the daily population weighted average for all the cells with ozone concentrations above 80 ppb.

All of the three-dimensional metrics showed a high level of inter-species consistency, i.e. different species had similar ranks in different metrics. In general, 3-D metrics were lower than box model scales for more reactive species, and closer to them (or even higher) for less reactive species. The largest difference with box model scales was observed for 8-hour MOIR-3D. The 3-D metrics also matched each other very well. Exposure and MIR-3D values were found to be very close to each other, but usually higher than MOIR-3D metrics for the more reactive species. It was also found that including the biogenic VOC emissions in the perturbation pattern had little effect on the results. Finally, looking at four different sites in the domain, some variability in RIRs was observed. Among the four sites (Fresno, Sacramento, Livermore, and San Jose), Fresno had lower RIRs for the more reactive species. Overall, these urban sites usually have higher RIRs for the more reactive species than the domain-wide metrics.

Summary of Major Findings

For most species studied here, reactivity scales developed using 3-D modeling resulted in similar rankings of individual VOC when compared to reactivity scales developed by Carter using a box model. We found that large site-to-site differences in the absolute incremental reactivity of VOC can occur, and that these differences are reduced when reactivity is measured on a relative rather than absolute basis. Differences in relative reactivity are likely to be magnified where absolute reactivities are low. In the South Coast Air Basin, we found that biogenic VOC such as isoprene and α-pinene were much less reactive than suggested by box model calculations, because the spatial distribution of these emissions placed most of the emissions downwind of the urban sites where reactivity was quantified.

Results for Central California are similar to those for the South Coast Air Basin. The same spatial distribution of emissions perturbations was used for all species, so the reactivity of biogenic VOC matched Carter's assessment of their relative reactivity more closely than results of the South Coast modeling. Use of different metrics of reactivity including MIR, MOIR, population exposure, and 1-hr vs. 8-hr average ozone, all yielded similar rankings of compounds in 3D modeling for Central California.

Alkenes and some carbonyls (especially formaldehyde and acetaldehyde) were found to exhibit greater site-to-site variability in reactivity than other classes of VOC. These differences were due to special features of the atmospheric chemistry of these compounds, such as direct reactions with ozone, photolysis to form HO_x radicals, and PAN formation.

Uncertainties in absolute incremental reactivity of the base VOC mixture were dominated by uncertainties in model input parameters such as rates of photolysis of NO_2, HCHO, and O_3, rate coefficients for the reactions HO + NO_2 and PAN decomposition, and NO_x emissions from stationary sources. Relative reactivities of individual VOC are strongly influenced by uncertainties in the rate parameters of their primary oxidation reactions.

2. Methodology

2.1 Development of Chemical Mechanism

The chemical mechanism used in this study is an extended version of the SAPRC99 mechanism (Carter, 2000a), which represents a complete update of the earlier SAPRC90 mechanism (Carter, 1990). Rate constants, absorption cross sections, quantum yields and mechanistic parameters were updated based on reviews conducted over the past decade by Roger Atkinson and by IUPAC and NASA panels (Carter, 2000a). Compared to previous versions of the mechanism the most significant change made to the inorganic chemistry incorporated in SAPRC99 was reducing the OH + NO_2 rate constant by approximately 30%, as recommended by DeMore et al. (1997). Changes to the organic chemistry of the base mechanism included adding explicit representation of methyl peroxy and acetyl peroxy radicals in order to improve O_3 predictions in low-NO_x conditions. In addition, methanol (MEOH) was added to the base mechanism. The representation of uncharacterized aromatic ring fragmentation products was updated, with a third dicarbonyl species (DCB3) added to eliminate the use of methyl glyoxal (MGLY) as a surrogate species. A new lumped parameter product for higher ketones that are more reactive than MEK was also added.

In consultation with ARB staff, we identified 31 chemical species for which detailed incremental reactivity calculations were performed in this research. We consider species that represent most of the important classes of VOC, including compounds that are of anthropogenic and biogenic origin. The full list of species that are studied here is presented in Table 2.1. Some of these species were already included in the base SAPRC99 mechanism. For the remaining species that were previously lumped together with other similar VOC, extra reactions were added to the mechanism so that all 31 species are represented explicitly. Propane is also represented explicitly in the extended version of the SAPRC99 mechanism used here, though it is not a species for which reactivity calculations were performed. The reactions that were added to the mechanism are listed in Appendix A.

Table 2.1. Chemical species considered in this research.

Category	Code	Species Name	MW ($g\ mol^{-1}$)	MIR	MOIR
Alkane	CH4	methane	16.0	0.01	0.01
	C2H6	ethane	30.1	0.31	0.20
	N-C4	n-butane	58.1	1.33	0.83
	N-C5	n-pentane	72.1	1.54	0.95
	IPNT	isopentane	72.1	1.68	1.02
	MCPT	methylcyclopentane	84.2	2.42	1.33
	224P	2,2,4-trimethylpentane	114.2	1.44	0.81
Alkene	ETHE	ethene	28.1	9.08	3.70
	PRPE	propene	42.1	11.58	4.43
	2MBT	2-methyl-2-butene	70.1	14.45	4.65
	BUTD	1,3-butadiene	54.0	13.58	4.83
	ISOP	isoprene	68.1	10.69	3.95
	APIN	α-pinene	136.2	4.29	1.56
	OLE1	lumped terminal olefins	70.1	7.79	3.11
Aromatic	C6H6	benzene	78.1	0.81	0.34
	TOLU	toluene	92.1	3.97	1.17
	XYLM	m-xylene	106.2	10.61	3.19
	XYLP	p-xylene	106.2	4.25	1.36
	124B	1,2,4-trimethylbenzene	120.2	7.18	2.32
Carbonyl	ACET	acetone	58.1	0.43	0.17
	MEK	methyl ethyl ketone	72.1	1.49	0.66
	HCHO	formaldehyde	30.0	8.97	2.56
	CCHO	acetaldehyde	44.1	6.84	2.56
	RCHO	propionaldehyde	58.1	7.89	2.97
	BALD	benzaldehyde	106.1	-0.61	-1.64
Other	C2H2	acetylene	26.0	1.25	0.49
	ETOH	ethanol	46.1	1.69	0.93
	IPOH	isopropanol	60.1	0.71	0.39
	MTBE	methyl tert-butyl ether	88.1	0.78	0.47
	BACT	n-butyl acetate	116.2	0.89	0.54
	CO	carbon monoxide	28.0	0.06	0.04

Note: MIR and MOIR values shown in this table are from Carter (2000b).

The final form of the chemical mechanism used in this study contains 104 species and 246 reactions. Of the 104 species, eight are lumped primary organic species: ALK1, ALK2 and ALK3 representing alkanes, ARO1 and ARO2 representing aromatics, OLE1 and OLE2 representing alkenes, and TRP1 representing terpenes. We used a version of the SAPRC99 mechanism with fixed oxidation product yields for all of the lumped organic species. Appendix A provides a list of the reactions and reaction rate parameter values that comprise the extended version of the SAPRC99 mechanism used in this study.

2.2 Incremental Reactivity Scales

In this study, the change in ozone was measured by the change in the concentration predicted in the lowest computational cell of the air quality model at the time of peak observed ozone at various receptor locations of interest. To express incremental reactivities on a mass basis, they are calculated as:

$$IR_j = \frac{MW_{O3}\, s^*_{ij}}{MW_j\, E_j} \qquad (2.1)$$

where s^*_{ij} is the semi-normalized sensitivity of ozone (ppm O_3) with respect to a dimensionless multiplier ε_j applied to emissions of organic compound j at all locations and times, MW is molecular weight, and E_j is the molar emissions rate of compound j throughout the modeling domain (or along an air parcel trajectory where a 1-D air quality model is used).

Differences in the chemical environment of individual receptor locations, including differences in the amount and timing of upwind VOC and NO_x emissions, are expected to affect the absolute incremental reactivities calculated from equation (2.1). Previous studies have suggested that normalizing reactivities to the reactivity of a base compound or mixture of compounds should decrease their variability (Russell et al., 1995). In this study, relative incremental reactivities (RIRs) are calculated as:

$$RIR_j = \frac{IR_j}{\sum_k w_k IR_k} \qquad (2.2)$$

where IR_k is the absolute reactivity of the k^{th} compound and w_k is its mass fraction in the mixture. The compounds included in the mixture and their mass fractions were 2% formaldehyde, 14% MEK, 37% n-butane, 26% 2,2,4-trimethylpentane, 2% propene, 17% ethanol, and 2% m-xylene. The mass fractions were determined so that the compounds would contribute approximately equally to the reactivity of the mixture. Note that this weighting is specific to this study, so the RIR values are only comparable within the study.

Incremental reactivity results calculated in this study are compared to incremental reactivities calculated by Carter (2000b) using a box model (see Table 2.1 for MIR and MOIR values for the compounds considered in this study). MIRs are defined for conditions in which NO_x levels are adjusted to maximize the overall incremental reactivity of a base VOC mixture, which typically occurs at VOC/NO_x ratios of 4-6 ppmC : 1 ppmNO_x. MOIRs are defined at a higher VOC/NO_x ratio where ozone formation is maximized for the base mixture. Because the conditions used in this study may not match MIR or MOIR conditions, comparisons are made for relative, not absolute incremental reactivities. Relative MIRs (R_MIRs) are calculated from Carter's MIR values using equation (2.2) and the mixture composition described in the previous paragraph.

3. VOC Reactivity in the South Coast Air Basin

The objective of the research presented in this chapter is to examine the influence of spatial variability on our assessment of VOC reactivity in Southern California. Spatial variability is important because the location of pollutant emissions and meteorological conditions affects how and where VOC and NO_x react to form ozone. For example, if VOC emissions are typically downwind of a particular site, then reactivity as determined in smog-chamber experiments or in box model estimates cannot specify how emission reductions will change ozone at that site. While vertically resolved trajectory models capture some spatial variability, a three-dimensional (3-D) model can more accurately represent transport in the atmospheric boundary layer, where wind shear is important.

A 3-D model was applied to determine VOC reactivity, and results were then compared to Carter's reactivity scales derived using a box model. This study considered a summertime episode in the South Coast Air Basin (SoCAB).

3.1 Model Application to the SoCAB

The period of study for this investigation was 23-25 June 1987. An extensive meteorological and air-quality-monitoring network that exists in Southern California was used to specify meteorological inputs and initial conditions for the air quality model. Supplemental upper air soundings were conducted during the Southern California Air Quality Study (SCAQS) during the 24-25 June 1987 intensive monitoring period. These soundings were performed every 4 hours at a network of 8 sites located along the coast and inland. Mixing depths were determined as the height to the base of the inversion layer in plots of potential temperature vs. altitude. Mixing depths, temperatures, surface winds, and winds aloft were interpolated using objective analysis procedures described by Goodin et al. (1979, 1980) to derive spatially and temporally-complete meteorological fields. Similar interpolation procedures were applied to observed concentrations of CO, NO, NO_2, O_3, and NMHC to derive initial conditions for these pollutants. By starting model simulations at 4 PM on 23 June 1987, observed pollutant concentrations at the surface could be used to estimate pollutant levels throughout the mixed layer. These input data were developed and used in a previous photochemical modeling study of the same episode (McNair et al., 1996). Inflow boundary conditions were based on a review of measurements of pollutant

concentrations at San Nicolas Island and in aircraft studies conducted offshore of southern California (Main et al., 1990).

Figure 3.1 shows the study domain and the boundary of the region of computation. Figure 3.1 also shows 8 sites at which incremental reactivity was specifically evaluated. The sites at Hawthorne and Long Beach, representative coastal sites, are characterized by coastal breezes and relatively clean air. Further inland, the Central Los Angeles and Anaheim sites, characterize the central domain, a region of high emissions and increased levels of air pollution. The inland sites Burbank, Azusa, Claremont, and Rubidoux are downwind of the core urban areas in the computational domain and downwind of most of the emissions. The inland sites experience the highest levels of ozone during the study period.

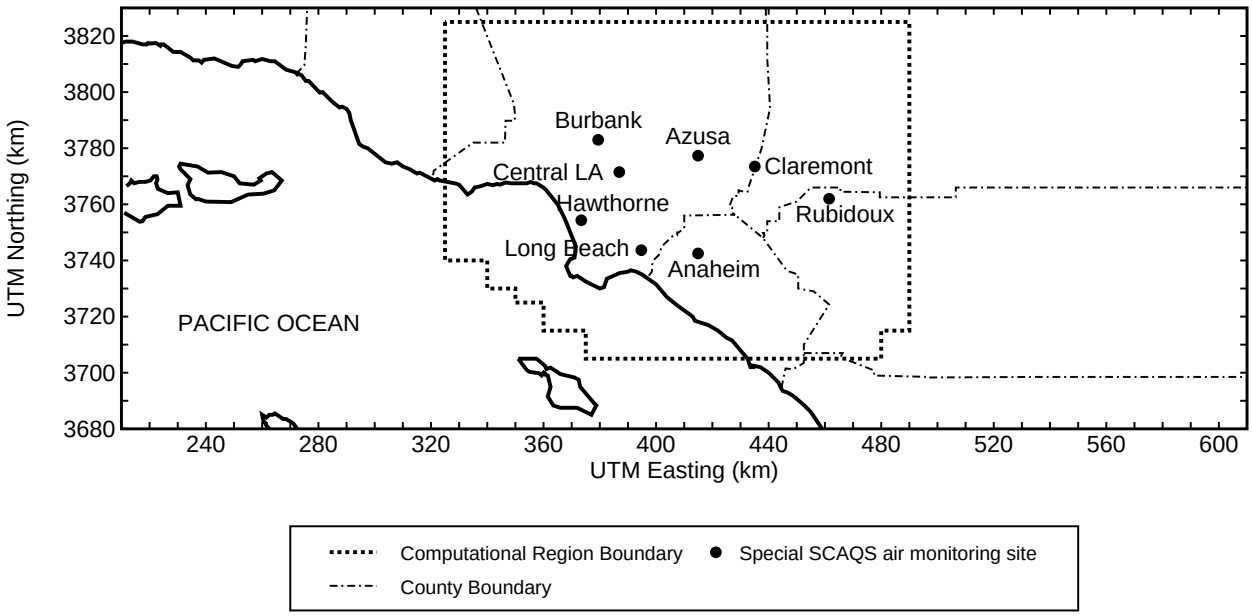

Figure 3.1. Modeling domain with selected measurement sites and the boundary of the computational region.

Emission-inventory estimates used in this research were provided by the California Air Resources Board (Allen, 1999). Estimates of mobile, area, and point source emissions are for summer 1987 typical weekday conditions. Baseline motor vehicle emissions estimates are based on EMFAC version 7G model predictions; stabilized exhaust VOC emissions from on-road

gasoline engines were multiplied by a factor of 3.7. This scaling was done to match estimates of VOC emissions from on-road vehicles made by Harley et al. (1997) using infrared remote sensing measurements of CO emissions and ambient NMOC/CO concentration ratios measured during the Southern California Air Quality Study (SCAQS). Day-specific estimates of biogenic VOC emissions were available for 23-25 June 1987, but day-to-day differences in emission estimates are negligible for this period. A summary of pollutant emissions by source category is provided below in Table 3.1.

Table 3.1: Summer 1987 typical weekday emission inventory estimates for the South Coast Air Basin used in this study.

	Emissions (10^3 kg/day)		
	CO	NMOC	NO_x
On-road vehicles	7000	2000	790
Area*	1500	800	420
Point	170	430	230
Biogenic	0	120	0
Total	8700	3400	1440

*Off-road mobile sources are included in totals shown here for area source emissions.

The spatial distribution of the daily total emissions of selected VOC species are shown (in units of kg/day per grid cell) in Figures 3.2.a through 3.2.c. The distribution of propene emissions (Figure 3.2.a), the primary source of which is automobile exhaust, is heavily concentrated in the central urbanized portion of the modeling domain. Likewise, isopropanol emissions (Figure 3.2.b), whose primary source is evaporating solvents, are also concentrated in the central region. The biogenic emissions, of which isoprene (Figure 3.2.c) is a good example, are distributed mostly to the north and east and downwind of the urbanized region.

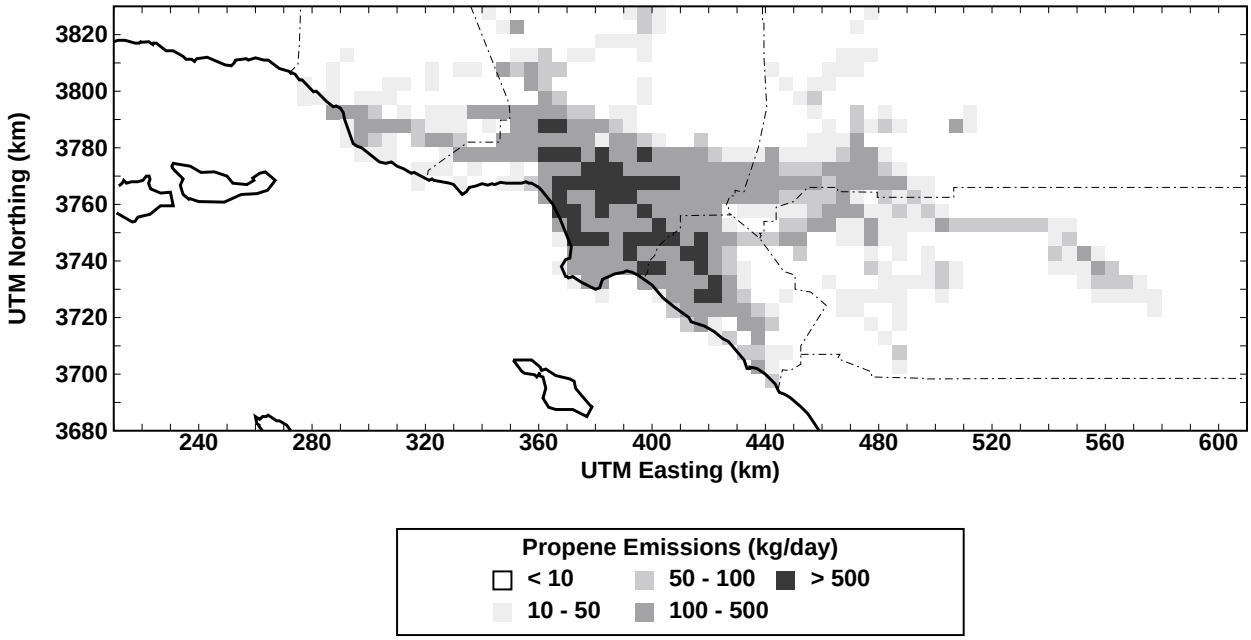

Figure 3.2.a. Estimated propene emissions in kg/day per grid cell for 25 June 1987.

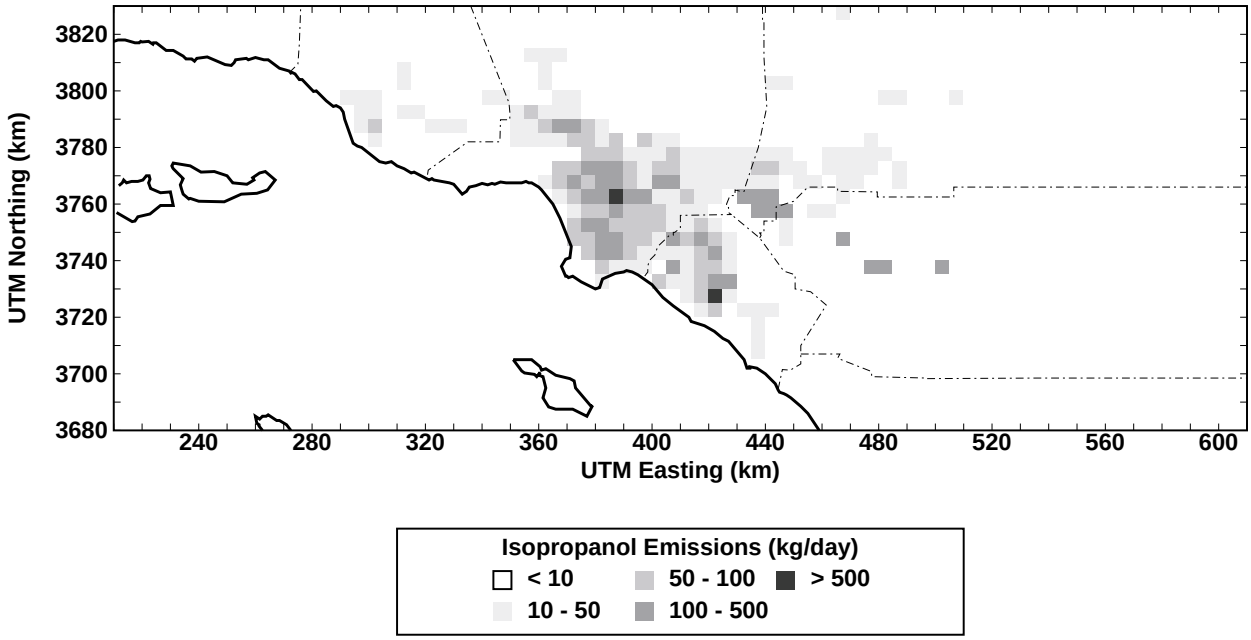

Figure 3.2.b. Estimated isopropanol emissions in kg/day per grid cell for 25 June 1987.

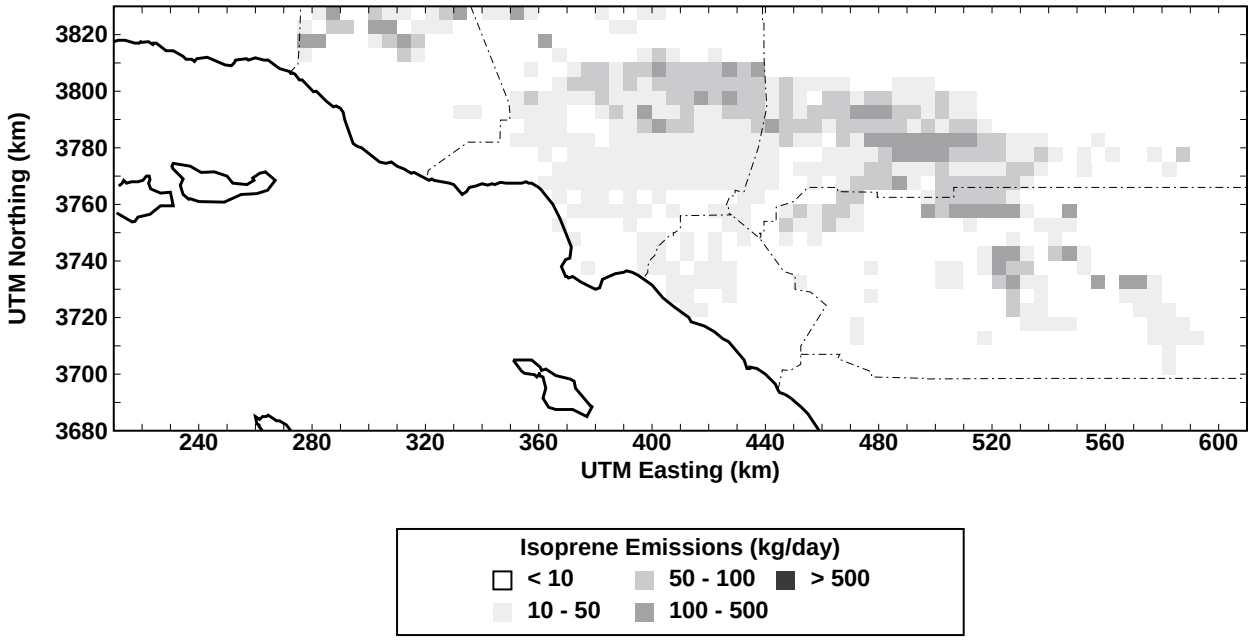

Figure 3.2.c. Estimated isoprene emissions in kg/day per grid cell for 25 June 1987.

All model simulations were started at 1600 PST on 23 June 1987 and continued until 2400 PST on 25 June. The 23rd was considered a model spin-up day; performance evaluations were done for both 24 and 25 June. Calculations of VOC reactivity were all done for 25 June in order to minimize the influence of uncertainties in initial conditions on the results.

3.2 Calculation Methods

The model applied here was the DDM-3D version of the CIT model (Yang et al., 1997). The formulation of DDM-3D is described in Chapter 1. This model was modified to use the SAPRC99 chemical mechanism (Carter, 2000a). The mechanism applied here was extended to treat many individual VOC explicitly, as described in Chapter 2. In this Chapter, absolute incremental reactivity (*AIR*) is determined from the semi-normalized sensitivity coefficients, $s^*_{O_3,j}$, using a modified version of equation (2.1):

$$AIR_j = \frac{s^*_{O_3,j}}{MW_j \cdot E_j}, \qquad (3.1)$$

where MW_j and E_j are, respectively, the molecular weight and the domain-total emissions (in moles) of species j. Relative incremental reactivity (*RIR*) for VOC species j is then

determined from AIR_j using equation (2.2). Since Carter (1994) defines MIR and MOIR at the time of peak ozone (see equations 1.1 and 1.3), in this chapter AIR and RIR at a given site are also calculated at the time of peak ozone. Chapter 5 explores the utility of other metrics.

Sensitivity coefficients and, subsequently, reactivities also can be computed using the so-called "brute-force" technique. For example, one could estimate $s^*_{O_3,j}$ using two model runs with different emissions of species j using a centered-difference approximation:

$$s^*_{O_3,j} \approx \frac{O_3(1+\Delta\varepsilon_j) - O_3(1-\Delta\varepsilon_j)}{2\Delta\varepsilon_j}, \qquad (3.2)$$

where $\Delta\varepsilon_j$ is an incremental change in the multiplicative scaling factor for the emissions of species j. $O_3(1\pm\Delta\varepsilon_j)$ represents the simulated ozone produced in a model run with a change in the emissions of species j.

The main advantage of using the DDM-3D method to estimate IR is that it reduces the number of runs required to produce IR estimates for the 31 species. With the brute-force technique, trial and error is required to select emission changes for each species large enough to produce a change in ozone that can be detected above the numerical noise in the model and yet small enough to yield an accurate estimate of the local derivative.

3.3 Results and Discussion

3.3.1 Performance Evaluation

Performance statistics for ozone (Table 3.2) indicate that the CIT model with the SAPRC99 chemical mechanism simulated the observed surface-level ozone (above 60 ppb) in this episode with a low bias and a moderate amount of error. Table 3.2 shows that model performance statistics on 24 and 25 June are similar. Normalized bias is about 7% and the normalized gross error is about 42% on both days.

Table 3.2. Ozone Performance Evaluation Statistics (Cutoff Value = 60 ppb).

Statistical Performance Measure	24 June	25 June
Bias (ppb)	+4.4	+3.8
Bias, Normalized (%)	+7	+6
Gross Error (ppb)	40	38
Gross Error, Normalized (%)	43	41
Std. Dev. of Residuals (ppb)	53.2	48.9

At the 8 sites where AIR and RIR are calculated, the time series plots (Figures 3.3.a - 3.3.b) show a high degree of consistency between observed and simulated ozone. At coastal sites Hawthorne and Long Beach, observed and predicted maximum ozone was about 70 ppb on both 24 and 25 June. Nighttime simulated ozone was predicted to be near zero on both days, whereas the observed ozone concentration was about 40 ppb at this time. At the central and inland sites, the magnitudes of the daily ozone peaks were usually within about 30 ppb of the observations and the times of the predicted peaks tended to be within an hour of the observed peak. Observed nighttime ozone values at the central and inland sites were near zero; nighttime model predictions matched these observations.

3.3.2 VOC Reactivity

To test that DDM-3D with the SAPRC99 chemical mechanism was producing accurate estimates for semi-normalized sensitivity coefficients, s^*, we compared the results of several DDM-3D simulations with estimates derived using the brute-force method. Toluene was one of the VOC for which the s^* values were checked using the brute-force technique (with a centered-difference approximation). A set of simulated ozone values was generated with toluene emissions uniformly increased by 50%; an otherwise identical set was generated with toluene emissions uniformly decreased by 50%. The difference in surface-level ozone values (ppb) for these two simulations is shown in Figure 3.4.a for 1600 PST on 24 June.

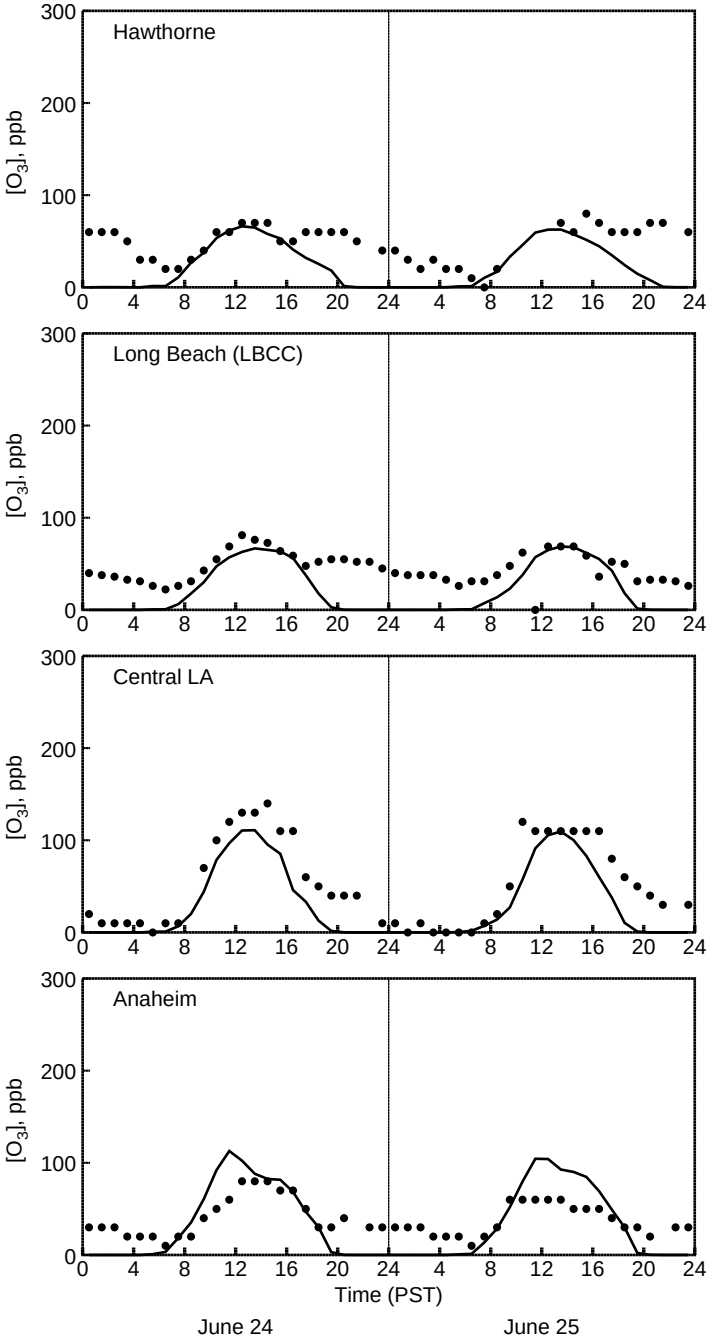

Figure 3.3.a. Ozone time series plots comparing observed (circles) and predicted (solid line) surface-level ozone at coastal and central sites.

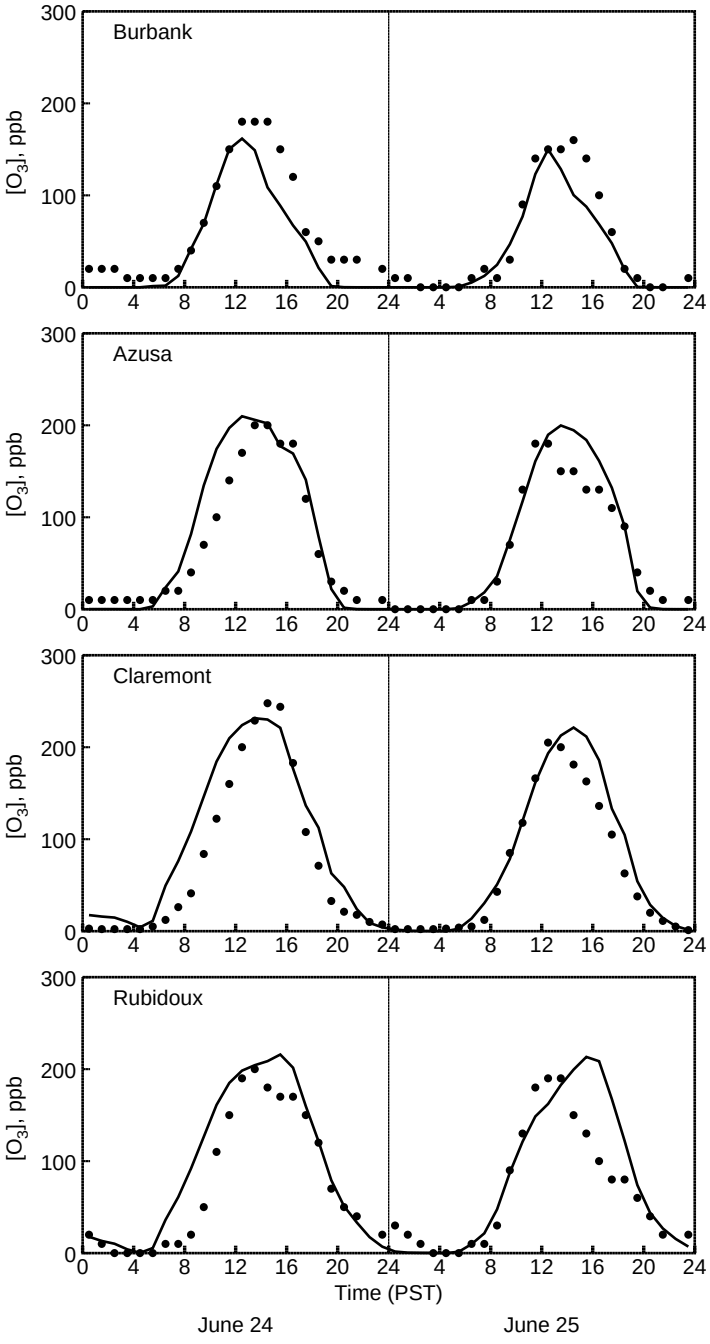

Figure 3.3.b. Ozone time series plots comparing observed (circles) and predicted (solid line) surface-level ozone at inland sites.

The difference contours indicate that, as expected, ozone increases with increasing toluene emissions in most areas. At hour 1600 PST near the center of the domain, there is more than a 10 ppb increase in ozone 100% increase in toluene emissions. The areas where ozone has decreased slightly with increased toluene (shaded area at upper right of Figure 3.4.a) are downwind of the primary emissions. Some of the NO_x that was previously converted to ozone in these downwind areas is now depleted sooner, resulting in lower ozone concentrations in these areas.

The DDM-3D estimate of the (semi-normalized) ozone sensitivity to toluene (Figure 3.4.b) is similar but not identical to the estimates using the "brute force" technique. Such differences are expected because, as discussed above, for a 50% change in toluene emissions, non-linear effects are encountered using the brute force technique that affect the estimate and, subsequently, the shape of the sensitivity contours. However, as the changes in the base case inventory are made smaller for the brute-force method, the results become closer to the results seen using the DDM-3D, indicating that DDM-3D has been implemented correctly and is working properly.

Tests were also performed for nitric oxide (NO) emissions, comparing the brute force technique to DDM-3D. Figure 3.5.a shows contours of the estimated semi-normalized sensitivity of ozone to NO using the brute force technique at hour 1600 PST 24 June. Figure 3.5.b provides the same contours, but using the DDM-3D. In this case, the centered-difference method used a 20% change in the base case NO emissions. Here again, the two methods produce similar but not identical results. The reason for the differences is the same as for the toluene tests. Again, as the changes to the base inventory are made smaller, the brute-force technique produces results closer to the DDM-3D.

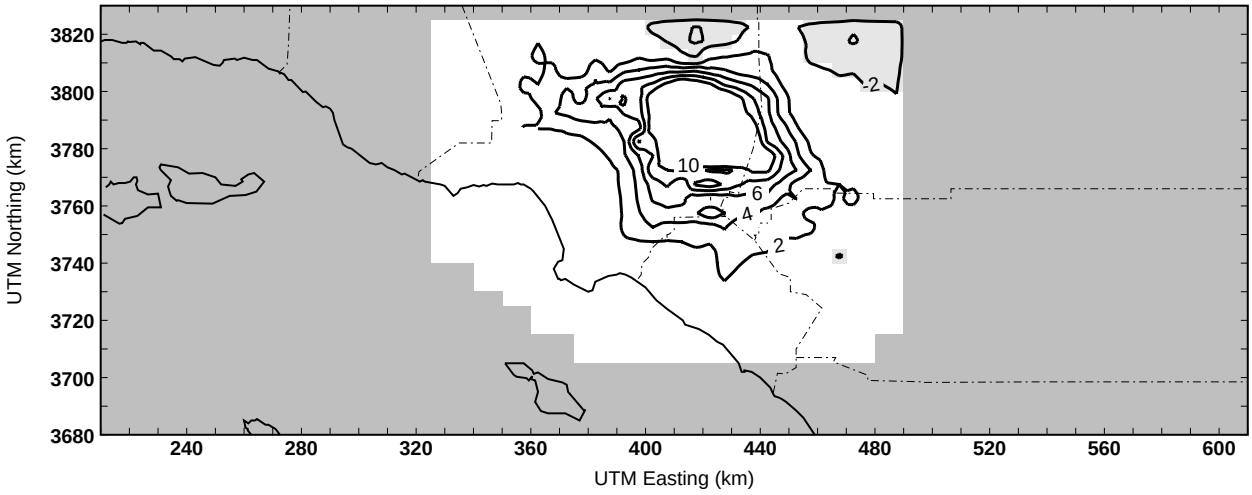

Figure 3.4.a. Estimated spatial distribution of the semi-normalized sensitivity (ppb) of ozone to toluene emissions at 1600 PST on 24 June 1987 using the centered-difference or "brute-force" method. Negative semi-normalized sensitivity values less than -2 ppb are shaded.

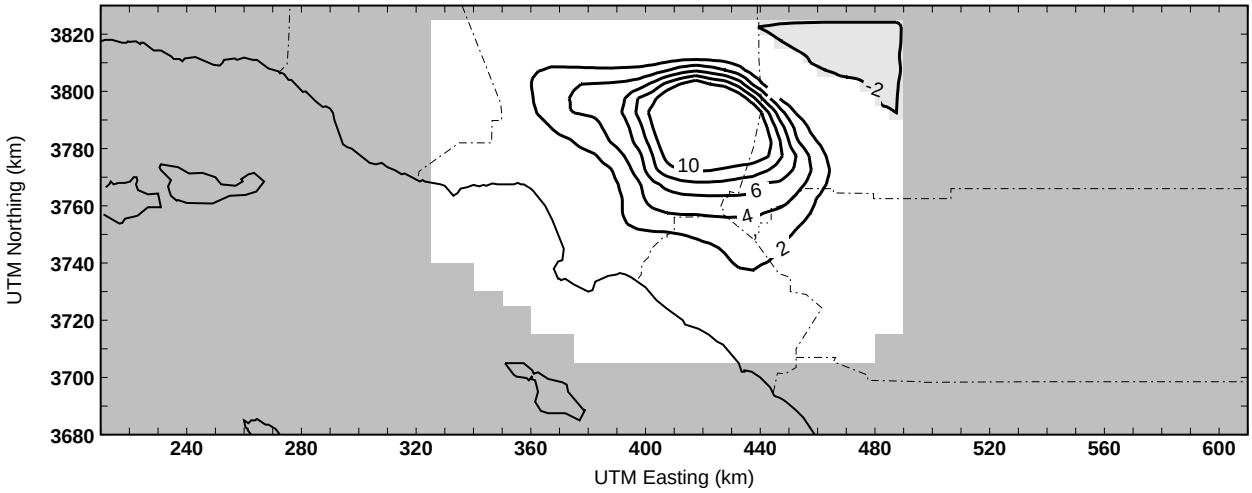

Figure 3.4.b. Same as 3.4.a. but using the DDM.

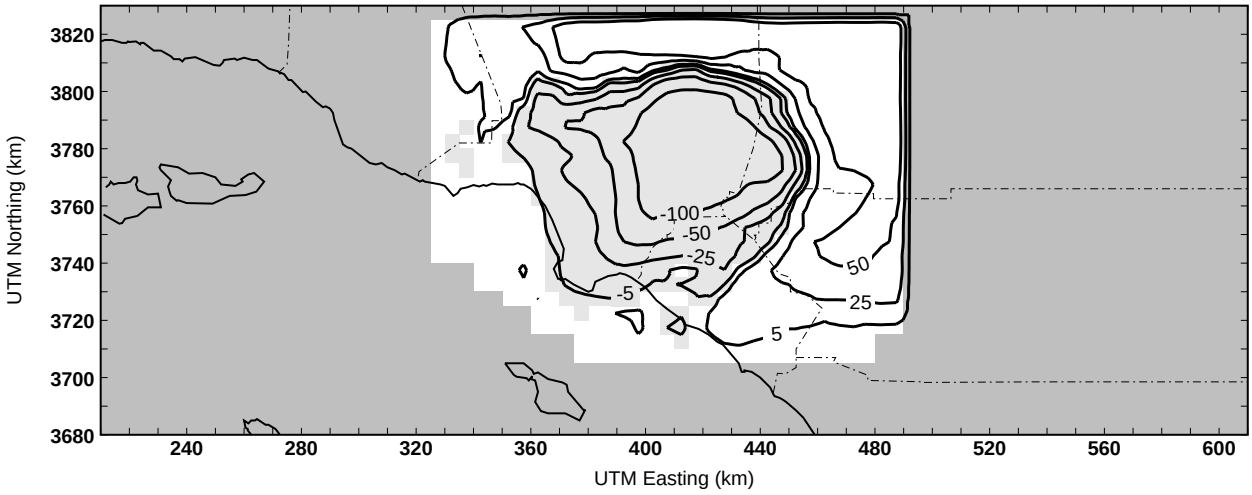

Figure 3.5.a. Estimated spatial distribution of the semi-normalized sensitivity (ppb) of ozone to nitric oxide emissions at 1600 PST on 24 June 1987 using the centered-difference or "brute-force" method. Negative semi-normalized sensitivity values less than -2 ppb are shaded.

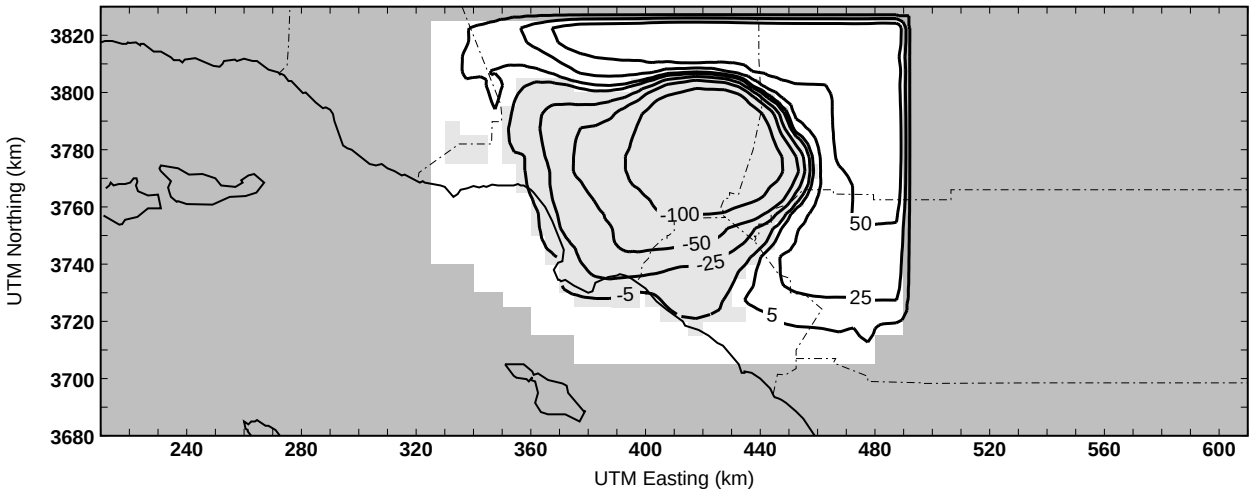

Figure 3.5.b. Same as 3.5.a. but using the DDM.

As illustrated in Figures 3.4-3.5, there are significant spatial variations in the sensitivity coefficients, and therefore one should expect significant variation in the AIR values calculated using equation (3.1). Figure 3.6 shows AIR values (ppb/kilotonne) at the time of maximum observed ozone at two locations: Hawthorne and Claremont. Each of the 31 species listed in Table 2.1 is represented and grouped according to species type. A comparison of the coastal Hawthorne site (Figure 3.6.a) with the inland Claremont site (Figure 3.6.b) reveals that, in fact, AIR at the inland site is larger by nearly an order of magnitude. Hawthorne and other coastal sites are upwind of most emissions, so ozone at these sites is only slightly reduced by VOC emission reductions. In contrast, at Claremont, and other inland sites, VOC reductions do significantly reduce ozone.

Absolute incremental reactivity is low at the coastal sites, increases near the central sites, and then decreases again at the furthest inland (downwind) sites. The spatial variation of the emissions and the landward transport of pollutants during the day create conditions that correspond roughly to the adjustments made by Carter (1994) to VOC/NO_x ratios to achieve either MOIR or MIR conditions. Maximum ozone conditions on both 24 and 25 June are achieved near the Claremont site; maximum incremental reactivity conditions are achieved near the Azusa site on both days. Appendix B contains plots of AIR for all 8 sites.

Normalizing the AIR values to produce RIR values (equation (2.2)), allows one to compare reactivity across the different sites. Figures 3.7.a-3.7.e plot RIR at all 8 sites for each VOC. These RIR values are also presented in a tabular format in Appendix B. The R_MIR from Carter (2000b) is included in Figures 3.7.a-3.7.e to compare the 3-D results to the accepted box model results. In these figures sites are ordered from coastal to inland (top to bottom). Note that the scaling of the vertical axis is varied from one figure to the next. In the discussion that follows, it will be useful to examine the mean and standard deviation of RIR for each species across the 8 sites. Table 3.3 includes this information as well as the R_MIR values from Carter (2000b).

In agreement with past results, the alkane species were not found to be particularly reactive (Figure 3.7a). Most of the alkane species have calculated RIR values that are consistent with the values of Carter (2000b). Notable exceptions to this are the RIR values for n-butane and n-pentane at the Long Beach site. This site is characterized by high concentrations of both n-butane and n-pentane from nearby refinery emissions; thus, ozone at this site is relatively more affected by changes in emissions of these species.

Alkenes (Figure 3.7b) are generally more reactive than the alkanes (note the significant change in scale between Figures 3.7a and 3.7b). Apart from the difference in magnitude, there are notable differences in the comparison to the R_MIR values. At the coastal and central sites for many of the alkene species, the estimated values of RIR from DDM-3D tend to be larger than the corresponding R_MIR values. At these locations, concentrations of radical species tend to be relatively low and alkenes, whose direct reactions with ozone initiate the production of radicals, therefore have a larger effect on ozone than they would at locations with a rich supply of radicals.

Important exceptions to the tendency for alkene RIR values to be greater than R_MIR values are the biogenic alkene species isoprene and α-pinene. The R_MIR values for both isoprene and α-pinene are higher than the corresponding DDM-3D estimates at all 8 sites. This difference is due to the spatial distribution of the biogenic emissions. As noted in the discussion of Figure 3.2.c above, the distribution of biogenic emissions places most of the isoprene and also the α-pinene downwind of these sites. Therefore, the effect of these species on ozone is much reduced relative to what would be predicted by a box model. Table 3.3 shows the 8-site mean of isoprene to be 1.34 whereas the R_MIR is 5.38.

Across the 8 sites, the estimated RIR values for aromatic species (Figure 3.7.c) are near but generally lower than the R_MIR values. There is a trend of increasing RIR from Hawthorne to Anaheim and a trend of decreasing RIR from Anaheim to Riverside. Apparently conditions at the Anaheim site are near the conditions for maximum incremental reactivity of aromatics. The RIR values at the Anaheim site agree most closely with the R_MIR values.

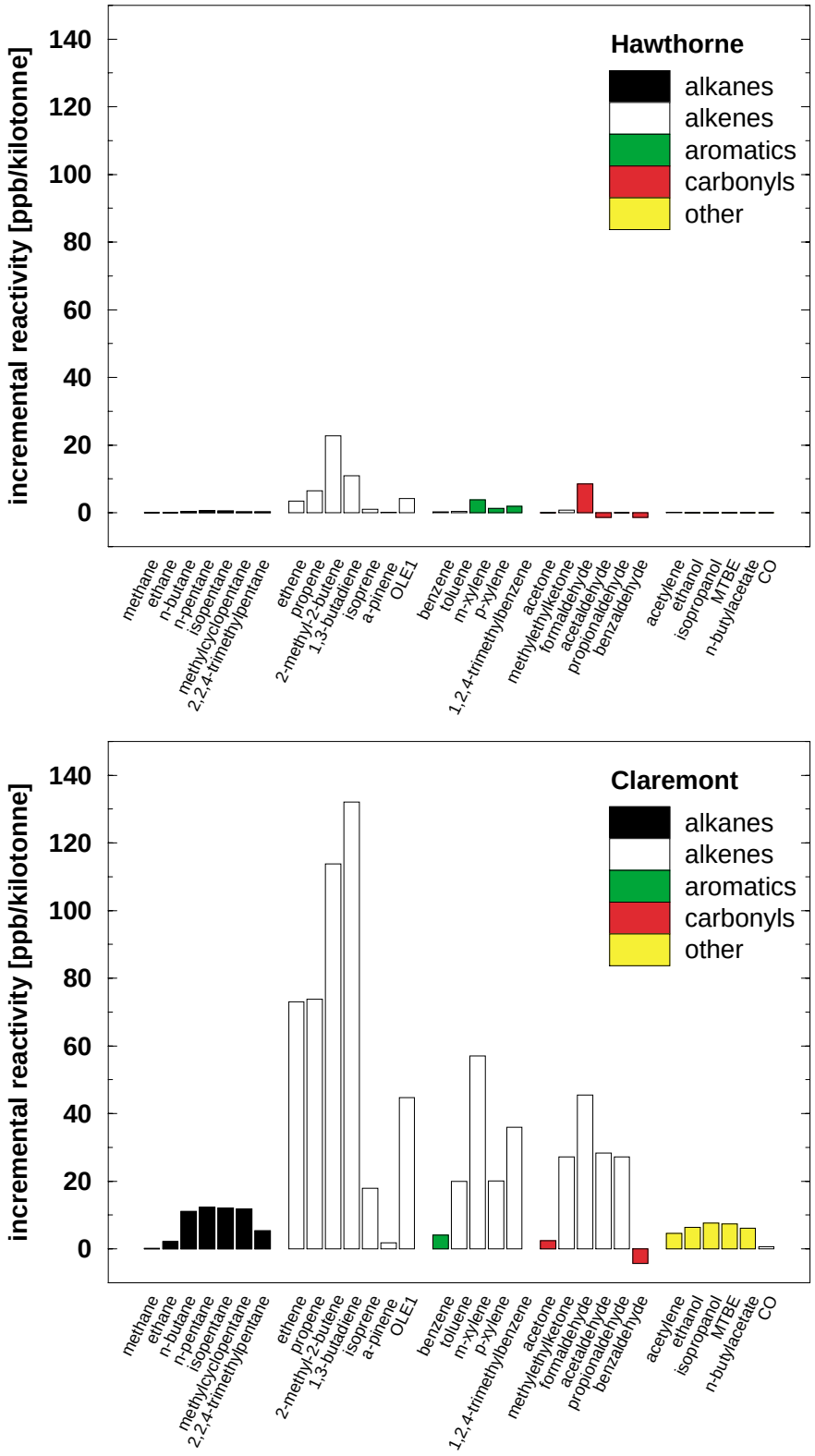

Figure 3.6. Absolute incremental reactivity calculated at the time of maximum observed ozone on 25 June 1987 at (a) coastal site Hawthorne and (b) inland site Claremont.

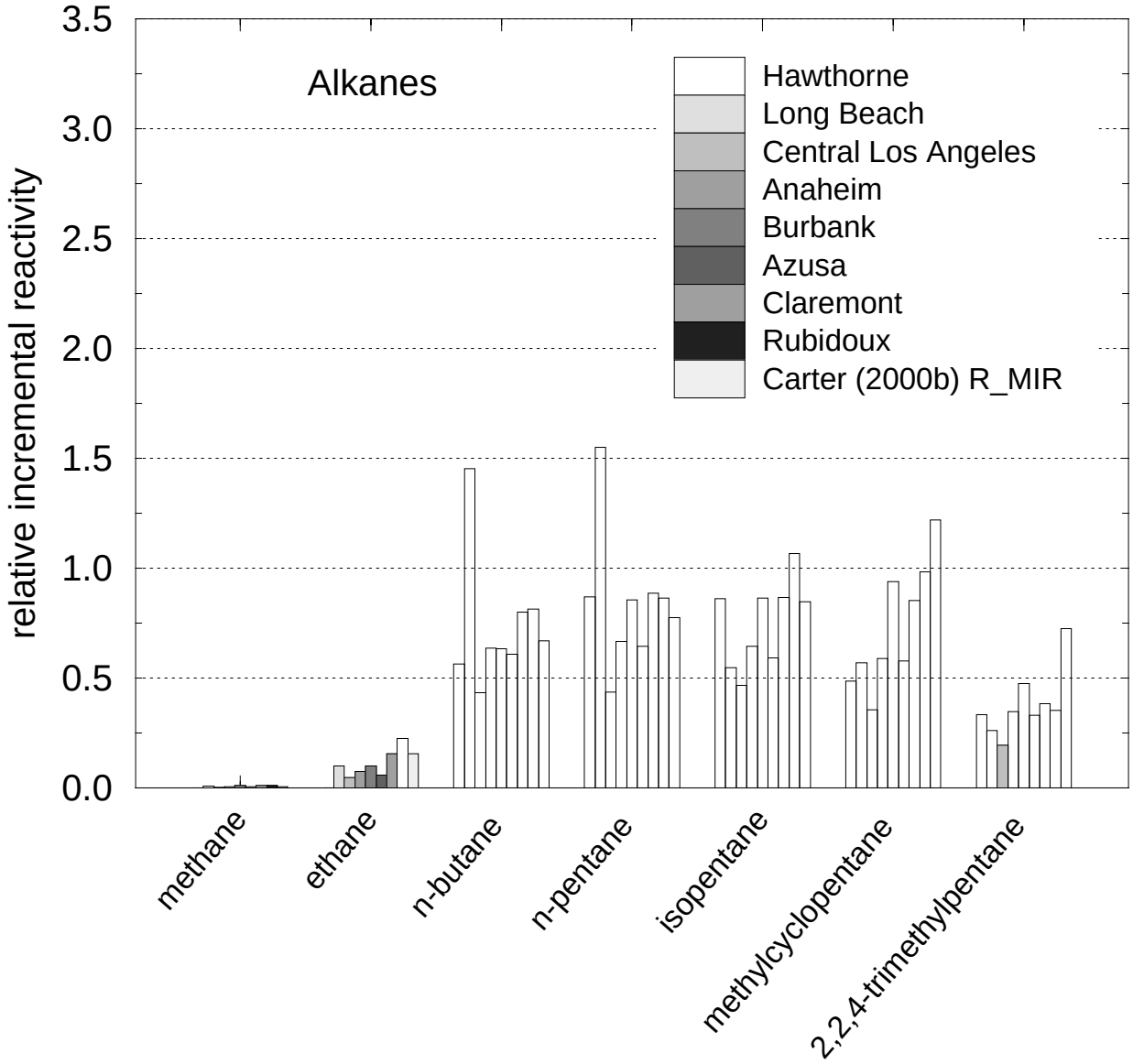

Figure 3.7.a. Relative incremental reactivity of alkanes calculated at the time of maximum ozone on 25 June 1987 at all sites. The R_MIR from Carter (2000b) is included for comparison.

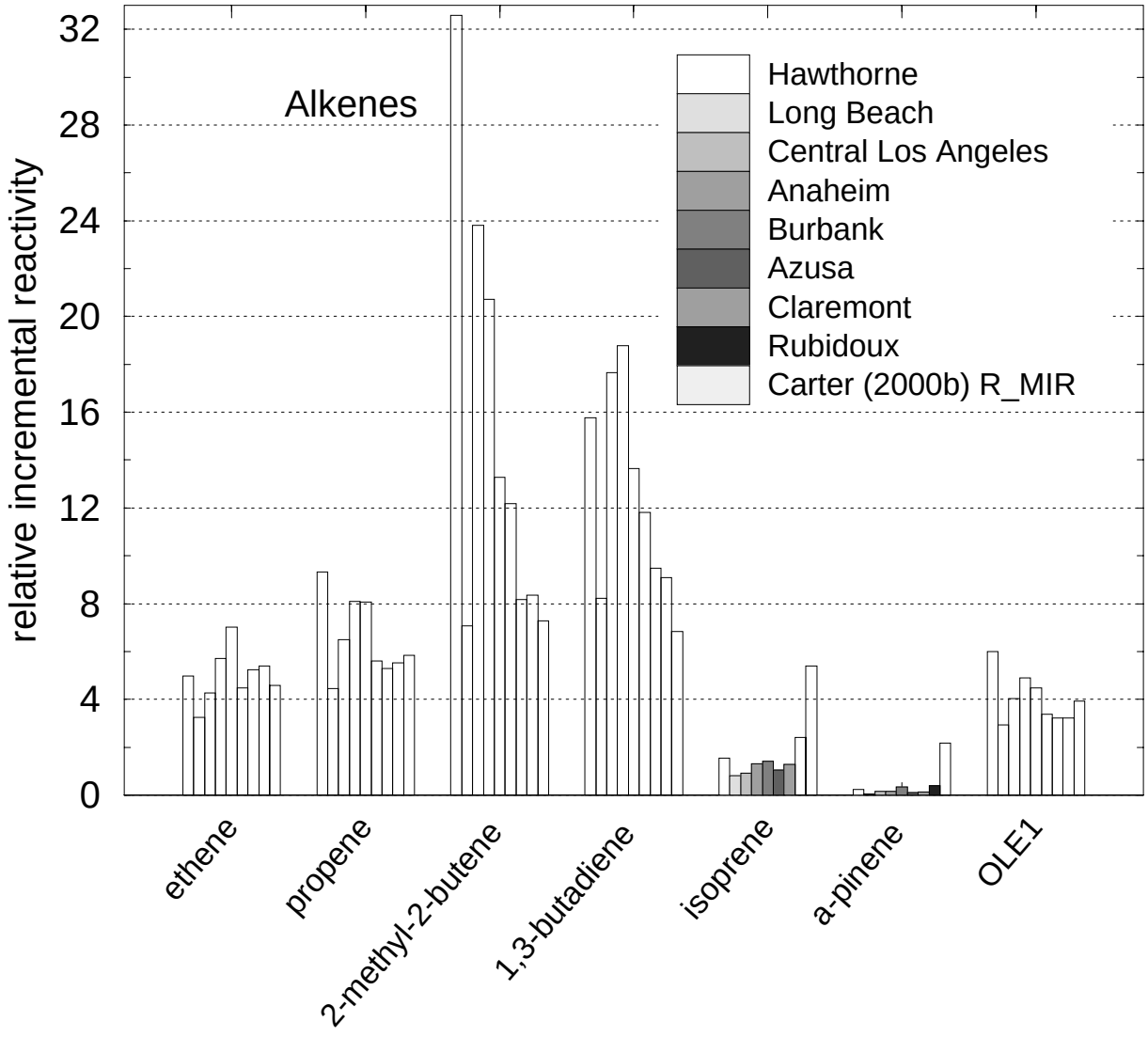

Figure 3.7.b. Relative incremental reactivity of alkenes calculated at the time of maximum ozone on 25 June 1987 at all sites. The R_MIR from Carter (2000b) is included for comparison.

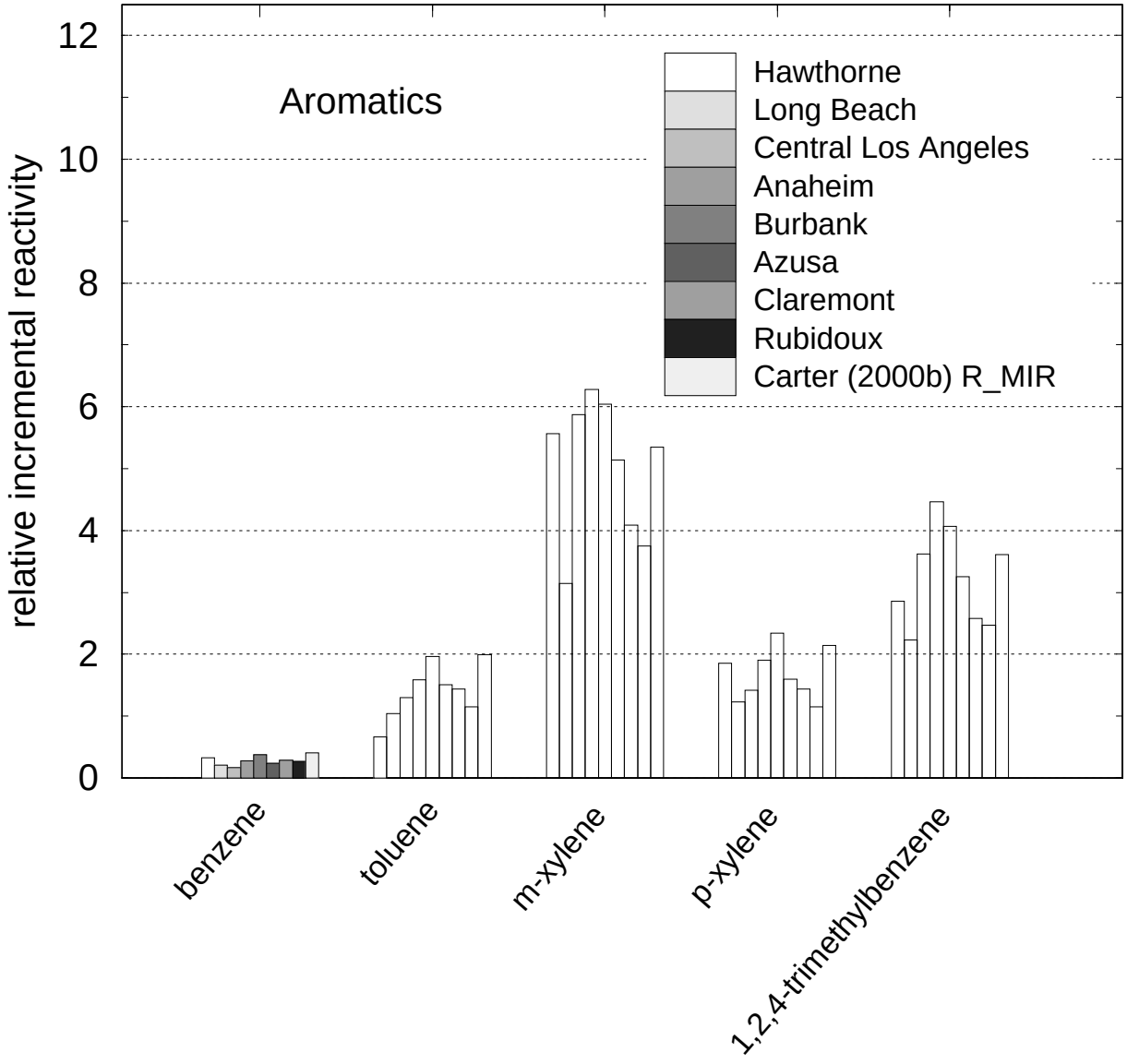

Figure 3.7.c. Relative incremental reactivity of aromatics calculated at the time of maximum ozone on 25 June 1987 at all sites. The R_MIR from Carter (2000b) is included for comparison.

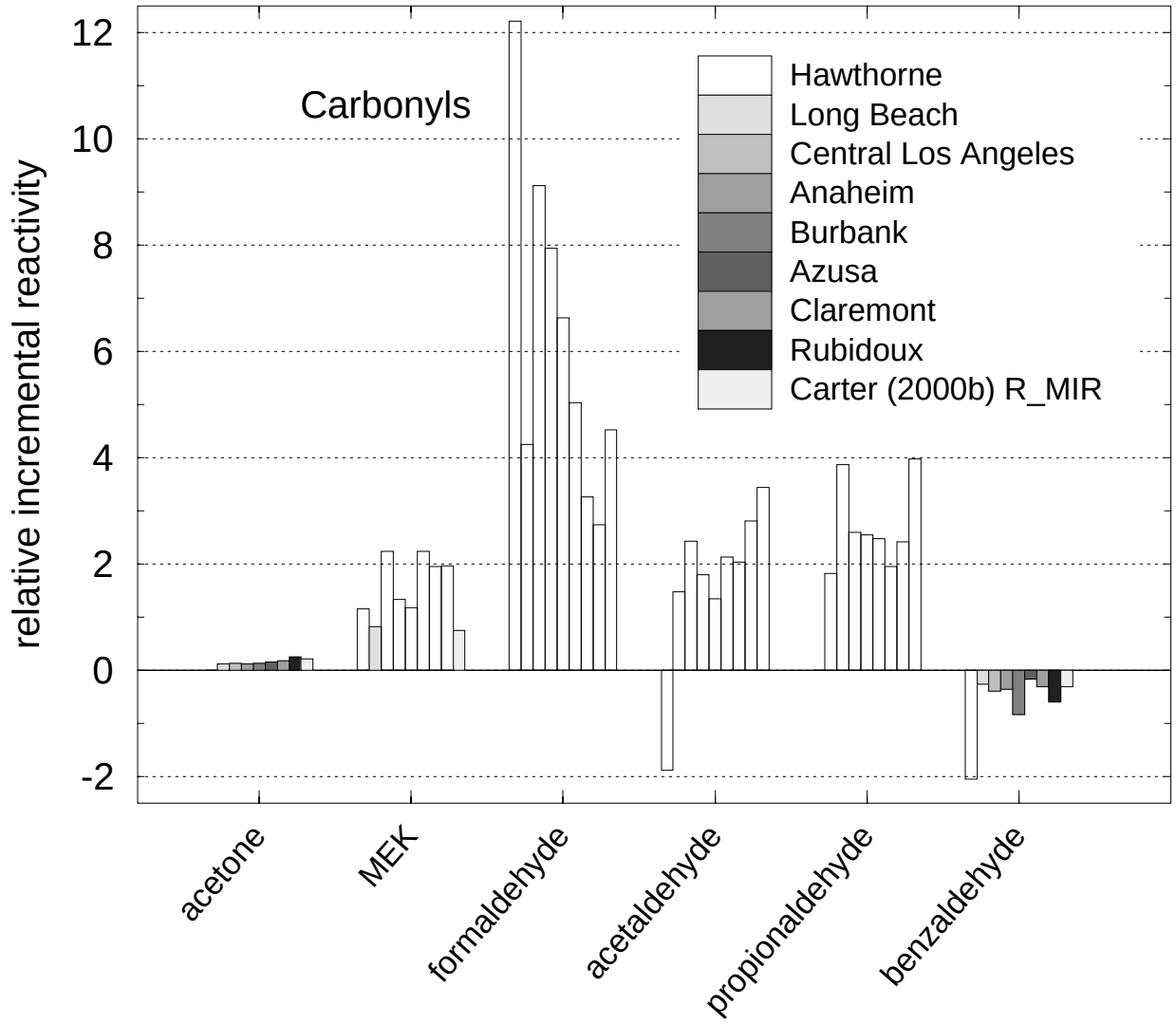

Figure 3.7.d. Relative incremental reactivity of carbonyls calculated at the time of maximum ozone on 25 June 1987 at all sites. The R_MIR from Carter (2000b) is included for comparison.

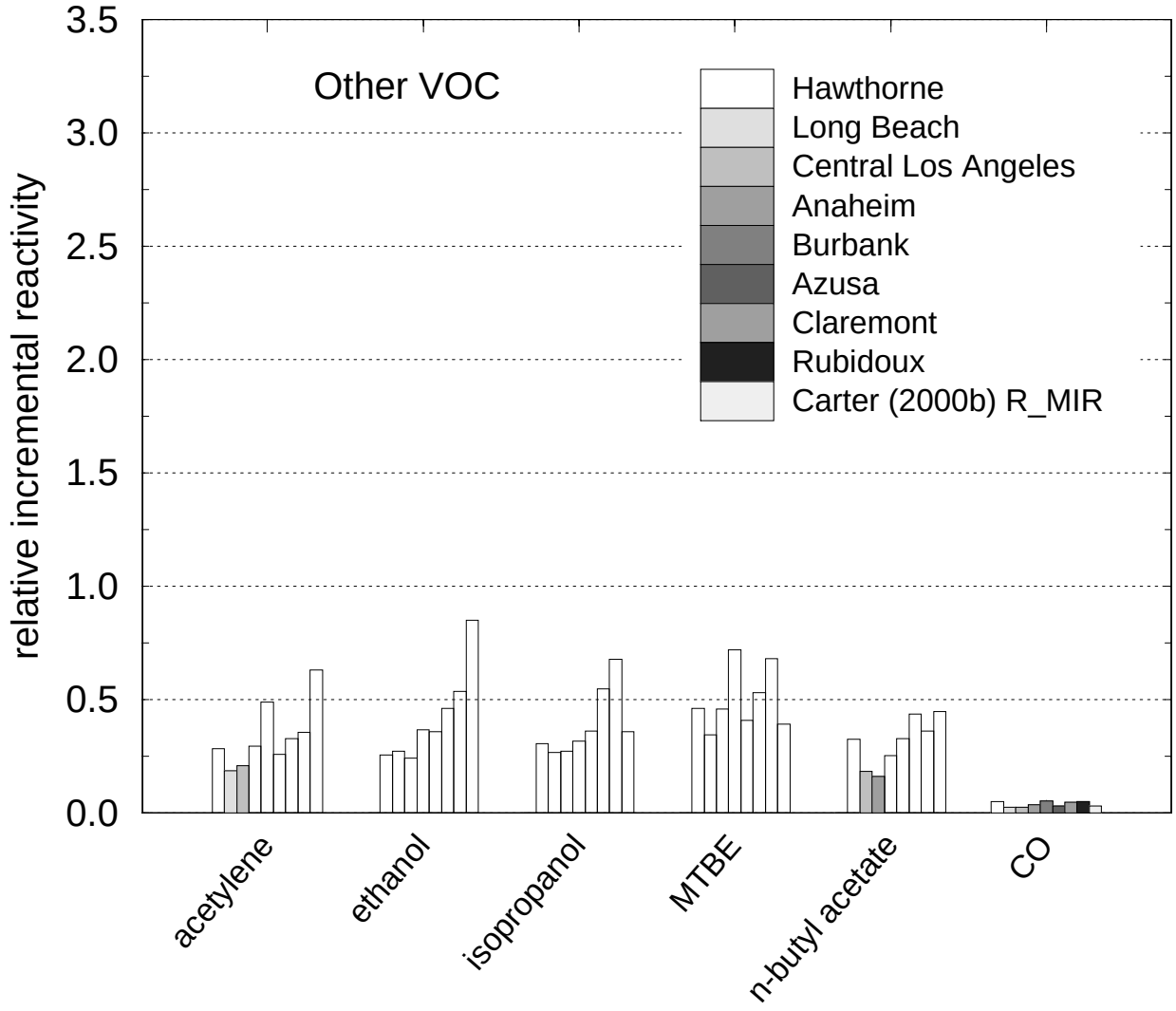

Figure 3.7.e. Relative incremental reactivity of other species calculated at the time of maximum ozone on 25 June 1987 at all sites. The R_MIR from Carter (2000b) is included for comparison.

The values of RIR for most of the carbonyls (Figure 3.7.d) are consistent for a given species across many of the sites. For some species, RIR and R_MIR values also agree. There are, however, several notable exceptions where significant variations are evident. The reactivity of formaldehyde, for example, varies widely from site to site and generally decreases from coastal to inland sites. Like the alkenes, formaldehyde reactions can initiate the formation of radicals ($HCHO + h\nu \rightarrow 2\,HO_2^{\bullet} + CO$). At sites where low radical concentrations limit the production of ozone, formaldehyde has particularly high RIR values. Interestingly, benzaldehyde RIR values at all sites and the R_MIR value are negative. This is because there is a NO_x sink in the reaction mechanism for benzaldehyde, which results in an overall reduction in ozone formation. (See Seinfeld and Pandis, 1998, p. 312.) At the Hawthorne site only, acetaldehyde has a negative RIR value. This is probably because at Hawthorne there is an increase in PAN production that competes with ozone formation via photolysis of NO_2.

Table 3.3. Mean and standard deviation of RIR across 8 sites in the SoCAB compared to R_MIR from Carter (2000b). Change in Rank and Discrepancy Index are defined on p. 38.

Compound	**R_MIR** Based on Carter (2000b)	**Mean & Std. Dev. RIR** (8 sites)	**Change in Rank** (31species)	**Discrepancy Index**
methane	0.01	0.01/0.01	0	0.00
ethane	0.16	0.09/0.06	0	0.00
n-butane	0.67	0.74/0.29	5	0.01
n-pentane	0.78	0.85/0.30	3	0.01
isopentane	0.85	0.74/0.19	0	0.00
methylcyclopentane	1.22	0.67/0.21	-3	-0.05
2,2,4-trimethylpentane	0.72	0.33/0.08	-1	-0.01
ethene	4.57	5.04/1.04	1	0.02
propene	5.83	6.61/1.59	0	0.00
2-methyl-2-butene	7.28	15.77/8.51	0	0.00
1,3-butadiene	6.84	13.06/3.79	0	0.00
isoprene	5.38	1.34/0.47	-9	-1.21
α-pinene	2.16	0.20/0.11	-14	-0.92
lumped terminal olefins	3.92	4.02/0.99	2	0.01
benzene	0.41	0.27/0.06	0	0.00
toluene	2.00	1.33/0.37	0	0.00
m-xylene	5.34	4.99/1.10	-1	-0.01
p-xylene	2.14	1.62/0.37	3	0.05
1,2,4-trimethylbenzene	3.62	3.19/0.75	2	0.03
acetone	0.22	0.13/0.07	0	0.00
methyl ethyl ketone	0.75	1.61/0.51	8	0.23
formaldehyde	4.52	6.40/3.03	3	0.19
acetaldehyde	3.44	1.52/1.36	-1	-0.06
propionaldehyde	3.97	2.21/1.01	-1	-0.06
benzaldehyde	-0.31	-0.62/0.57	0	0.00
acetylene	0.63	0.30/0.09	-1	-0.01
ethanol	0.85	0.31/0.15	-6	-0.11
isopropanol	0.36	0.34/0.19	6	0.00
methyl tert-butyl ether	0.39	0.45/0.21	6	0.01
n-butyl acetate	0.45	0.26/0.13	-2	-0.01
carbon monoxide	0.03	0.04/0.01	0	0.00

The other species (Figure 3.7.e) all have RIR values of 0.5 or less. While there is fair agreement with R_MIR values, the R_MIR values are larger than the 8-site mean of the RIR values (See also Table 3.3). There is a tendency for increasing RIR values with distance from the coast. This trend is probably due to the increase in radical availability at inland sites and the fact that alkenes and formaldehyde are relatively high at the coastal and central sites.

One of the advantages of assigning incremental reactivity values to VOC compounds is that it allows the compounds to be ranked in order of their potential to form ozone. Figure 3.8.a shows R_MIR of each of the 31 species sorted in order of decreasing (from top to bottom) MIR values. Near the top of Figure 3.8.a with the highest R_MIR values are many of the alkenes, followed by m-xylene, formaldehyde, and propionaldehyde. The sort order is not altered greatly if one examines R_MOIR instead of R_MIR. Figure 3.8.b shows R_MOIR values ranked in order of decreasing MIR value for each VOC compound. There are cases where the rankings change, but not by many positions. For example, an MOIR ranking would place 1,3-butadiene first instead of second and 2-methyl-2-butene would be second instead of first, in each case a change of just one position.

It is instructive to rank RIR from DDM-3D in MIR order to examine the variation in rankings at different sites. Figure 3.9 plots RIR ranked in MIR order for two sites: Central L.A., which is representative of the coastal and central sites, and Claremont, which is representative of the inland sites. In Figure 3.9.a, one first notes that the largest values of RIR for the top 2 alkenes are larger than the corresponding values of R_MIR shown in Figure 3.8.a. Also, near the bottom of Figure 3.9.a, the smallest values of RIR are smaller than the corresponding R_MIR values. However, it is clear that for most species the sort order would not shift by many positions. An exception to this is formaldehyde, which, as noted above, is an important chain initiator for radical species. For coastal and central locations, formaldehyde would move up in the rank order. While the rankings of anthropogenic alkenes such as 2-methyl-2-butene are high in all cases, the reactivity of these alkenes is much higher, even on a relative basis, at coastal sites compared to inland sites.

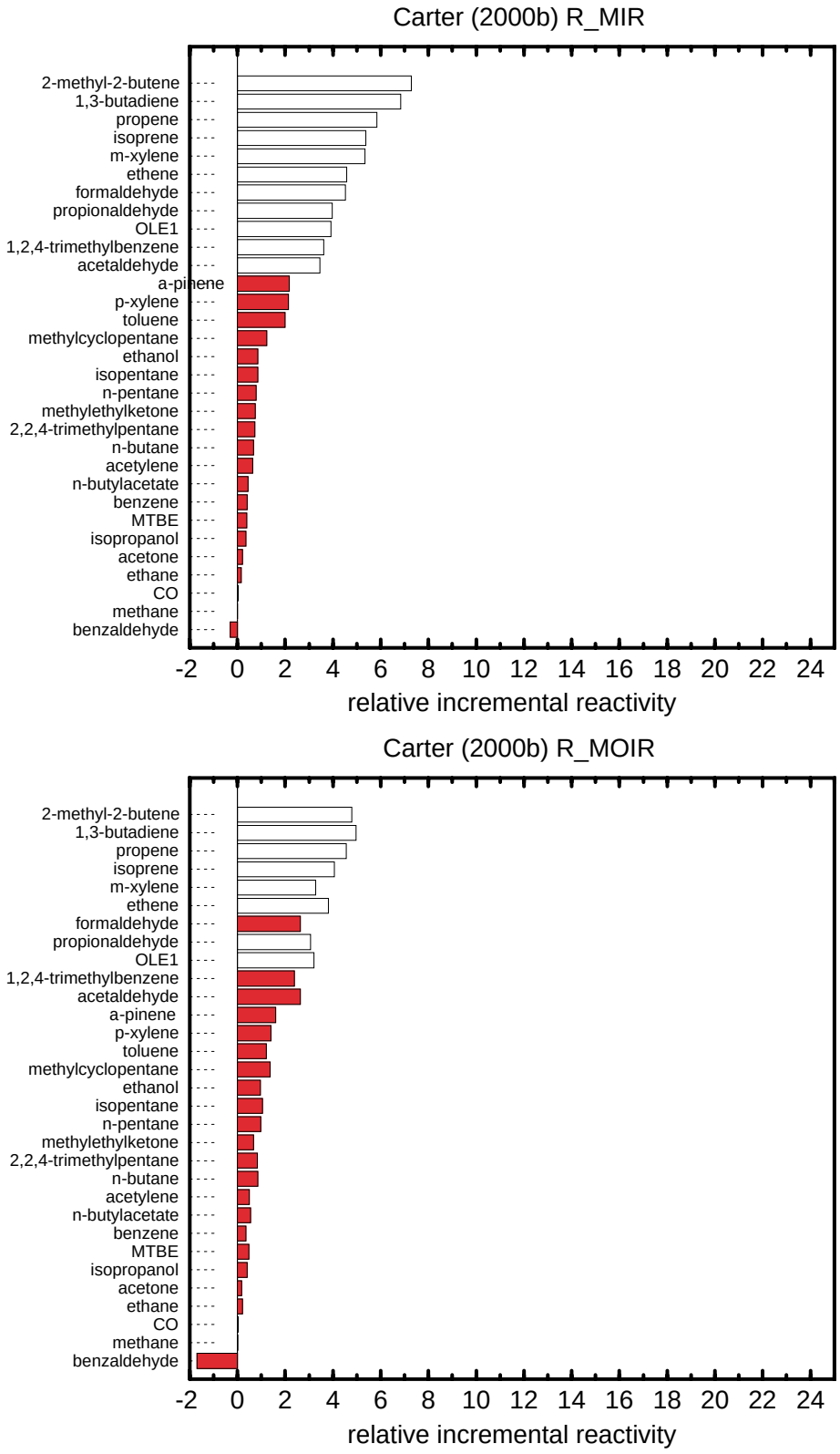

Figure 3.8. The R_MIR (a) and R_MOIR (b) from Carter (2000b) are shown sorted in order of decreasing MIR in both cases.

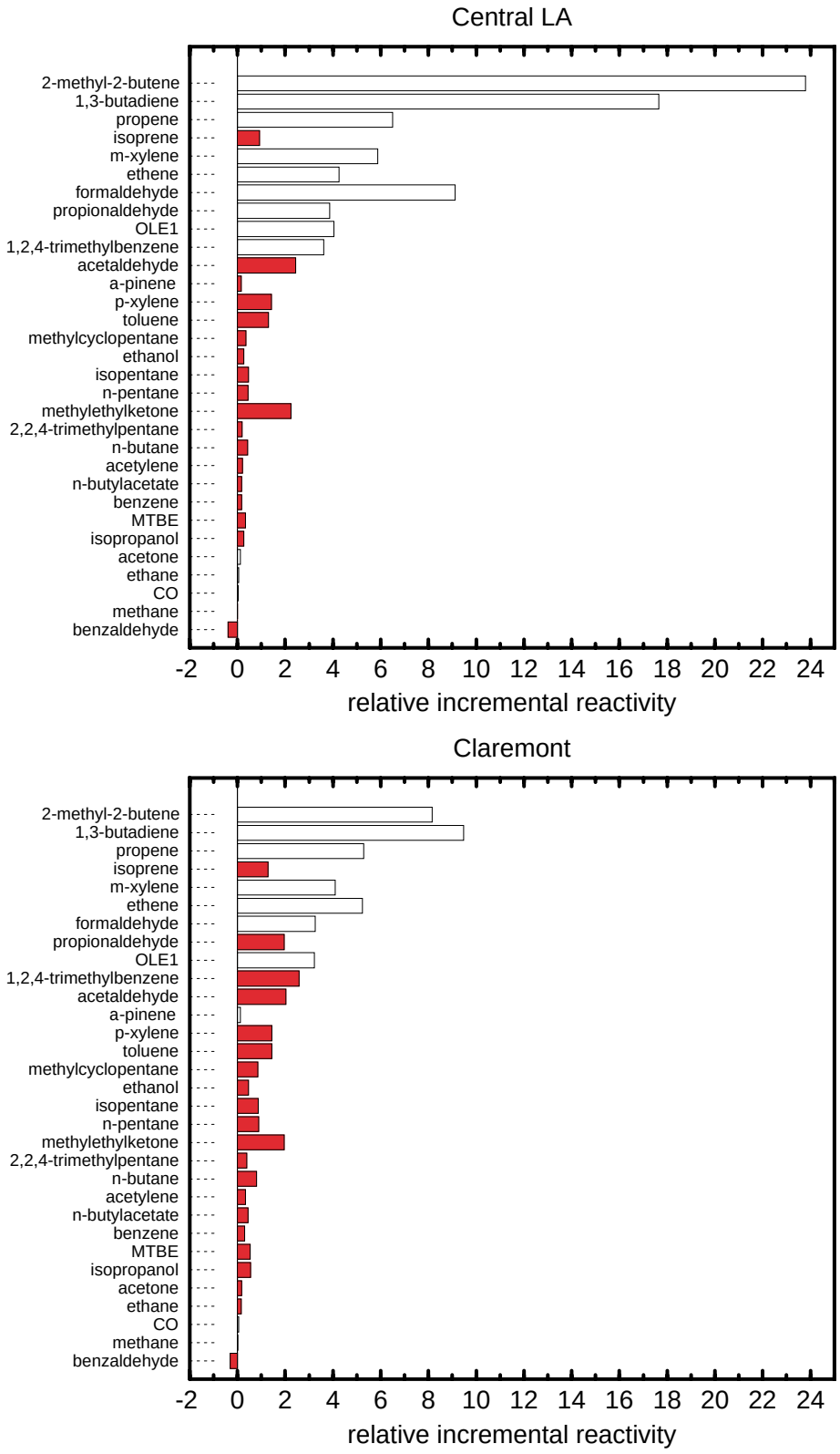

Figure 3.9. RIR calculated at the time of maximum ozone on 25 June 1987 at Central Los Angeles (a) and Claremont (b). The sort order is based on the MIR of Carter (2000b).

The biogenic species isoprene and α-pinene stand out in Figure 3.9; these compounds would move down in sort order relative to the MIR rankings. The reason for this, as noted above, is that the spatial distribution of the biogenic emissions is such that most of the emissions occur downwind of the sites examined here. The timing of the biogenic emissions, which peak at midday when insolation and temperatures are high, may also be a factor. The late release of the biogenic emissions may make them relatively less reactive at the sites we examined compared to emissions from anthropogenic sources that peak earlier.

Compared to the Central L.A. site, the inland Claremont site (Figure 3.9.b) more nearly resembles the R_MIR plot (Figure 3.8.a). This is because the inland site is removed from the important spatial inhomogeneity formed by the Pacific coast. At the inland site, formaldehyde falls more nearly into the MIR ranking. However, note that the RIR values of the biogenic species are still greatly reduced and would drop in rank order even at the inland sites.

Table 3.3 includes two statistics that quantify the difference between mean RIR across the 8 sites and R_MIR. The change in rank is defined by

$$\Delta\, rank = rank_{MIR} - rank_{RIR} \tag{3.3}$$

where $rank_{MIR}$ is the rank number of the 31 species sorted from largest to smallest by MIR and $rank_{RIR}$ is the rank number sorted by RIR. The discrepancy index is defined by

$$\delta = \left|\overline{RIR} - R\_MIR\right| \cdot \frac{\Delta\, rank}{N_{species} - 1} \tag{3.4}$$

where $\overline{RIR}$ is the mean RIR across the 8 sites and $N_{species}$ is the number of species (31 in this case). This index is useful for identifying those species for which the magnitude of RIR differs significantly from that of R_MIR and for which the ranking by MIR differs from ranking by RIR. Table 3.3 shows that the largest changes in rank and discrepancy index are those of the biogenic species isoprene and α-pinene. The discrepancy index of both of these biogenic species is near -1; for all other species, the discrepancy index has a magnitude of less than 0.25. For most other species, the discrepancy index is at or near zero.

3.4 Summary

The main results presented above are summarized in this section. For a multi-day ozone episode in the SoCAB in June 1987, the CIT airshed model with DDM-3D was applied to examine the importance of spatial variability on the assessment of incremental reactivity for 31 VOC species. The CIT model performance for ozone was evaluated and found to have low bias (+6-7%) and moderate error (about 40%) for both days of the simulation. The semi-normalized sensitivity calculations of DDM-3D with SAPRC99 were found to be consistent with values computed using the "brute-force" method.

The application of DDM-3D yielded sensitivities from which RIR values were determined for each of 8 sites in the South Coast Air Basin at the time of maximum observed ozone on 25 June 1987. Analysis of these results led to the following findings:

- Normalized or relative IR values are more useful than absolute values for comparing and ranking VOC reactivities across different sites. As shown in Figure 3.6, AIR values varied by an order of magnitude across sites, whereas Figure 3.7 shows that RIR values are closer for a given VOC at different sites.
- For most species, RIR values and rank order are consistent with the R_MIR values and rank order. The discrepancy index, listed in Table 3.3 for each species and defined by equation (3.4), is within ± 0.25 for all but two species, indicating a high degree of consistency with R_MIR values and rankings.
- The spatial distribution of emissions and pollutant transport patterns can affect determinations of incremental reactivity within an airshed.
- At coastal and central sites in the SoCAB, VOC such as formaldehyde and alkenes that initiate radical formation have higher reactivity than at inland sites on both absolute and relative bases.
- A consistent finding for all 8 sites examined was that biogenic VOCs, while ranked high in box model determinations of MIR, have low RIR at South Coast urban monitoring sites. The discrepancy index for isoprene is –1.21 for isoprene and –0.92 for α-pinene.
- Differences in relative reactivity can be magnified when the absolute reactivities are low (such as at coastal sites).

4. Uncertainty and Variability in Incremental Reactivities

The objective of the research presented in this chapter is to estimate uncertainties and explore variability in incremental reactivities that are calculated for realistic atmospheric conditions. Reactivities are estimated for selected compounds using the vertically-resolved trajectory version of the California Institute of Technology (CIT) photochemical air quality model incorporating the SAPRC99 chemical mechanism (Carter, 2000a). Trajectories ending at four monitoring locations in the South Coast Air Basin at the time that peak ozone concentrations were observed on 25 June 1987 were used in the analysis. The monitoring locations are at Anaheim, Azusa, Claremont and Riverside. Uncertainties in critical chemical parameters, emissions rates and deposition parameters were propagated through the reactivity calculations using Monte Carlo analysis with Latin Hypercube Sampling.

4.1 Trajectory model formulation and inputs

For each simulation, the trajectory version of the CIT model simulates a parcel of air traveling across an airshed by solving the Lagrangian formulation of the atmospheric diffusion equation:

$$\frac{\partial C_i}{\partial t} = \frac{\partial}{\partial z}\left(K_{zz} \frac{\partial C_i}{\partial z} \right) + R_i(\underline{C}), \qquad i=1,\ldots,n \tag{4.1}$$

where C_i is the ensemble mean concentration of species i, K_{zz} is the turbulent eddy diffusivity in the vertical direction, and $R_i(\underline{C})$ is the net rate of generation of species i by chemical reactions. The initial condition is $C_i(z,0)=C_i^0(z)$, and the boundary conditions are:

$$v_g^i C_i - K_{zz} \frac{\partial C_i}{\partial z} = E_i \text{ at the surface, and}$$

$$K_{zz} \frac{\partial C_i}{\partial z} = 0 \text{ at the top of the column.}$$

Here, v_g^i is the surface deposition velocity and E_i is the surface emissions flux of species i. The trajectory column modeled in this study is comprised of five vertical layers. The most significant limitations of the trajectory formulation are its inability to account for horizontal diffusion and wind shear. Nevertheless, the trajectory model is useful because it accounts for more physical

detail than a box model, while remaining computationally tractable in the context of the hundreds of model runs required for Monte Carlo analysis.

The same meteorological and emissions inputs described above in Chapter 3 were used in trajectory modeling described here. Multi-day air parcel back-trajectories were computed using surface layer wind fields. The trajectories were computed so that air parcels arrived at each of the receptor air monitoring sites of interest at the time of the observed maximum ozone concentration. Relevant emissions and meteorological input data for the air quality model were recorded along the calculated path of each air parcel trajectory.

As a preliminary step, results obtained from the CIT trajectory model using SAPRC99 were compared to results obtained with the SAPRC97 version of the mechanism (Carter, 1996) that we have used in previous incremental reactivity uncertainty studies (Wang et al., 2000). Table 4.1 presents final concentration values for Azusa and Riverside for several key output species. For these two locations, as well as others that we examined, SAPRC99 generally gives lower concentrations of O_3, HNO_3, PAN and H_2O_2 and higher concentrations of NO_2 than SAPRC97. This is consistent with Carter's (2000) description of the SAPRC99 mechanism as less "reactive" than the previous version.

Table 4.1. Comparison of trajectory model results obtained with SAPRC97 and SAPRC99

	Ozone (ppm)		H_2O_2 (ppm)		HNO_3 (ppm)	
	SAPRC97	SAPRC99	SAPRC97	SAPRC99	SAPRC97	SAPRC99
Azusa	0.163	0.138	2.74×10^{-3}	1.45×10^{-3}	2.57×10^{-2}	1.89×10^{-2}
Riverside	0.135	0.135	5.34×10^{-3}	2.88×10^{-3}	9.17×10^{-3}	7.71×10^{-3}

	NO_2 (ppm)		PAN (ppm)	
	SAPRC97	SAPRC99	SAPRC97	SAPRC99
Azusa	3.24×10^{-2}	4.36×10^{-2}	1.03×10^{-2}	5.80×10^{-3}
Riverside	4.74×10^{-3}	5.97×10^{-3}	3.94×10^{-3}	3.22×10^{-3}

4.2 Incremental reactivity calculations

With the trajectory model, unlike the airshed models, incremental reactivities were estimated using finite perturbations to the emissions of a particular VOC. Absolute incremental reactivities were calculated as:

$$\frac{MW_{O3}\left([O_3]_{[base\ VOC]} - [O_3]_{[base\ VOC]-\Delta[VOC_j]}\right)}{MW_j\ f_j \sum_{i=1}^{n} \frac{E_{j,i}}{H_i} \Delta t_i} \qquad (4.2)$$

where $[O_3]$ is the concentration in ppm(v) units, MW is molecular weight, E_{ji} is the emissions flux of compound j over time interval i (ppm m min^{-1}), Δt_i is the length of the time interval over which emissions are held constant (min), H_i is the mixing height (m) over that time interval, n is the total number of time intervals comprising the trajectory, and f_j is a fractional reduction in emissions which is applied uniformly with respect to time. The magnitude of f_j used for each compound was determined so that comparable changes in ozone concentrations would be produced across compounds for a given trajectory endpoint. For a representative subset of compounds, a series of tests was conducted with a range of values of f_j, to ensure that the reductions used in the final calculations were in the linear range over which incremental reactivies are independent of the magnitude of f_j.

4.3 Uncertainty analysis

Monte Carlo analysis with Latin hypercube sampling (Iman and Shortencarier, 1984) was used to estimate uncertainties in base case ozone concentrations and in incremental reactivity estimates. A total of 33 uncertain input parameters were treated as random variables, as listed in Table 4.2. The parameters treated as uncertain include rate constants, product yields, emissions rates and deposition parameters determined previously to be influential for box model reactivity calculations (Wang et al., 2000) or for the response of ozone concentrations to VOC emissions reductions, as predicted with a trajectory model (Bergin et al., 1999). Unless indicated otherwise in Table 4.2, all of the uncertainties were incorporated in the model as multiplicative factors, drawn from independent lognormal distributions with a mean of 1.0. The derivations or sources for the uncertainty estimates are given in Bergin et al. (1999) unless otherwise noted.

Multivariate linear regression analysis is applied to the Monte Carlo results to identify the influence of the random input variables on the incremental reactivity estimates.

4.4 Results

Table 4.3 shows the average and coefficient of variation (COV = standard deviation divided by the mean) of the final ozone concentrations from the Monte Carlo simulations of each trajectory. The table also shows regression results indicating which model parameters contribute most to the uncertainty in the final ozone values. The uncertainties range from 17% ($\pm$ 1 σ, relative to the mean) for the ozone concentration at Riverside, to 33% for the ozone concentration at Azusa. For the ozone concentration at Anaheim, the largest source of uncertainty is the deposition affinity of ozone, a parameter that is also influential for the ozone concentrations at Claremont and Riverside. The motor vehicle emissions rate, EMCO, is the most influential parameter for the ozone concentrations at Claremont and Riverside and the second most influential source of uncertainty in the value at Azusa. Rate constants for the reactions HO + NO2 and NO2 + hv and for PAN chemistry are influential for ozone concentrations at all four sites. At Azusa, uncertainties in non-mobile emissions of NO_x and VOCs are also influential. This set of influential parameters is similar to those identified by Bergin et al. (1999) for trajectories ending at Azusa, Burbank, Claremont and Riverside for an August 1987 episode.

Table 4.2. Trajectory model inputs and parameters treated as random variables in the Monte Carlo/LHS calculations

Parameter	COV	Notes	Parameter	COV	Notes
NO2 + hv	0.18	1	ARO2+HO	0.27	1
O3 + NO	0.1	1	PRPE+HO	0.14	1
O3 + hv	0.27	1	N-C4+HO	0.18	1
O1D2+H2O	0.18	1	224P+HO	0.18	1
O1D2+M	0.18	1	XYLM+HO	0.2	1,5,8
HO+NO2	0.27	1,6	ETOH+HO	0.18	1
HO+CO	0.27	1	DCB2,XYLM	0.3	2,5
HO2+NO	0.18	1	DCB3,XYLM	0.3	2,5
CCO-O2+NO2	0.16	1,7	MGLY,XYLM	0.3	2,5
PAN	0.4	1	EMCO	0.25	3
CCO-O2+NO	0.34	1	EMNX	0.06	3
PAN2	0.66	1	EMHC	0.06	3
RCO-O2+NO	0.75	1	EONX	0.15	3
HCHO+hv	0.34	1,9	EOHC	0.29	3
MEK+hv	0.42	1	DPO3	0.29	4
CRES+NO3	0.75	1	DPN2	0.29	4

1 Rate parameter of the indicated reaction treated as uncertain.
2 Yield of the indicated product of the reaction of XYLM + HO treated as uncertain.
3 Uncertainty factors for emissions rates. EMCO is an uncertainty factor for general motor vehicle emissions, applied to CO, NO_x and NMOC (non-methane organic compounds). EMHC and EMNX are separate uncertainty factors for NMOC and NO_x emissions from motor vehicles, respectively. EOHC and EONX are uncertainty factors applied to other anthropogenic sources of NMOC and NO_x.
4 Deposition affinity for O_3 or NO_2, as indicated, treated as random variable from a uniform distribution.
5 Uncertainty estimates adapted from Wang et al. (2000).
6 Correlated with DCB2, XYLM ($\rho = 0.5$); DCB3, XYLM ($\rho = 0.5$); and MGLY, XYLM ($\rho = 0.5$) based on Wang et al. (2000).
7 Correlated with CCO-O2 + NO ($\rho = 0.7$).
8 Correlated with DCB2, XYLM ($\rho = -0.6$); DCB3, XYLM ($\rho = -0.6$); and MGLY, XYLM ($\rho = -0.5$) based on Wang et al. (2000).
9 Applied to both HCHO+hv $\rightarrow$ 2HO2 + CO and HCHO+hv $\rightarrow H_2$ + CO.

Table 4.3 Final ozone concentrations (mean in ppm units with associated COV in parentheses), and regression results indicating the model parameters that contribute most to their uncertainties.

Anaheim (O_3 = 0.061 (0.21); R^2 = 0.96)				Azusa (O_3 = 0.131 (0.33); R^2 = 0.96)			
Parameter	COV[1]	Reg. Coef.[2]	UC (%)[3]	Parameter	COV	Reg. Coef.	UC (%)
DPO3	0.29	-0.48	23.2	HO + NO2	0.27	-0.51	26.3
HO + NO2	0.27	-0.45	19.9	EMCO	0.25	0.39	15.3
NO2 + hv	0.18	0.40	16.3	HCHO + hv	0.34	0.29	8.7
RCO-O2+NO	0.75	0.23	5.1	NO2 + hv	0.18	0.27	7.3
CCO-O2+NO	0.34	0.22	4.8	EONX	0.15	-0.26	6.8
O3 + hv	0.27	0.22	4.7	EMHC	0.06	0.21	4.4
EMCO	0.25	0.20	4.0	EOHC	0.29	0.21	4.4
PAN	0.4	0.18	3.4	CCO-O2+NO	0.34	0.19	3.6

Claremont (O_3 = 0.168 (0.25); R^2 = 0.96)				Riverside (O_3 = 0.128 (0.17); R^2 = 0.95)			
Parameter	COV	Reg. Coef.	UC (%)	Parameter	COV	Reg. Coef.	UC (%)
EMCO	0.25	0.46	21.4	EMCO	0.25	0.47	22.5
HO + NO2	0.27	-0.39	15.1	NO2 + hv	0.18	0.45	20.6
NO2 + hv	0.18	0.33	10.7	HO+NO2	0.27	-0.34	11.3
DPO3	0.29	-0.28	8.1	DPO3	0.29	-0.30	9.0
HCHO + hv	0.34	0.20	4.2	RCO-O2+NO	0.75	0.25	6.2
CCO-O2+NO	0.34	0.20	4.1	CCO-O2+NO	0.34	0.20	4.1
RCO-O2+NO	0.75	0.20	4.0	PAN	0.4	0.20	4.1
PAN	0.4	0.18	3.4	O3 + NO	0.1	-0.18	3.2

[1]COV is the coefficient of variation (standard deviation divided by the nominal value) of the parameter.

[2]Reg. Coef. is the standardized regression coefficient, which indicates the influence of the parameter on the output variable.

[3]UC is the uncertainty contribution, which is defined as the percentage contribution of uncertainty in the parameter to the variance in the output variable.

Figure 4.1 shows absolute incremental reactivities (AIRs) for eight compounds and the base mixture, calculated from the ozone concentrations at the endpoints of the four trajectories. The average values from the Monte Carlo simulations are shown, with the standard deviations in the Monte Carlo results indicated by error bars. For HCHO, N-C4, PRPE, XYLM and the base mixture, the incremental reactivities are lowest for the Riverside trajectory, while those for ETOH and MEK are lowest for the Anaheim trajectory. The coefficients of variation for the eight compounds and base mixture range from 0.16 for XYLM at Anaheim to 0.63 for HCHO at Riverside, with most of the values falling in the range of 0.3 to 0.4. The uncertainty in the absolute incremental reactivities is generally highest at Riverside.

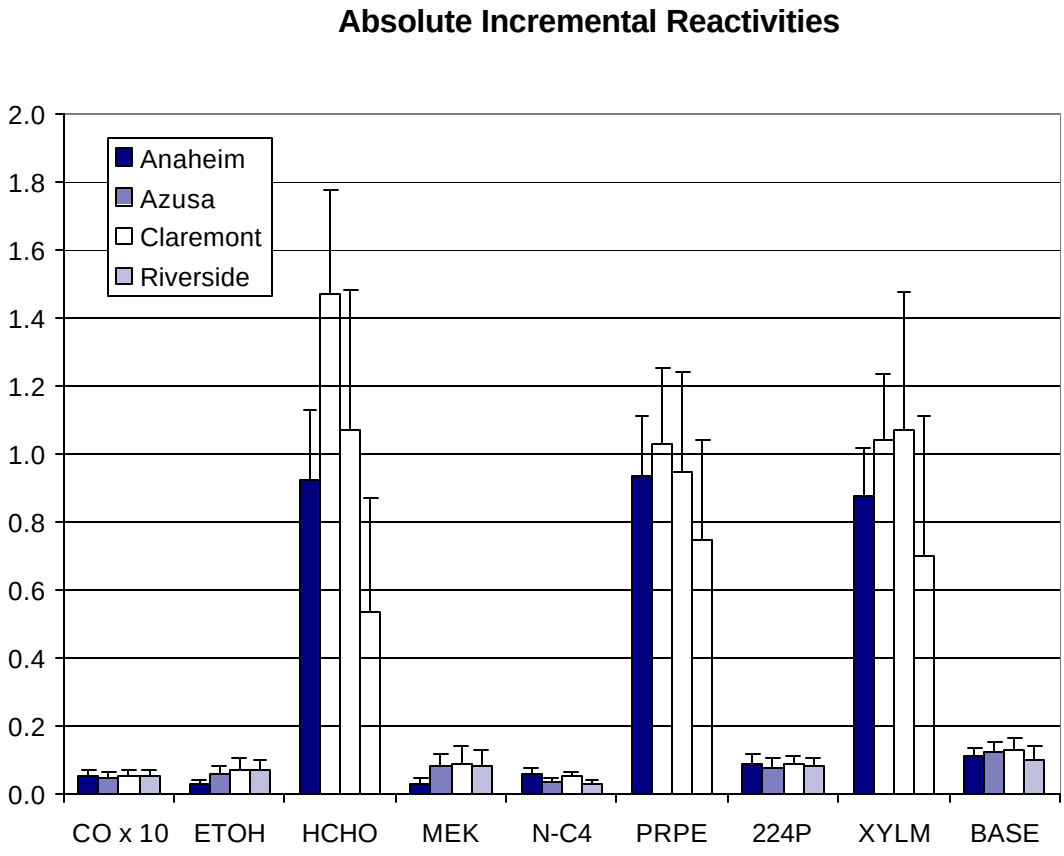

Figure 4.1. Absolute incremental reactivities and associated uncertainties for selected compounds and the base mixture.

Relative incremental reactivities for the eight compounds, normalized by the incremental reactivities of the base mixture, are shown in Figure 4.2. Accounting for uncertainties in the inputs for a given trajectory, COVs for the RIRs range from 0.08 for PRPE at Anaheim and Azusa to 0.49 for CO at Riverside. Coefficients of variation for most of the RIRs range from 0.2 to 0.35. With a few exceptions, uncertainties in the RIRs are lower than those in the AIRs. In general, normalizing the reactivities also reduces variability across locations. Comparing Figures 4.1 and 4.2, the average RIRs of all of the compounds except CO and ETOH are less variable across trajectories than the average AIRs.

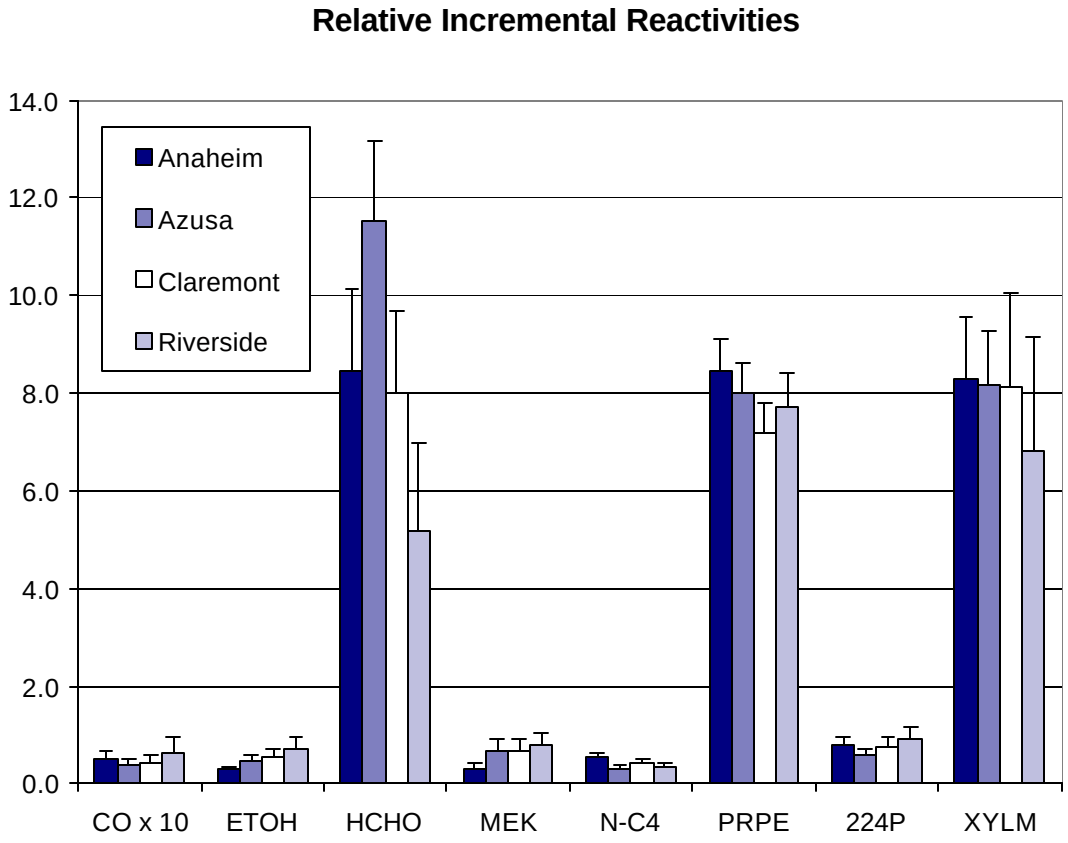

Figure 4.2. Relative incremental reactivities and associated uncertainties for selected compounds.

Table 4.4 shows the eight uncertain input parameters with the greatest influence on uncertainty in the absolute incremental reactivity estimates for the base mixture, as calculated for each of the trajectory endpoints. A total of 16 parameters are included in the top eight for one or more of the trajectories. Six of them: the rate parameters for NO2 + hv, HCHO + hv, O3 + hv, HO + NO2 and PAN decomposition, and the emissions rates for non-mobile NO_x emissions, appear in the top eight for three locations. The standardized regression coefficients shown in the table indicate the sign of the response of the mixture incremental reactivity to an increase in the value of each parameter. These signs differ across the trajectories for parameters that control the amount of NO_x or radicals in the air parcel. For the Claremont and Riverside trajectories, the incremental reactivity of the mixture increases with increased NO_x emissions or a reduced NO_2 deposition rate. For the Azusa trajectory, the sensitivity of the mixture AIR to increased NO_x emissions or reduced NO_2 deposition is negative, whereas the mixture AIR for the Anaheim trajectory is insensitive to these parameters. The incremental reactivity of the base mixture for the Riverside trajectory displays negative sensitivity to parameters that would increase the supply of radicals (e.g., O_3 + hv, HCHO + hv) while the opposite is true for Anaheim and Azusa.

Motor vehicle emissions and associated uncertainty estimates were defined using results of previous research (Harley et al., 1997; Bergin et al., 1999). CO emissions were based on fuel sales and an on-road infrared remote sensing study of vehicle emissions conducted in southern California shortly after the 1987 SCAQS field experiment. Ratios of NMOC/CO and NO_x/CO in vehicle emissions were calculated via regression analysis of ambient pollutant concentrations measured during SCAQS for morning commuter peak periods (see Harley et al., 1997). NMOC and NOx emissions were computed as the product of absolute CO emissions and the appropriate ambient concentration ratio described above. These estimates of vehicle emissions were used to scale gridded motor vehicle emission inventory data provided by ARB.

In this study, EMCO represents the uncertainty common to motor vehicle emissions of all pollutants (i.e., CO, NMOC and NO_x), and was estimated from site-to-site variability in on-road remote sensing measurements for CO emissions. This uncertainty applies not only to CO, but also to the other pollutants, because NMOC and NO_x emissions were estimated as the product of CO emissions and ambient pollutant ratios. Additional, independent uncertainties in NMOC and

NO_x emissions from motor vehicles are represented by the parameters EMHC and EMNX. These additional uncertainties, which are relatively small, arise from the uncertainties in the regression analysis of ambient concentrations of NMOC and NO_x versus CO.

As shown in Tables 4.3 and 4.4, standardized regression coefficients for EONX (uncertainty in NO_x emissions from other sources) are higher than those for EMNX (independent uncertainty in motor vehicle NO_x emissions) indicating that EONX contributes more to the uncertainty in ozone concentrations and base mixture reactivities. This is primarily because EONX is larger than EMNX (see Table 4.2), while NO_x emissions from on-road motor vehicles and other sources in the SoCAB are similar in magnitude (Table 3.1). As mentioned above, EMNX represents only part of the uncertainty in NO_x emissions from motor vehicles. The larger part of the uncertainty is represented by the parameter EMCO, which applies equally to NO_x, NMOC and CO emissions. Although ozone concentrations are sensitive to the common uncertainty represented by EMCO, incremental reactivities tend to be less affected when emissions of all three pollutants increase or decrease together than when NO_x or NMOC emissions are changed independently.

The comparison between motor vehicle and other emissions of NMOC is somewhat different than the parallel comparison for NO_x. For NMOC, motor vehicle emissions are relatively large compared to those from other anthropogenic sources (Table 3.1). Moreover, NMOC emissions from motor vehicles tend to be more reactive than those from other anthropogenic sources. For these two reasons, ozone concentrations and base mixture reactivities are more sensitive to changes in motor vehicle emissions of NMOC than to equal percentage changes in other anthropogenic NMOC emissions. Due to this difference in sensitivities, the relatively small independent uncertainty in motor vehicle NMOC emissions (EMHC) is more influential than the larger uncertainty in other NMOC emissions (EOHC) for some trajectories and output variables.

Regression results for relative incremental reactivities of individual compounds are shown in Table 4.5. Representative results from this table are discussed below, beginning with those for the less reactive compounds such as N-C4.

Table 4.4 Absolute incremental reactivities of the base mixture (mass basis) and regression results indicating the model parameters that contribute most to their uncertainties. COV is the coefficient of variation. Reg. Coef. is the standardized regression coefficient. UC is the uncertainty contribution.

Anaheim (AIR = 0.11 (0.18); R^2 = 0.92)				Azusa (AIR = 0.13 (0.20); R^2 = 0.85)			
Parameter	COV	Reg. Coef.	UC (%)	Parameter	COV	Reg. Coef.	UC (%)
NO2 + hv	0.18	0.48	22.8	HCHO + hv	0.34	0.45	20.1
HCHO + hv	0.34	0.43	18.5	CCO-O2+NO	0.34	0.36	12.7
DPO3	0.29	-0.33	10.6	NO2 + hv	0.18	0.33	10.9
CCO-O2+NO	0.34	0.29	8.5	PAN	0.4	0.26	6.6
O3 + hv	0.27	0.27	7.2	EONX	0.15	-0.21	4.4
PAN	0.40	0.20	3.8	HO + NO2	0.27	-0.20	3.9
HO + NO2	0.27	-0.19	3.6	RCO-O2+NO	0.75	0.19	3.4
HO2 + NO	0.18	0.18	3.4	O3 + hv	0.27	0.18	3.1
Claremont (AIR = 0.13 (0.29); R^2 = 0.78)				Riverside (AIR = 0.10 (0.39); R^2 = 0.95)			
Parameter	COV	Reg. Coef.	UC (%)	Parameter	COV	Reg. Coef.	UC (%)
HO + NO2	0.27	0.41	16.8	EONX	0.15	0.58	33.7
DPN2	0.29	-0.32	10.3	EOHC	0.29	-0.43	18.2
EONX	0.15	0.31	9.8	DPN2	0.29	-0.41	16.6
EMHC	0.06	-0.23	5.5	O3 + hv	0.27	-0.40	16.4
NO2 + hv	0.18	0.23	5.5	O1D2 + H2O	0.18	-0.24	5.5
EMCO	0.25	-0.22	4.8	O1D2 + M	0.18	0.23	5.1
EOHC	0.29	-0.20	4.1	HCHO+hv	0.34	-0.19	3.5
PAN	0.40	0.20	3.8	EMHC	0.06	-0.18	3.4

Table 4.5 Relative incremental reactivities of selected compounds and regression results indicating the model parameters that contribute most to their uncertainties. COV is the coefficient of variation. Reg. Coef. is the standardized regression coefficient. UC is the uncertainty contribution.

Anaheim				Azusa			
Parameter	COV	Reg. Coef.	UC (%)	Parameter	COV	Reg. Coef.	UC (%)
CO (RIR = 0.05 (0.29); R^2=0.98)				CO (RIR = 0.04 (0.31); R^2 = 0.97)			
HO + CO	0.27	0.93	86.5	HO + CO	0.27	0.86	73.8
HO + NO2	0.27	-0.25	6.2	HO + NO2	0.27	-0.36	12.8
O3 + hv	0.27	0.21	4.5	DCB2,XYLM	0.30	-0.19	3.5
HCHO+hv	0.34	-0.19	3.6	EONX	0.15	-0.16	2.6
N-C4 + HO	0.18	-0.17	2.7	XYLM + HO	0.20	-0.16	2.4
O1D2 + H2O	0.18	0.14	2.1	EOHC	0.29	0.15	2.4
O1D2 + M	0.18	-0.12	1.3	O3 + hv	0.27	0.14	2.1
224P + HO	0.18	-0.10	1.1	DCB3,XYLM	0.30	-0.13	1.7
ETOH (RIR = 0.29 (0.25); R^2 = 0.96)				ETOH (RIR = 0.48 (0.22); R^2 = 0.94)			
ETOH + HO	0.18	0.51	26.5	ETOH + HO	0.18	0.70	49.6
CCO-O2 + NO	0.34	0.34	11.9	CCO-O2 + NO	0.34	0.39	15.2
PAN	0.40	0.19	3.7	PAN	0.40	0.24	5.9
RCO-O2 + NO	0.75	-0.19	3.5	RCO-O2 + NO	0.75	-0.18	3.3
N-C4 + HO	0.18	-0.15	2.3	NO2 + hv	0.18	0.16	2.5
NO2 + hv	0.18	0.14	1.9	EMCO	0.25	-0.14	2.1
EMCO	0.25	-0.13	1.7	CCO-O2 + NO2	0.16	-0.13	1.7
CCO-O2 + NO2	0.16	-0.12	1.5	N-C4 + HO	0.18	-0.13	1.6
HCHO (RIR = 8.45 (0.20); R^2 = 0.97)				HCHO (RIR = 11.54 (0.14); R^2 = 0.95)			
HCHO + hv	0.34	0.52	27.5	HO + NO2	0.27	0.52	26.8
O3 + hv	0.27	-0.45	20.5	HCHO + hv	0.34	0.46	20.9
EMCO	0.25	0.33	11.0	NO2 + hv	0.18	-0.36	12.8
O1D2 + M	0.18	0.30	8.8	MEK + hv	0.42	-0.27	7.5
NO2 + hv	0.18	-0.29	8.3	CCO-O2 + NO	0.34	-0.23	5.3
HO + NO2	0.27	0.28	8.0	O3 + hv	0.27	-0.21	4.2
CCO-O2 + NO	0.34	-0.24	5.6	224P + HO	0.18	-0.20	4.2
PAN	0.40	-0.23	5.3	O3 + NO	0.10	0.20	4.1

MEK (RIR = 0.30 (0.35); R^2 = 0.97)

MEK + hv	0.42	0.85	71.6
HO + NO2	0.27	0.26	7.0
HCHO + hv	0.34	-0.24	5.5
O3 + hv	0.27	-0.18	3.4
CCO-O2 + NO	0.34	0.18	3.2
O1D2 + H2O	0.18	-0.14	1.9
DPO3	0.29	0.13	1.6
224P + HO	0.18	-0.11	1.2

MEK (RIR = 0.67 (0.35); R^2 = 0.98)

MEK + hv	0.42	0.87	75.0
HCHO + hv	0.34	-0.37	13.4
HO + NO2	0.27	0.33	10.9
EONX	0.15	0.14	2.1
EMCO	0.25	-0.10	0.9
DCB2,XYLM	0.30	-0.09	0.8
XYLM + HO	0.20	-0.08	0.7
224P + HO	0.18	-0.08	0.7

N-C4 (RIR = 0.53 (0.18); R^2 = 0.98)

N-C4 + HO	0.18	0.70	48.7
O3 + hv	0.27	0.34	11.3
EMCO	0.25	-0.24	6.0
HCHO + hv	0.34	-0.24	5.8
HO + NO2	0.27	-0.21	4.3
O1D2 + M	0.18	-0.20	4.1
O1D2 + H2O	0.18	0.20	3.8
NO2 + hv	0.18	0.15	2.2

N-C4 (RIR = 0.31 (0.20); R^2 = 0.96)

N-C4 + HO	0.18	0.77	59.2
HO + NO2	0.27	-0.38	14.7
O3 + hv	0.27	0.21	4.6
NO2 + hv	0.18	0.16	2.5
HCHO + hv	0.34	-0.15	2.1
ARO2 + HO	0.27	0.14	2.0
CCO-O2 + NO	0.34	0.13	1.6
O1D2 + H2O	0.18	0.11	1.3

PRPE (RIR = 8.45 (0.08); R^2 = 0.92)

PRPE + HO	0.14	0.52	27.0
224P + HO	0.18	-0.44	19.2
N-C4 + HO	0.18	-0.39	15.3
RCO-O2 + NO	0.75	-0.28	8.0
O3 + hv	0.27	-0.26	6.6
MEK + hv	0.42	-0.20	3.9
O1D2 + M	0.18	0.19	3.7
CCO-O2 + NO	0.34	0.17	3.0

PRPE (RIR = 7.99 (0.08); R^2 = 0.94)

PRPE + HO	0.14	0.62	38.1
MEK + hv	0.42	-0.42	18.0
224P + HO	0.18	-0.34	11.8
N-C4 + HO	0.18	-0.21	4.3
HCHO + hv	0.34	0.18	3.3
ETOH + HO	0.18	-0.18	3.2
DCB2,XYLM	0.30	-0.15	2.3
XYLM + HO	0.20	-0.13	1.7

224P (RIR = 0.80 (0.18); R^2 = 0.96)

224P + HO	0.18	0.69	47.5
HO + NO2	0.27	-0.38	14.5
O3 + hv	0.27	0.31	9.6
RCO-O2 + NO	0.75	0.21	4.4
O1D2 + M	0.18	-0.19	3.7
O1D2 + H2O	0.18	0.18	3.3
HCHO + hv	0.34	0.16	2.5
N-C4 + HO	0.18	-0.16	2.4

224P (RIR = 0.60 (0.22); R^2 = 0.95)

224P + HO	0.18	0.63	39.6
HO + NO2	0.27	-0.56	31.0
HCHO + hv	0.34	0.37	13.9
EONX	0.15	-0.19	3.8
O3 + hv	0.27	0.17	2.8
EOHC	0.29	0.16	2.4
RCO-O2 + NO	0.75	0.13	1.8
NO2 + hv	0.18	0.13	1.8

XYLM (RIR = 8.30 (0.15); R^2 = 0.95)			
HCHO + hv	0.34	-0.53	27.6
DCB2,XYLM	0.3	0.42	17.7
XYLM + HO	0.2	0.37	13.8
HO + NO2	0.27	0.30	8.9
224P + HO	0.18	-0.24	5.9
N-C4 + HO	0.18	-0.21	4.6
O3 + hv	0.27	-0.20	3.9
EMCO	0.25	0.20	3.8

XYLM (RIR = 8.15 (0.14); R^2 = 0.93)			
HCHO + hv	0.34	-0.63	39.1
DCB2,XYLM	0.30	0.46	21.3
XYLM + HO	0.20	0.44	19.8
MEK + hv	0.42	-0.24	5.8
HO + NO2	0.27	0.17	3.0
224P + HO	0.18	-0.16	2.7
N-C4 + HO	0.18	-0.15	2.2
ETOH + HO	0.18	-0.12	1.4

Claremont			
Parameter	COV	Reg. Coef.	UC (%)
CO (RIR = 0.04 (0.40); R^2 = 0.85)			
HO + CO	0.27	0.62	38.9
HO + NO2	0.27	-0.58	33.2
O3 + hv	0.27	0.26	6.6
DPN2	0.29	0.21	4.6
EOHC	0.29	0.20	4.0
EONX	0.15	-0.20	3.9
O1D2 + H2O	0.18	0.19	3.8
EMCO	0.25	0.17	2.9
ETOH (RIR = 0.55 (0.28); R^2 = 0.88)			
ETOH + HO	0.18	0.54	28.7
CCO-O2 + NO	0.34	0.44	19.7
PAN	0.40	0.33	10.6
RCO-O2 + NO	0.75	-0.24	5.8
EMCO	0.25	-0.19	3.8
CCO-O2 + NO2	0.16	-0.17	3.0
N-C4 + HO	0.18	-0.16	2.6
NO2 + hv	0.18	0.13	1.7

Riverside			
Parameter	COV	Reg. Coef.	UC (%)
CO (RIR = 0.065 (0.49); R^2 = 0.83)			
HO + CO	0.27	0.52	27.5
O3 + hv	0.27	0.39	15.5
O1D2 + H2O	0.18	0.33	11.1
HO + NO2	0.27	-0.26	6.8
EOHC	0.29	0.26	6.7
EONX	0.15	-0.25	6.4
O1D2 + M	0.18	-0.24	5.6
DPN2	0.29	0.20	4.0
ETOH (RIR = 0.73 (0.34); R^2 = 0.89)			
ETOH + HO	0.18	0.43	18.8
PAN	0.40	0.41	17.1
CCO-O2 + NO	0.34	0.40	16.0
RCO-O2 + NO	0.75	-0.34	11.3
O3 + hv	0.27	0.24	5.8
PAN2	0.66	-0.23	5.3
NO2 + hv	0.18	0.23	5.1
HCHO + hv	0.34	0.17	2.9

HCHO (RIR = 8.01 (0.21); R^2 = 0.91)

HO + NO2	0.27	0.66	44.2
O3 + hv	0.27	-0.34	11.3
NO2 + hv	0.18	-0.31	9.4
EONX	0.15	0.24	5.8
PAN	0.40	-0.24	5.7
CCO-O2 + NO	0.34	-0.23	5.2
224P + HO	0.18	-0.22	4.8
MEK + hv	0.42	-0.20	4.2

HCHO (RIR = 5.18 (0.35); R^2 = 0.91)

O3 + hv	0.27	-0.54	29.2
EONX	0.15	0.33	11.0
O1D2 + M	0.18	0.30	8.9
O1D2 + H2O	0.18	-0.27	7.5
NO2 + hv	0.18	-0.26	6.8
HO + NO2	0.27	0.24	5.6
EOHC	0.29	-0.21	4.4
PAN	0.40	-0.20	4.1

MEK (RIR = 0.66 (0.37); R^2 = 0.96)

MEK + hv	0.42	0.73	53.9
HO + NO2	0.27	0.47	22.0
HCHO + hv	0.34	-0.36	12.7
DPN2	0.29	-0.18	3.2
O3 + hv	0.27	-0.16	2.7
XYLM + HO	0.20	-0.15	2.4
EONX	0.15	0.15	2.2
DCB2,XYLM	0.30	-0.15	2.2

MEK (RIR = .80 (0.32); R^2 = 0.94)

MEK + hv	0.42	0.67	44.8
HO + NO2	0.27	0.38	14.8
O3 + hv	0.27	-0.26	6.6
HCHO + hv	0.34	-0.25	6.3
O1D2 + H2O	0.18	-0.21	4.3
DPN2	0.29	-0.19	3.8
EMCO	0.25	-0.19	3.5
O1D2 + M	0.18	0.17	2.9

N-C4 (RIR = 0.42 (0.26); R^2 = 0.84)

HO + NO2	0.27	-0.65	42.3
N-C4 + HO	0.18	0.50	25.3
EOHC	0.29	0.33	11.0
O3 + hv	0.27	0.31	9.6
O1D2 + H2O	0.18	0.21	4.4
HCHO + hv	0.34	0.17	3.0
DPN2	0.29	0.17	2.9
O1D2 + M	0.18	-0.15	2.3

N-C4 (RIR = 0.33 (0.24); R^2 = 0.92)

O3 + hv	0.27	0.51	25.6
N-C4 + HO	0.18	0.46	20.7
HO + NO2	0.27	-0.36	13.3
O1D2 + H2O	0.18	0.33	11.1
EONX	0.15	-0.24	5.7
O1D2 + M	0.18	-0.23	5.3
EMCO	0.25	0.20	3.8
DPN2	0.29	0.18	3.4

PRPE (RIR = 7.17 (0.09); R^2 = 0.81)

EMCO	0.25	-0.43	18.1
224P + HO	0.18	-0.40	15.6
MEK + hv	0.42	-0.38	14.1
PRPE + HO	0.14	0.37	13.5
EOHC	0.29	0.32	10.1
HO + NO2	0.27	0.30	8.7
O3 + hv	0.27	-0.29	8.2
N-C4 + HO	0.18	-0.25	6.4

PRPE (RIR = 7.73 (0.09); R^2 = 0.90)

MEK + hv	0.42	-0.43	18.6
PRPE + HO	0.14	0.39	15.2
224P + HO	0.18	-0.35	12.4
PAN2	0.66	-0.28	8.0
RCO-O2 + NO	0.75	-0.28	8.0
O3 + hv	0.27	-0.26	6.9
ETOH + HO	0.18	-0.24	5.9
HCHO + hv	0.34	0.20	4.2

224P (RIR = 0.74 (0.29); R^2 = 0.87)				224P (RIR = 0.91 (0.27); R^2 = 0.86)			
HO + NO2	0.27	-0.63	39.2	224P + HO	0.18	0.39	15.4
224P + HO	0.18	0.44	19.2	O3 + hv	0.27	0.35	12.4
HCHO + hv	0.34	0.36	13.1	HO + NO2	0.27	-0.27	7.4
EOHC	0.29	0.30	9.2	O1D2 + H2O	0.18	0.26	6.8
O3 + hv	0.27	0.24	5.7	EMCO	0.25	0.25	6.1
DPN2	0.29	0.21	4.5	PAN	0.40	-0.23	5.4
O1D2 + H2O	0.18	0.20	4.1	O1D2 + M	0.18	-0.22	5.0
EONX	0.15	-0.18	3.2	CCO-O2 + NO	0.34	-0.22	4.8
XYLM (RIR = 8.11 (0.24); R^2 = 0.86)				XYLM (RIR = 6.82 (0.34); R^2 = 0.91)			
HCHO + hv	0.34	-0.52	27.3	O3 + hv	0.27	-0.43	18.2
HO + NO2	0.27	0.49	24.0	HCHO + hv	0.34	-0.39	15.1
DCB2,XYLM	0.30	0.24	5.8	HO + NO2	0.27	0.35	12.5
O3 + hv	0.27	-0.22	4.8	DCB2,XYLM	0.30	0.30	9.1
O1D2 + H2O	0.18	-0.17	3.0	O1D2 + H2O	0.18	-0.28	8.0
224P + HO	0.18	-0.17	3.0	O1D2 + M	0.18	0.23	5.4
MEK + hv	0.42	-0.15	2.3	DPN2	0.29	-0.19	3.6
XYLM + HO	0.20	0.13	1.6	224P + HO	0.18	-0.19	3.5

For all four trajectories, the RIR of n-butane (N-C4) is sensitive to the rate constant for its reaction with HO, and to parameters that control the availability of HO radicals. Regression results for the CO and 2,2,4-trimethylpentane (224P) RIRs are similar, showing high positive sensitivity to their HO reaction rates and to reaction rates for O3 + hv and O1D + H2O, and negative sensitivity to reaction rates for HO + NO2, and O1D + M. As shown in Table 4.5, the regression results for the ethanol (ETOH) RIR are somewhat different from those of other slowly reacting compounds, due to the influence of uncertainties in PAN chemistry. Results for the ETOH RIR are relatively consistent across trajectories. In contrast to those compounds that react only with OH, the primary oxidation pathway for MEK is its photolysis reaction. At all four locations, the RIR for MEK is most sensitive to the rate of this reaction. In contrast to the low-reactivity compounds that are oxidized by HO, the RIR for MEK is also strongly negatively influenced by parameters that increase the rate of HO production or reduce its consumption rate (e.g., HO + NO2).

In general, the RIR for HCHO is sensitive to parameters that affect other sources and sinks of radicals, e.g., O3 + hv, and displays negative sensitivity to parameters that increase the absolute incremental reactivity of other components of the base mixture, including the rate constants for NO2 + hv and CCO-O2 + NO. Uncertainty in the HCHO photolysis rate is highly influential for the HCHO RIR for the Anaheim and Azusa trajectories but not for the relatively NO_x-limited trajectories ending at Claremont and Riverside. The results shown in Table 4.5 for m-xylene (XYLM) are typical of those for other rapidly reacting compounds, such as propene (PRPE), which react primarily with HO. Parameters of the XYLM reaction mechanism that directly affect its absolute reactivity, such as the rate constant for its reaction with HO and its DCB2 yield, are influential. Otherwise, the XYLM RIR shows strong negative sensitivity to parameters that increase the reactivity of other compounds in the base mixture, including the rate constants for their primary oxidation reaction steps and rates of reactions that produce hydroxyl or peroxy radicals. Although the order changes, the set of parameters that are most influential for XYLM is relatively consistent across trajectories.

RIRs for several compounds show relatively high sensitivity to uncertainty in emissions rates. The responses are mixed, with the sign of the RIR sensitivities determined by whether the absolute incremental reactivity of the compound is more or less sensitive to the emissions parameter than the incremental reactivity of the base mixture is. For example, at Claremont and Riverside, the incremental reactivity of the base mixture displays positive sensitivity to the non-motor vehicle NO_x emissions (EONX) parameter, as do the absolute incremental reactivities of HCHO and CO. However, AIRs of CO and HCHO respectively are less and more sensitive to EONX than the AIR of the base mixture. Correspondingly, the sensitivity coefficients for the CO RIR values are negative and those for the HCHO RIR values are positive.

Table 4.6 compares the nominal relative incremental reactivities calculated from trajectory model runs for Azusa and Riverside with RIRs calculated using Maximum Incremental Reactivity values from Carter (2000b). For this comparison, the individual absolute incremental reactivities were normalized by the weighted sum of the reactivities of seven compounds (equation 2.2), as described previously in Section 2.2. The RIRs calculated with the trajectory model agree reasonably well with those calculated from Carter's MIRs. The average absolute

difference between the RIRs for Azusa and those calculated from Carter's MIRs is 38%, and the correlation coefficient between these pairs of values is $\rho = 0.93$. Comparing the Riverside RIRs with Carter's values, the average absolute difference is 31% and the correlation coefficient is 0.95. For the Azusa trajectory, the RIRs of the more reactive compounds such as HCHO and propene tend to be relatively high, compared to relative reactivities calculated from Carter's MIRs. As shown in Figure 4.2, reactivities calculated for the Azusa trajectory for HCHO and PRPE are high compared to those calculated for the other trajectories, as well.

As indicated by the footnotes, emissions of a number of the compounds listed in Table 4.6 come primarily from motor vehicles, whereas for other compounds non-vehicle sources dominate. As illustrated in Figure 4.3 for n-butane emissions, the temporal profiles of emissions from motor vehicles versus other sources can differ significantly. To begin to explore the effect of emissions timing on VOC reactivities, AIRs for four compounds were calculated both from reductions in motor vehicle emissions and separately from reductions in all other anthropogenic sources. The results of these calculations are shown in Table 4.7.

Table 4.6. Comparison of RIRs calculated from nominal trajectory simulations in this study with normalized Maximum Incremental Reactivities (R_MIRs) from Carter (2000b).

Compound	MW	R_MIR	Azusa	Riverside
carbon monoxide	28.0	0.03	0.03[1]	0.06
formaldehyde	30.0	4.50	11.56	5.18
acetaldehyde	44.1	3.43	3.17	3.96
acetone	58.1	0.22	0.18	0.18[2]
methyl ethyl ketone	72.1	0.74	0.66[2]	0.82[2]
methane	16.0	0.01	0.01	0.00[2]
ethene	28.1	4.55	6.26[1]	7.23[1]
isoprene	68.1	5.36	6.39	8.00[2]
acetylene	26.0	0.63	0.57[1]	0.83[1]
ethane	30.1	0.16	0.06	0.08[2]
n-butane	58.1	0.67	0.30	0.33[2]
propene	42.1	5.81	7.95[1]	7.75[1]
α-pinene	136.2	2.15	2.47[2]	0.61[2]
benzene	78.1	0.41	0.28	0.35
toluene	92.1	1.99	2.12	1.80
m-xylene	106.2	5.32	8.31	6.84
p-xylene	106.2	2.13	2.36	2.17
1,2,4-trimethylbenzene	120.2	3.60	5.01[1]	4.17[1]
2,2,4-trimethylpentane	114.2	0.72	0.60[1]	0.95
2-methyl-2-butene	70.1	7.24	14.83[1]	6.50
n-butyl acetate	116.2	0.45	0.55[2]	0.43[2]
methylcyclopentane	84.2	1.21	0.46[1]	1.37[1]
isopentane	72.1	0.84	0.51[1]	0.67[1]
n-pentane	72.1	0.77	0.33	0.41
1,3-butadiene	54.0	6.81	7.85[1]	5.88[1]
ethanol	46.1	0.85	0.48[2]	0.72[2]
isopropanol	60.1	0.36	0.14[2]	0.24[2]

[1] More than 80% of emissions are from motor vehicles. [2] More than 80% of emissions are from other sources.

Table 4.7. Comparison of absolute incremental reactivities (mass basis) calculated by perturbing motor vehicle versus other anthropogenic emissions, or by perturbing both by the same fraction.

	Anaheim			Azusa		
Compound	MV	Other	Combined	MV	Other	Combined
CO	0.0059	0.0041	0.0057	0.0048	0.0048	0.0048
HCHO	1.05	0.63	0.97	1.73	1.39	1.63
N-C4	0.06	0.077	0.064	0.047	0.038	0.042
XYLM	1.03	0.65	0.96	1.25	1.00	1.17
	Claremont			Riverside		
CO	0.0055	0.006	0.0056	0.0053	0.0053	0.0053
HCHO	1.10	1.01	1.08	0.51	0.38	0.45
N-C4	0.055	0.056	0.055	0.056	0.024	0.029
XYLM	1.05	1.26	1.10	0.56	0.66	0.59

AIR estimates calculated by perturbing non-motor vehicle sources range from over 50% lower to about 30% higher than those calculated by adjusting motor vehicle emissions. AIRs calculated using motor vehicle versus non-motor vehicle emissions for CO at Azusa, Claremont and Riverside and for HCHO and N-C4 at Claremont show less than a 10% difference. The incremental reactivities for HCHO are higher in each case when estimated from motor vehicle emissions perturbations than other emissions. For the other compounds, which estimate is highest depends on the trajectory. For the four compounds examined, differences in AIRs calculated using motor vehicle versus non-motor vehicle emissions appear comparable to the variability in AIRs across trajectories. For AIRs, this degree of variability is comparable to the uncertainty due to model inputs and parameters.

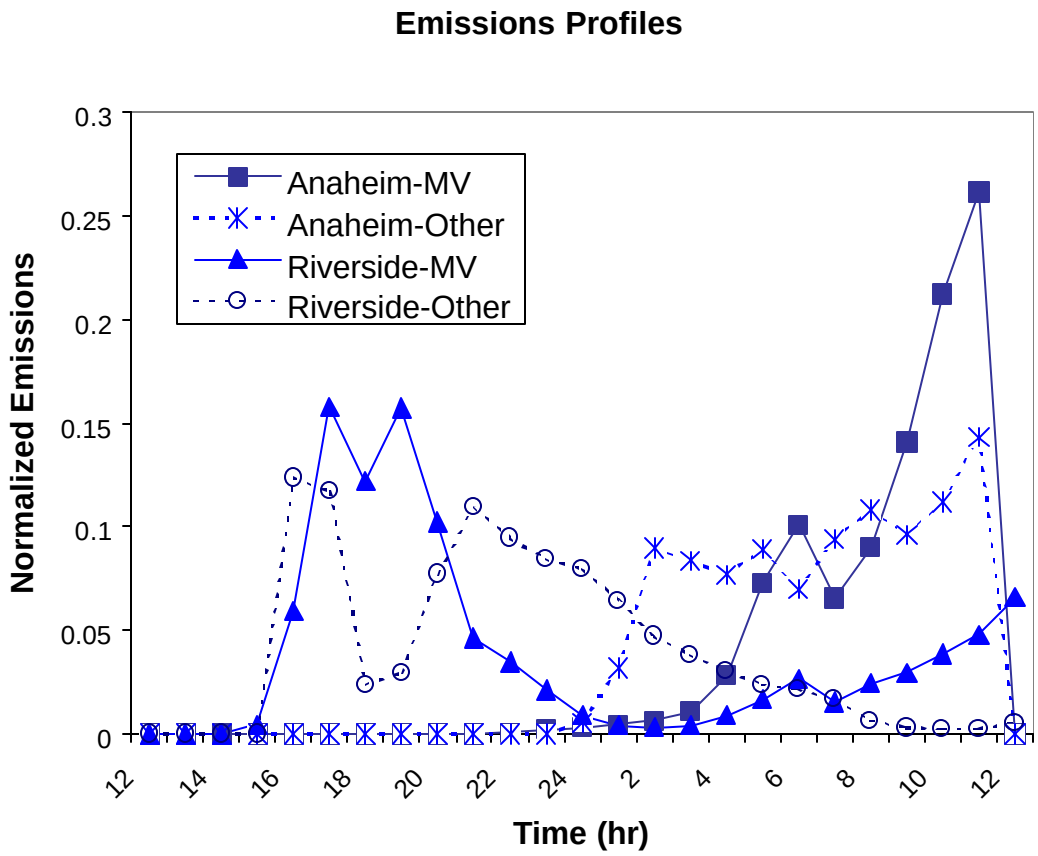

Figure 4.3. Emissions profiles for n-butane from motor vehicle and other sources along the Anaheim and Riverside trajectories. Profiles are normalized to total emissions from the source category. Values are shown starting at noon on June 24 although the trajectory simulations actually start 12 hours earlier.

4.5 Discussion

Calculated incremental reactivities for organic compounds are subject to both variability due to environmental conditions, including the magnitude and timing of emissions, and uncertainty due to model inputs and parameter values. Illustrating variability due to environmental conditions, relative incremental reactivities calculated for a realistic trajectory ending at Azusa on 25 June 1987 differ from relative values of maximum incremental reactivities calculated by Carter (2000), by 38%, on average. RIRs calculated for a trajectory ending at Riverside differ by 31%, on average, from Carter's R_MIRs. For the eight compounds that were studied in detail, the coefficients of variation across trajectories in the average absolute incremental reactivities range from 8% for CO and 224P to 37% for MEK and 39% for HCHO (Figure 4.1). The coefficients of variation in the relative incremental reactivities across trajectories range from 7% for PRPE to 35% for both ETOH and MEK.

Overall uncertainties of the absolute incremental reactivities of the base mixture ranged from 18% for the AIR calculated for the Anaheim trajectory to 39% for the AIR of the Riverside trajectory. Photolysis rates for NO_2, HCHO, and O_3, rate constants for HO + NO_2 and PAN decomposition and the non-mobile NO_x emissions rate are among the influential parameters. However, the AIRs calculated for different trajectories respond somewhat differently to uncertainties in model inputs and parameters, depending on whether the ozone concentrations at the trajectory endpoint are limited by the availability of NO_x or radicals.

Uncertainties in the RIRs of the eight compounds studied in detail range from 8% for PRPE at Anaheim and Azusa to 49% for CO at Riverside. Uncertainties in the RIRs are generally lower than those in the AIRs. The largest contributors to uncertainty in the RIRs include rate parameters for the primary oxidation pathway of the compound. For relatively slowly reacting compounds that react primarily with OH, parameters that control the abundance of the radical are also influential. The RIRs of the more reactive compounds show negative sensitivity to parameters that increase the reactivity of other compounds in the base mixture.

The results of this study suggest that for a single pollution episode, the variability in incremental reactivity estimates across trajectories within the South Coast Air Basin is comparable in magnitude to the uncertainty in the values that is attributable to chemical and deposition parameters and emissions inputs. A distinction that is often made between variability and uncertainty is that the former is irreducible, for a given metric, whereas the latter may be reduced through research. This study supports previous research (Russell et al., 1995; Yang and Milford, 1996) that suggests that using relative values rather than absolute values as a reactivity metric can reduce, though not eliminate, both variability and uncertainty.

The next chapter describes results of incremental reactivity modeling for Central California. The propagation of input data uncertainties through the model described here for the SoCAB is not repeated for Central California. Instead, a variety of reactivity metrics are considered and presented, providing a complementary analysis to that presented for the SoCAB.

5. Regional Reactivity Assessment in Central California

5.1 Introduction

Tropospheric ozone is a secondary pollutant whose precursors are oxides of nitrogen (NOx) and Volatile Organic Compounds (VOCs). Consequently, all ozone control measures rely on reducing emissions of one (or both) of these precursor classes. VOC controls are traditionally based on the total mass of organic compounds, not taking into account the unique characteristics of each individual species. However, individual VOCs behave differently in the atmosphere, and have differing ozone formation potentials. Therefore the concept of organic reactivity has been introduced to quantify the relative importance of organic compounds in producing ozone.

While a variety of reactivity measures have been proposed, they are usually developed using box model calculations. The physics of the atmosphere (i.e. meteorology), as well as spatial variability in precursor emissions and concentrations are not reflected in conventional box model calculations. Therefore, the applicability of reactivity scales in predicting atmospheric response to VOC control has been a controversial subject with significant policy implications. Three-dimensional air quality models (AQMs), on the other hand, incorporate physical details into their calculations and consider temporal/spatial variability of different species, and are considered to provide more realistic estimates of organic reactivities. Different investigators have used airshed models for reactivity estimation (e.g., McNair et al., 1992, Russell et al., 1995, Bergin et al., 1995). These studies have been mostly, although not solely (Khan et al., 1999), limited to urban modeling and/or brute-force calculations. In this paper, three-dimensional organic reactivities for a regional domain are developed using a direct sensitivity technique.

5.2 Methodology

The Incremental Reactivity (IR) of an organic compound is defined as the amount of ozone produced per unit mass of VOC added to an organic mixture, or:

$$IR_i = \frac{\Delta O_3}{\Delta VOC_i} \qquad (5.1)$$

The Maximum Incremental Reactivity (MIR) (Carter, 1994) is the main box model reactivity scale used in VOC control regulations in California (CARB, 1990). The MIR is calculated as the maximum IR for a given VOC mixture and any amount of NOx addition. MIR conditions are likely to occur in VOC-limited urban air mass, where because of low VOC-to-NOx ratios, the mixture is most sensitive to organic compounds. MIR conditions are of high practical significance because they represent areas of dense human population where ozone exposure is highest. Another box model reactivity scale, Maximum Ozone Incremental Reactivity (MOIR), is defined as the change in the peak ozone concentration for a given VOC mixture. MOIR conditions are likely to happen at higher VOC-to-NOx ratios than MIR, more typical of aged urban air masses. Reactivity scales are instantaneous values, but they can also be averaged over time. In light of the proposed 8-hour ozone standard, 8-hour reactivity scales have been developed (Carter, 2000).

Reactivities by definition are the sensitivity of ozone to individual organic compounds, and therefore, different sensitivity analysis techniques can be applied for their assessment. Reactivity scales can be written as:

$$MIR_i = \max\left(\frac{\partial O_3}{\partial VOC_i}\right) \qquad (5.2)$$

and,

$$MOIR_i = \frac{\partial O_3}{\partial VOC_i}\Big|_{\max(O_3)} \qquad (5.3)$$

Box model reactivity scales are traditionally calculated by a brute-force approach where the response of ozone to a change in the initial amount of an individual VOC is

estimated. Three-dimensional reactivities have also been estimated by this method, i.e. one-at-a-time perturbation of VOC emissions. The brute-force method is straightforward and easy to implement for few VOCs, but as the number of VOCs increases, the method becomes cumbersome and computationally expensive. More importantly, in brute-force method a large perturbation can change the original characteristics of the mixture, while a small perturbation may result in numerical noise. Disadvantages of the brute-force approach can be avoided by using a direct method, where sensitivity equations are derived from model equations and solved. One such technique is the Direct Decoupled Method (DDM) which integrates sensitivity equations decoupled from concentrations (Dunker, 1984). AQMs usually follow the time evolution of pollutants by solving the Atmospheric Diffusion Equation (ADE):

$$\frac{\partial C_i}{\partial t} = -\nabla(\boldsymbol{u}C_i) + \nabla(\boldsymbol{K}\nabla C_i) + R_i + E_i \qquad (5.4)$$

where **u** is the three-dimensional wind field, and **K** is the turbulent diffusivity tensor. *C*, *E*, and *R* are grid average concentration, emission rate, and chemical reaction rate of species *i*, respectively. The corresponding sensitivity equation can be derived by differentiating ADE with respect to the emissions of VOC_j (Yang et al., 1997):

$$\frac{\partial S_{ij}}{\partial t} = -\nabla(\boldsymbol{u}S_{ij}) + \nabla(\boldsymbol{K}\nabla S_{ij}) + \boldsymbol{J}S_{ij} + E_j\boldsymbol{d}_{ij} \qquad (5.5)$$

where S_{ij} is sensitivity of species i to semi-normalized emission of species j (in this case a VOC). **J** is the Jacobian matrix ($J_{ik} = \partial R_i/\partial C_k$) of the reaction rates, and $\boldsymbol{d}_{ij}$ is the Kronecker delta function. Equation 5.5 is structurally similar to the ADE and can be integrated (for the most part) by the same numerical integration routines, while maintaining the structure of the AQM. DDM sensitivity (reactivity) calculations can be carried out for large number of VOCs in an efficient manner, and computational overhead

for additional VOCs is minimal. It is important to note that unlike concentrations, sensitivity equations, when decoupled from concentrations, are linear and can be solved accordingly.

5.3 Application

Three-dimensional reactivities are evaluated using the Multiscale Air Quality SImulation Platform (MAQSIP) (Odman and Ingram, 1996), which is a state-of-the-science, highly modular AQM, and the prototype for the Community Model for Air Quality (CMAQ) of EPA's Models-3. SARMAP (DaMassa et al., 1996) was chosen as the modeling domain for this study because a comprehensive emission inventory and meteorological modeling results for the domain are available. Additionally, reactivity-based regulations for mobile sources are already in use in California (CARB, 1990) and are being extended to other sources. The modeled episode is August 2-6 (Thursday to Monday), 1990. The first two days are considered to be a ramp-up period, but results for the whole 5-day period are analyzed.

For the purpose of reactivity assessment, few modifications were made to the original version of MAQSIP. These changes include:

- The original chemical mechanisms available in MAQSIP (CB-IV and RADM) were not considered suitable for a detailed reactivity study; therefore, the latest version of the Statewide Air Pollution Research Center (SAPRC-99) chemical mechanism (Carter, 2000) was integrated into the model and additional explicit VOCs were added to the chemistry. The emissions for SAPRC-99 were prepared from an intermediate SAPRC-97 emission inventory. No emissions were assigned to the newly added explicit VOCs, as they were only perturbed in the sensitivity field.
- DDM sensitivity calculations were implemented in MAQSIP, while maintaining its original structure and modularity. DDM implementation was separately tested for CB-IV and SAPRC-99 chemical mechanisms.

- Original western boundary conditions for SARMAP domain were unrealistically high (Sillman et al., 2001). Therefore, a more reasonable set of boundary conditions were used.
- The QSSA chemical solver was substituted by a hybrid solver. QSSA solver was found to give erroneous results, especially in constructing brute-force sensitivity coefficients.
- A mass conservation scheme through the adjustment of vertical wind profiles (Odman et al., 2000) was incorporated in the original advection subroutine to avoid producing artificial sinks and sources.

Table 5.1 gives a summary of the MAQSIP/SAPRC-99 model. Table 5.2 shows a list of 31 organic species and CO that are considered for reactivity assessment and explicitly expressed in the mechanism, along with their MIR and MOIR reactivity scales from box model calculations (for both instantaneous and 8-hour averaging periods).

5.4 Results and Discussion

Figure 5.1 shows a comparison between the ozone simulations of SAPRC-99 and CB-IV versions of MAQSIP, for Sacramento, and peak ozone location. Reasonable agreement between the two mechanisms is observed, while SAPRC-99, shows a more dynamic behavior, tending to predict higher peak and lower minimum ozone concentrations. Table 5.3 shows the performance evaluation summary for the modeling domain. Normalized error is low throughout the simulation period, and the bias is also at a reasonable level with the exception of the last day. It should be noted, however, that much of the lower predicted ozone concentrations can be ascribed to lower (but more reasonable) boundary conditions. The impact of the lower boundary conditions are seen as the bias decreases throughout the modeled period.

DDM sensitivity results were comprehensively tested and compared to various brute-force sensitivity approximations. Figure 5.2 shows snapshots of such comparison for the sensitivity of ozone to a 25% reduction in domain-wide NO emissions. NO sensitivity is chosen as a benchmark because it triggers the most dynamic and spatially varying model

response among the species. In general, DDM results are in very good agreement with different brute-force approximations (also tested for 10% and 50% perturbations). Brute-force results with small perturbations tend to be noisy at times, and larger perturbation is prone to non-linearity problems. Perturbations in the range of 10-30 percent appear to produce stable and close-to-linear brute-force approximations. DDM and brute-force sensitivities to organic emissions are also in very good agreement, as shown in Figure 5.3 for the sensitivity of ozone to a 25% reduction in domain-wide isoprene emissions.

Absolute VOC reactivities are calculated by perturbing the emissions sensitivity field. This perturbation (E_j in equation 5.5) is done equally (on a mass basis) for all the VOCs, by a fraction (α) of the total VOC emissions. For each grid cell:

$$E_j = a \sum_k E_k \qquad (5.6)$$

where index k indicates any VOC with anthropogenic emissions, and E_j is the emission perturbation for species j (in units of *gm VOC / cell – min*). The perturbation, unlike the brute-force method, is insensitive to numerical noise for small values. Due to linearity of the sensitivity equations, the perturbation fraction is chosen arbitrarily. In other words, since the reactivities are only calculated on a relative basis (to each other), any magnitude of perturbation can be applied, as long as it is done equally for all species. Perturbation is only applied to the sensitivity field, and due to the decoupled nature of the method, concentrations remain intact. This method is applied to ensure that three-dimensional reactivity estimation is based on the real spatial and temporal emissions distribution of organic compounds. In addition, since all VOCs are perturbed equally (on a mass basis) their ozone formation potential can be readily compared to each other. This method of perturbation produces the same effect as previous brute-force studies (Bergin et al., 1995), while avoiding the non-linearity problems that are encountered when changing the concentration field.

For this study all VOCs were perturbed by two percent of the total anthropogenic VOC emissions ($\alpha = 0.02$) for each grid cell, and at each simulation hour. As mentioned before, the magnitude of this perturbation is arbitrary, and does not affect the calculation. Figures 5.4, and 5.5 show examples of spatial and temporal variability in absolute reactivities. Spatial snapshots are made at the time of daily maximum photochemical activity, and the time series are chosen to represent two different predominant chemical regimes, i.e. VOC-limited urban air mass and a remote location that is more NOx-limited.

Absolute reactivities show a great deal of temporal and spatial variability, which can only be captured in a physically meaningful way through a three-dimensional modeling approach. As can be seen from the plots, depending on the location, time, and species, absolute reactivities can span a range of few orders of magnitude. Another interesting observation is that formaldehyde may be more or considerably less reactive than m-xylene, depending on the chemical regime. Since the sensitivity perturbation follows the pattern of the total VOC emissions, high VOC reactivities are found in areas (or downwind of areas) where anthropogenic emissions of both VOC and NOx are highest. Figure 5.5 also shows that organic reactivities, as expected, are considerably higher for VOC-limited air masses, where the peak ozone usually occurs.

Carter's reactivity scales are given in units of *gm O_3 / gm VOC*; which is possible since a box model is used. A similar value is not appropriate for three-dimensional reactivities because emissions from the whole domain are being perturbed, and concentrations all over (in three dimensions) are responding. Of interest, however, is how surface level ozone responds to domain-wide perturbation. For practical applications (i.e. development of ozone control strategies), it is the relative magnitude of individual reactivities, as opposed to their absolute values, that are meaningful. Therefore, three –dimensional Relative Incremental Reactivities (RIRs) are defined as:

$$RIR_i = \frac{R_{3D_i}}{R_{Base}} \qquad (5.7)$$

where R_{3D_i} is the absolute reactivity of species *i* (in units of $ppm\ O_3 / gm\ VOC$) calculated from three-dimensional modeling (S_{ij} in equation 5.5), and R_{Base} is the reactivity of a base VOC mixture. On a mass basis, the base mixture is comprised of 2% formaldehyde, 14% MEK, 37% n-butane, 26% 2,2,4-trimethylpentane, 2% propene, 17% ethanol, and 2% m-xylene. The mass fractions are determined such that each compound would contribute equally to the reactivity of the mixture.

Unlike box model calculations, three-dimensional simulations result in a spatial distribution of reactivities. Therefore, a metric (or metrics) can be chosen to compare an ensemble measure from spatial distribution to the box model scales. MIR-3D metric is defined as the instantaneous RIR of each species, at the time and location where the base mixture has its daily maximum reactivity. MOIR-3D is defined as the instantaneous RIR of each species at the time and location of the daily maximum ozone concentration. MIR-$3D_{8hr}$, and MOIR-$3D_{8hr}$ metrics are calculated in the same manner but for 8-hour averaging periods. Incremental population exposure metric is defined as daily population weighted average of reactivities, relative to exposure of the base mixture:

$$PE_i = \frac{\sum_{time}\sum_{cell} IR_i(time, cell) \times P(cell)}{\sum_{time}\sum_{cell} IR_{Base}(time, cell) \times P(cell)} \qquad (5.8)$$

where P is the time-independent population of the modeling grid. This exposure metric is usually calculated for grid cells and times with ozone concentration above a threshold value that is considered harmful to human health.

Relative reactivity metrics of different species are calculated using equation 5.7. Three-dimensional relative maximum incremental reactivity (MIR-3D), and maximum ozone incremental reactivity (MOIR-3D) metrics, as well as those of 8-hour moving averages (MIR-$3D_{8hr}$, and MOIR-$3D_{8hr}$) are then evaluated. Relative daily population exposure metrics are also calculated for an ozone concentration threshold of 80 ppb. This threshold value is chosen to reflect the new national ambient ozone standard. These domain-wide

metrics are shown in Figures 5.6a-5.6e. Given the significant temporal and spatial variability in absolute reactivities, the relative reactivity metrics are reasonably constant. They are also fairly consistent with box model reactivity scales, considering the observed day-to-day variability in those metrics, as well as the uncertainty in box model scales. In general, organic species show a less dynamic behavior in three-dimensional metrics than box model calculations. In other words, all metrics are usually lower than box model values for more reactive species, while they match box model scales for less reactive compounds.

It should be noted that for more reactive species (with important exceptions in isoprene and butadiene) box model reactivity scales tend to be higher than corresponding three-dimensional metrics. Of particular interest for regulatory ozone attainment is the pronounced deference between the 8-hour box model MOIR and MOIR-$3D_{8hr}$ for more reactive species. The exposure metric is usually closer to the MOIR than the MIR scale, mainly because box model MIR reflects more extreme conditions that are less common in the atmosphere. Estimated values for the exposure metric, to a large extent depend on the selected threshold concentration. Increasing the threshold ozone concentration for exposure calculations shifts the metric closer to MOIR-3D or MOIR-$3D_{8hr}$ metrics.

Figure 5.7 compares four different three-dimensional metrics. Different metrics are in very good agreement with each other, particularly in terms of relative ranking. MOIR-3D and MOIR-$3D_{8hr}$ metrics are generally very close to each other, and lower than exposure and MIR-3D metrics. The exposure metric is more heavily affected by highly populated urban areas, where maximum three-dimensional reactivities are also expected to occur. Therefore, when the selected threshold ozone concentration includes these locations in calculating the exposure metric, it closely follows the MIR-3D metric, as can be seen in Figure 5.7. Although these results are specific to the modeled domain and episode, it appears that relative reactivity metrics, as suggested by previous urban studies (e.g., Bergin et al., 1995), exhibit a fairly consistent behavior in a regional domain.

All of the metrics discussed so far are domain-wide measures of organic reactivity. Figures 5.8a and 5.8b show RIRs for six specific locations in the modeling domain (San Jose, Sacramento, Fresno, Livermore, Bakersfield, and Monterey). The RIR values are averaged over five days in the episode, and are taken at the time of the daily peak simulated ozone at each location. Among these six sites, Livermore and Monterey are not locally affected by large anthropogenic emissions, although Livermore receives a polluted urban plume from the Bay area. Relative reactivities at Fresno and Bakersfield are very similar and consistent, and somewhat distinctive from the other four sites. Monterey shows a negative reactivity for acetaldehyde. As expected, local relative reactivities show higher variability than the domain-wide relative metrics. The variability, as well as the magnitude of the local relative reactivities can be affected by the composition of the base VOC mixture, and including more species in the mixture can decrease the variability. Table 5.4 shows the average of the relative reactivities at these six sites, at the time of observed peak ozone at each site. The change in the reactivity rank of each species, compared to the box model MIR is also shown.

Sensitivity perturbation for all the above-mentioned results is a fraction of the total anthropogenic VOC emissions, as opposed to the total (including biogenic) organic emissions. This method is chosen because it represents the portion of emissions that can be targeted for ozone control policies. For comparison, simulations perturbing the total VOC (anthropogenic and biogenic) emissions were also conducted. Figure 5.9 shows a comparison for MIR-3D and MOIR-3D metrics. Given the day-to-day variability, MIR-3D metric estimates for both cases are very similar, while MOIR-3D results are virtually identical. Species that behave most differently in the MIR-3D metric are mainly those who react strongly with ozone. By including biogenics in total emissions of the grid, more of these species are injected into the sensitivity field, and their reaction with ozone decreases the absolute reactivity in the vicinity of emission sources (generally close to MIR conditions). Further downwind (MOIR conditions), these species have had enough time to produce their share of ozone, and inclusion of biogenics has less effect.

5.5 Summary

A three-dimensional modeling approach reveals a great deal of spatial and temporal variability in organic absolute reactivities that is difficult to capture with traditional box model calculations. Direct sensitivity calculation was shown to be a suitable and efficient method for three-dimensional reactivity assessment. Absolute reactivities of different compounds were calculated by injecting equal amounts (on a mass basis) of each species into the sensitivity field. The perturbation followed the same spatial pattern as total anthropogenic VOC emissions. The absolute reactivity values for different organic species, or for the same species at different locations and times, can cover a range of few orders of magnitude.

Relative reactivity of each VOC was calculated with reference to a base mixture, and different domain-wide metrics were defined. The relative reactivities are fairly similar and very consistent with each other, independent of which endpoint is chosen; MIR-3D, MOIR-3D, or exposure, and with different averaging periods. Exposure and MIR-3D metrics give very similar results, and are somewhat higher than both MOIR-3D metrics. The metrics compare reasonably well (for most species) with box model scales and exhibit very low day-to-day variability for the modeled episode and domain. Metrics with 8-hour averaging period are more different from the corresponding box model scales, with MOIR-$3D_{8hr}$ being considerably lower for some reactive species. Finally, perturbing the sensitivity field based on the total anthropogenic emissions or total organic emissions (including biogenics) produced very similar results.

Table 5.1 MAQSIP specifications

Chemistry	SAPRC-99
total number of species	107
steady state species	7
explicit VOCs	40
total number of reactions	246
number of photolytic reactions	30
chemical solver	hybrid (Young and Boris, 1977)
Horizontal Transport	separate diffusion and advection
advection scheme	PPM (Colella and Woodward, 1984)
Emissions	processed with vertical diffusion
total number of emitted species	39

Table 5.2 Detailed species for reactivity assessment and box model scales (Carter, 2000)

Name	Name in the mechanism	MIR	MOIR	MIR_{8rh}	$MOIR_{8hr}$
2-Methyl 2-butene	2MBT	14.450	4.650	9.610	7.040
1,3-Butadiene	BUTD	13.580	4.830	7.900	5.520
Propene	PRPE	11.580	4.430	6.500	4.570
Isoprene	ISOP	10.690	3.950	6.250	4.210
m-Xylene	XYLM	10.610	3.190	6.240	4.170
Ethylene	ETHE	9.080	3.700	4.770	3.560
Formaldehyde	HCHO	8.970	2.560	5.910	4.060
Higher aldehydes	RCHO	7.880	2.970	4.520	2.870
Higher lumped olefines	OLE1	7.800	3.110	4.280	2.910
1,2,4 Trimethyl benzene	124B	7.180	2.320	4.110	2.710
Acetaldehyde	CCHO	6.840	2.560	3.890	2.520
a-Pinene	APIN	4.290	1.560	2.580	1.780
p-Xylene	XYLP	4.250	1.360	2.200	1.450
Toluene	TOLU	3.970	1.170	2.000	1.310
Methylcyclopentane	MCPT	2.420	1.330	1.140	0.870
Ethanol	ETOH	1.690	0.930	0.770	0.610
iso-Pentane	IPNT	1.670	1.020	0.790	0.670
n-Pentane	N_C5	1.540	0.960	0.710	0.600
Methyl ethyl ketone	MEK	1.480	0.650	0.740	0.500
2,2,4 Trimethyl pentane	224P	1.440	0.810	0.690	0.570
n-Butane	N_C4	1.330	0.830	0.610	0.520
Acetylene	C2H2	1.250	0.490	0.590	0.430
n-Butyl acetate	BACT	0.890	0.540	0.410	0.330
Benzene	C6H6	0.820	0.340	0.370	0.270
Methyl t-butyl ether	MTBE	0.780	0.470	0.380	0.340
Methanol	MEOH	0.710	0.340	0.340	0.270
Isopropyl alcohol	IPOH	0.710	0.390	0.370	0.320
Acetone	ACET	0.430	0.170	0.220	0.140
Ethane	C2H6	0.310	0.200	0.140	0.120
Carbon monoxide	CO	0.060	0.040	0.030	0.030
Methane	CH4	0.010	0.010	0.010	0.010
Benzaldehyde	BALD	-0.610	-1.640	-0.550	-1.090

Table 5.3 Performance evaluation summary (60 ppb cut-point).

	Aug. 2^{nd}	Aug. 3^{rd}	Aug. 4^{th}	Aug. 5^{th}	Aug. 6^{th}
Normalized error (%)	14.2	16.4	16.0	16.2	21.3
Normalized bias (%)	4.9	5.8	5.4	-4.2	-17.0

Table 5.4 Average RIRs (average is for six Central California sites), and their standard deviation. The change in rank is with respect to the box model MIR.

species	average	standard deviation	change in rank
2MBT	9.26	4.58	-1
BUTD	11.46	4.72	1
PRPE	4.63	1.18	-1
ISOP	8.94	3.94	1
XYLM	3.75	1.05	-2
ETHE	2.37	0.51	-3
HCHO	3.79	1.95	1
RCHO	1.69	1.14	-3
OLE1	3.81	0.88	4
124B	2.48	0.58	2
CCHO	1.21	1.38	-4
APIN	2.20	0.87	2
XYLP	1.32	0.20	-1
TOLU	1.10	0.11	-2
MCPT	0.84	0.22	-3
ETOH	1.52	0.16	3
IPNT	0.70	0.15	-2
N_C5	0.69	0.19	-2
MEK	1.02	0.18	2
224P	0.60	0.11	-1
N_C4	0.54	0.18	-1
C2H2	0.18	0.03	-5
BACT	0.37	0.13	-1
C6H6	0.22	0.05	-1
MTBE	0.40	0.06	2
MEOH	0.21	0.03	0
IPOH	1.58	0.46	14
ACET	0.10	0.03	-1
C2H6	0.11	0.05	1
CO	0.03	0.00	0
CH4	0.01	0.00	0
BALD	-0.48	0.17	0

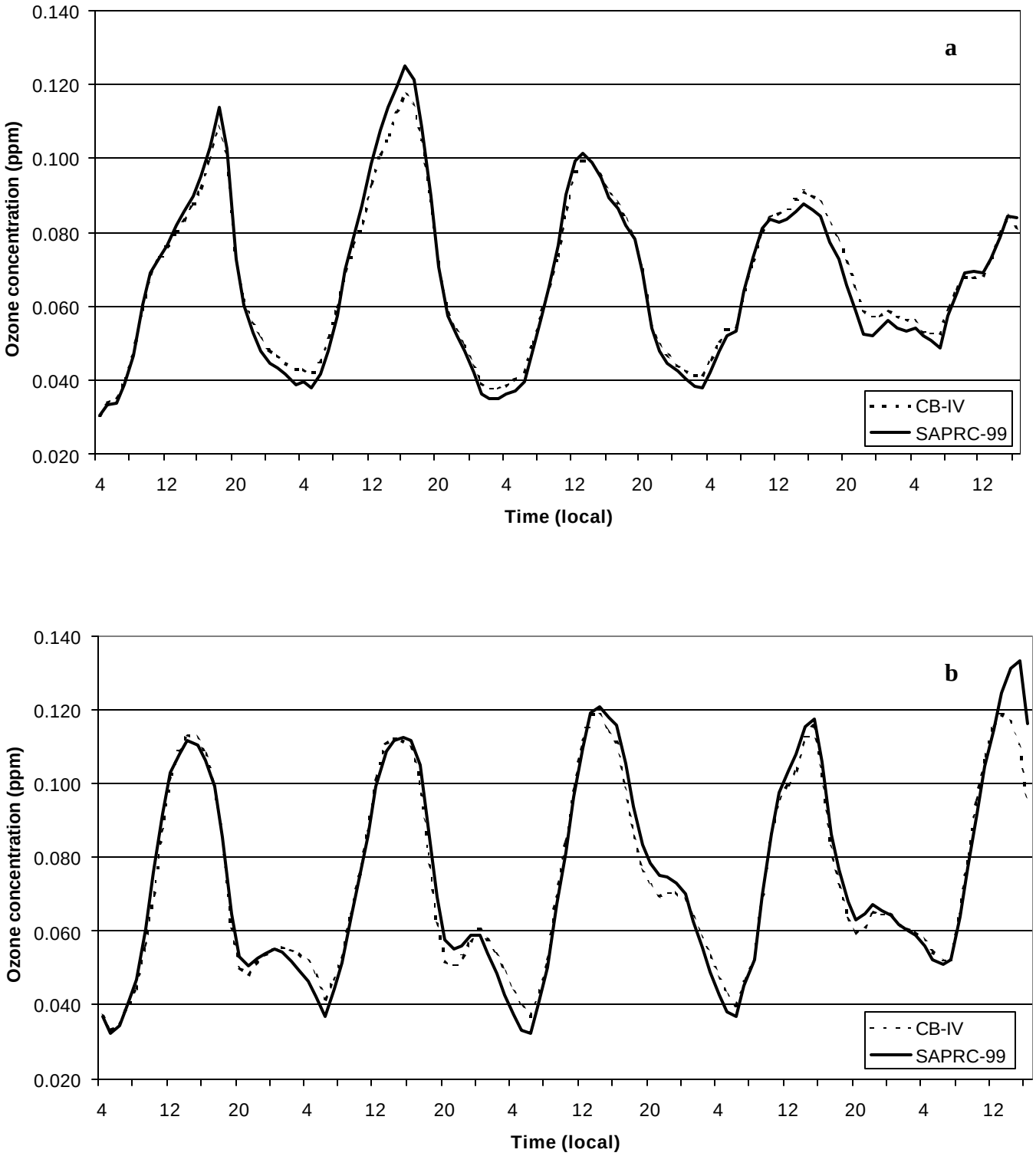

Figure 5.1 Comparison between SAPRC-99 and CB-IV chemical mechanisms in predicting ozone concentrations at a) Sacramento, b) episode's peak ozone location.

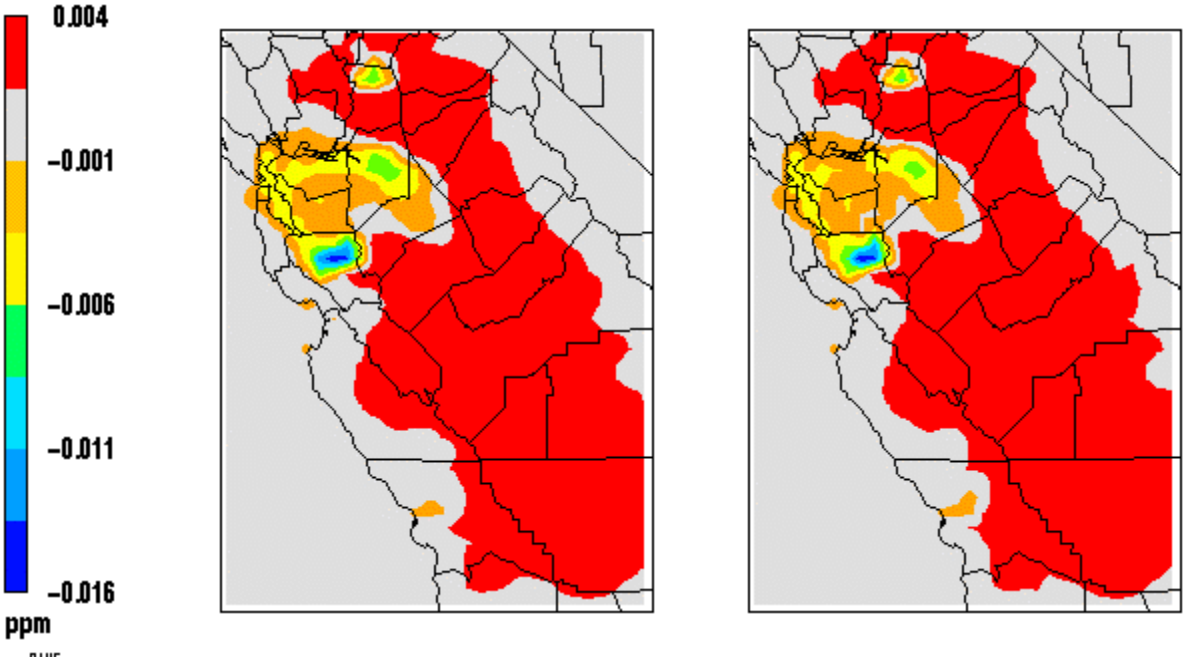

Figure 5.2 DDM (left) and brute-force (right) ozone sensitivity (3 pm, local time) to 25% domain-wide reduction in NO emissions. Brute-force values are central difference approximations.

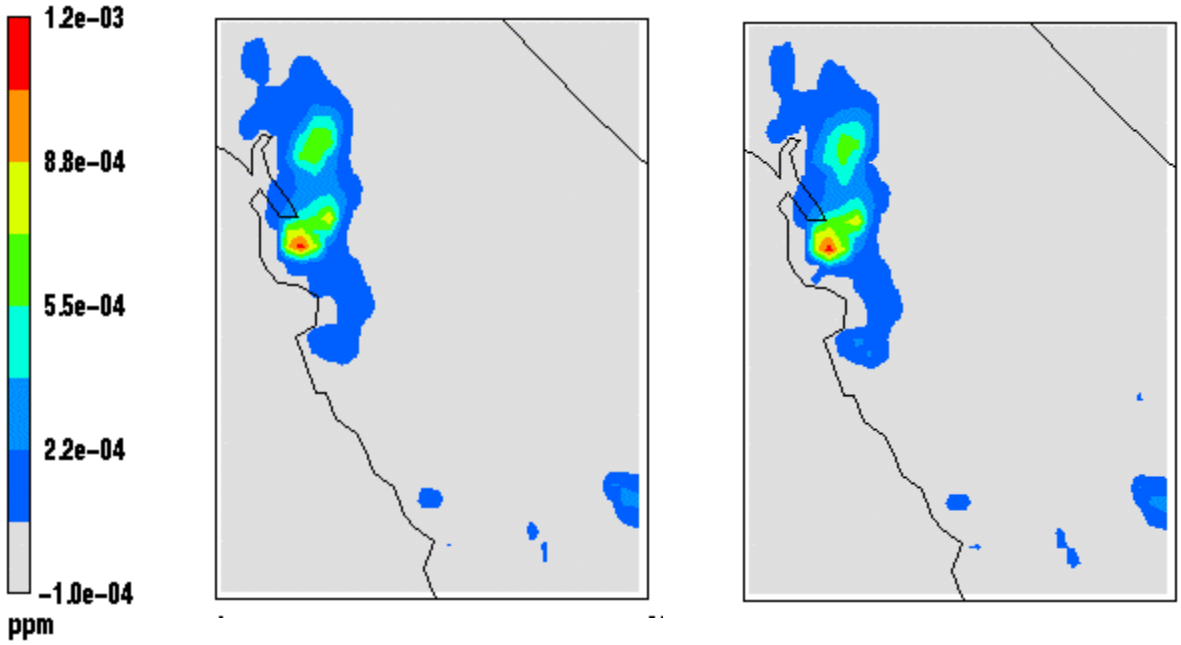

Figure 5.3 DDM (left) and brute-force (right) ozone sensitivity (local noon) to 25% domain-wide reduction in Isoprene emissions. Brute-force values are central difference approximations.

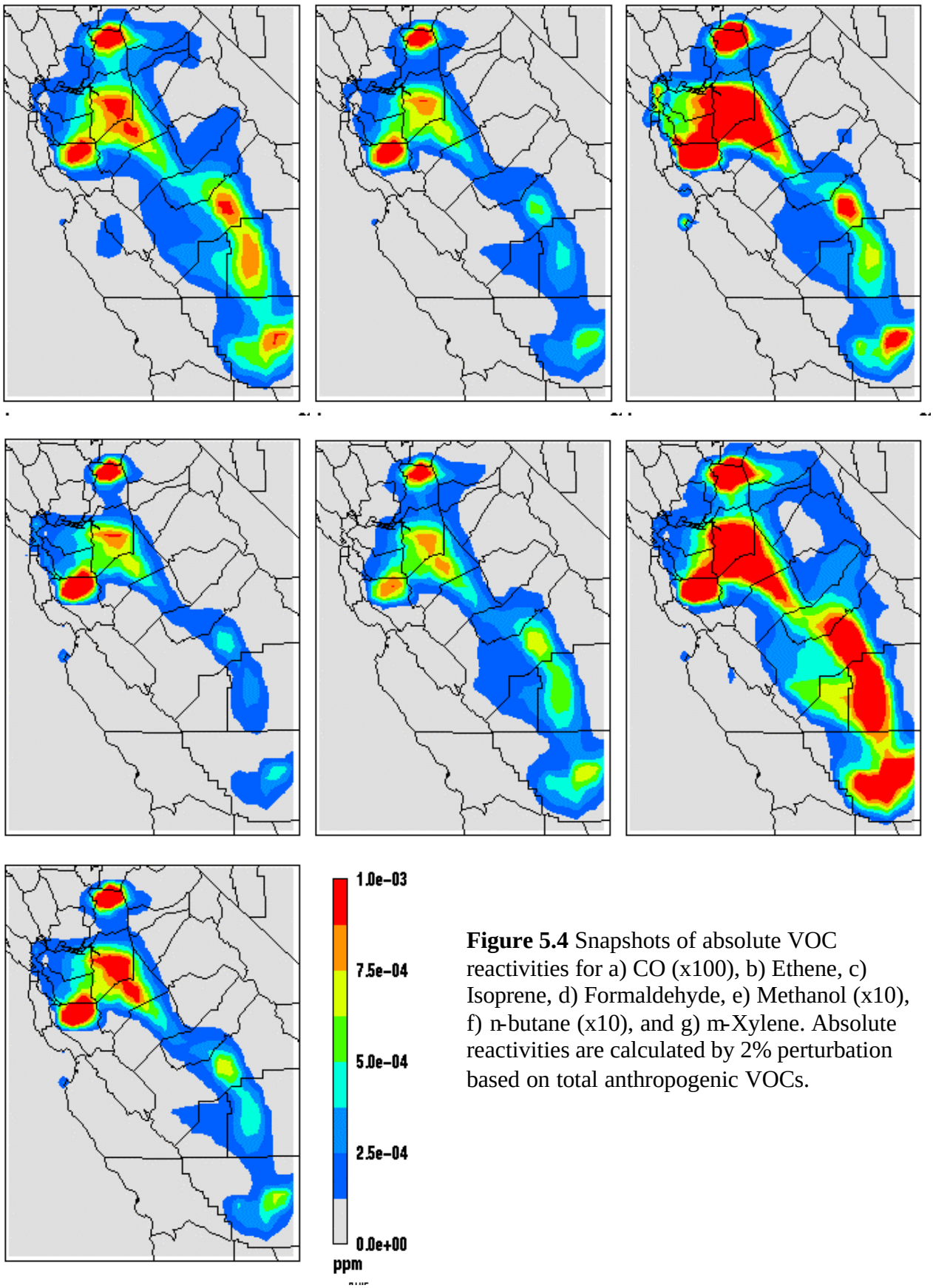

Figure 5.4 Snapshots of absolute VOC reactivities for a) CO (x100), b) Ethene, c) Isoprene, d) Formaldehyde, e) Methanol (x10), f) n-butane (x10), and g) m-Xylene. Absolute reactivities are calculated by 2% perturbation based on total anthropogenic VOCs.

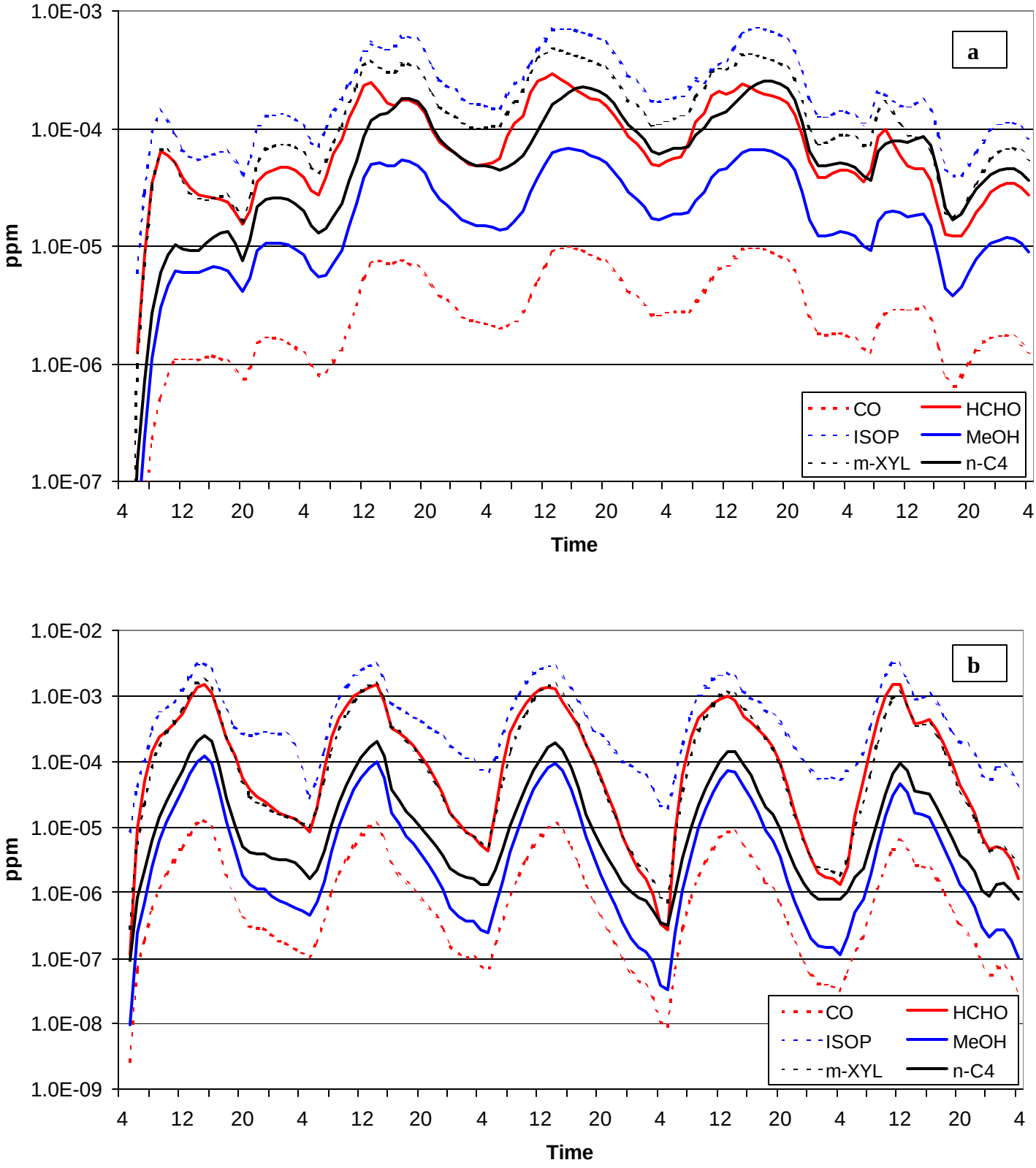

Figure 5.5 Time series of absolute reactivity of different VOCs for a) NOx-limited, and b) VOC-limited locations.

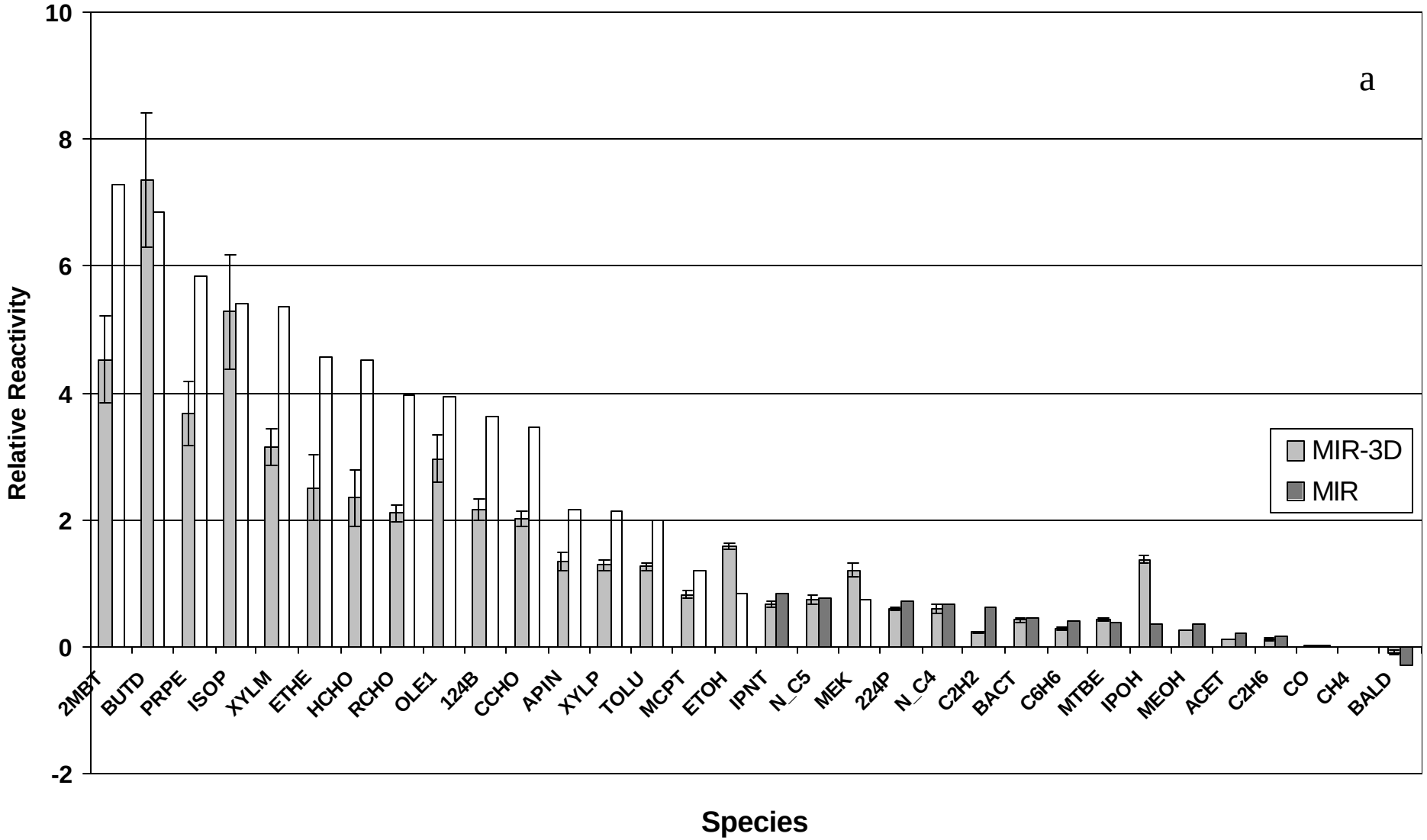

Figure 5.6a MIR-3D metric. Error bars are 1-σ variability for 5 modeling days.

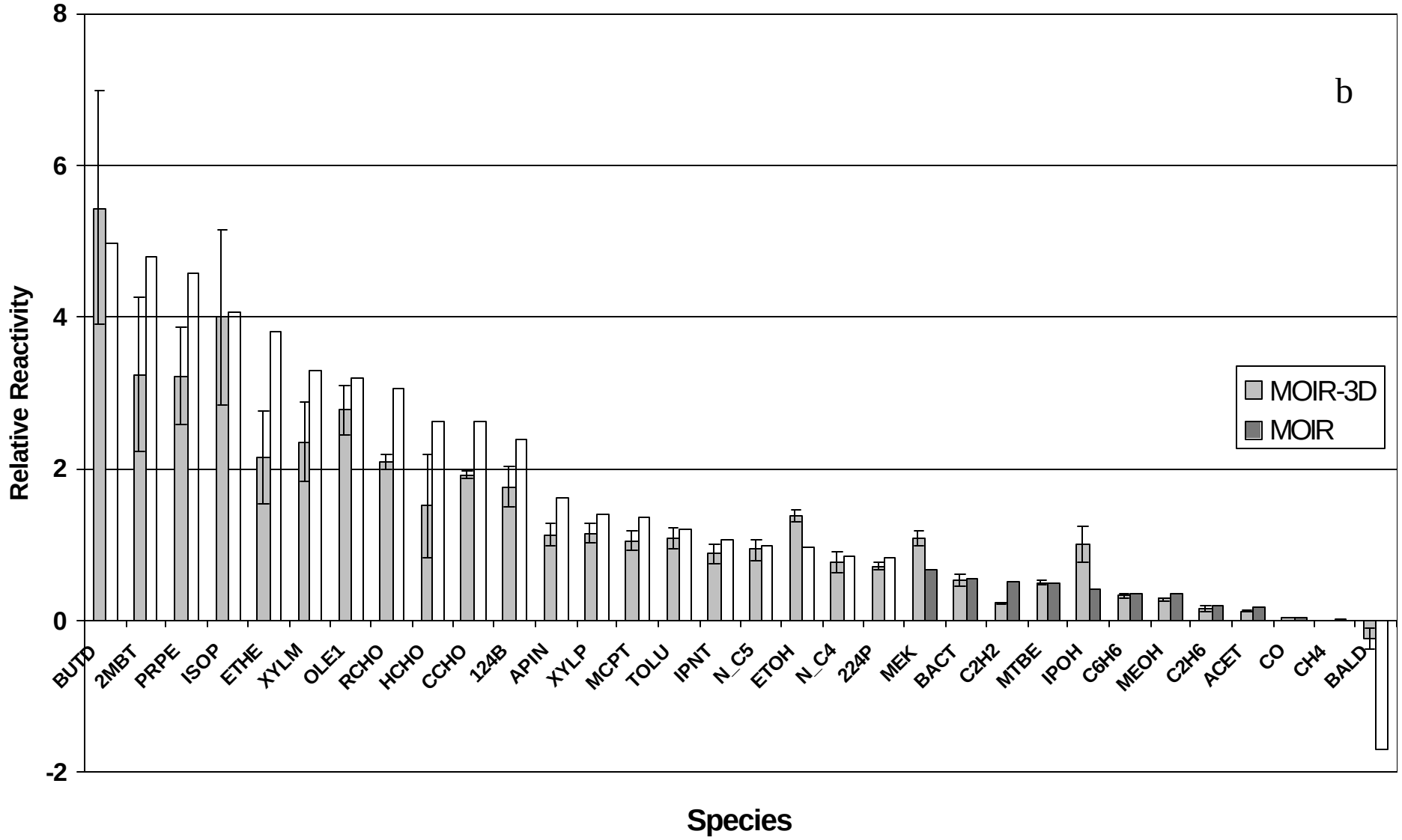

Figure 5.6b MOIR-3D metric. Error bars are 1-σ variability for 5 modeling days.

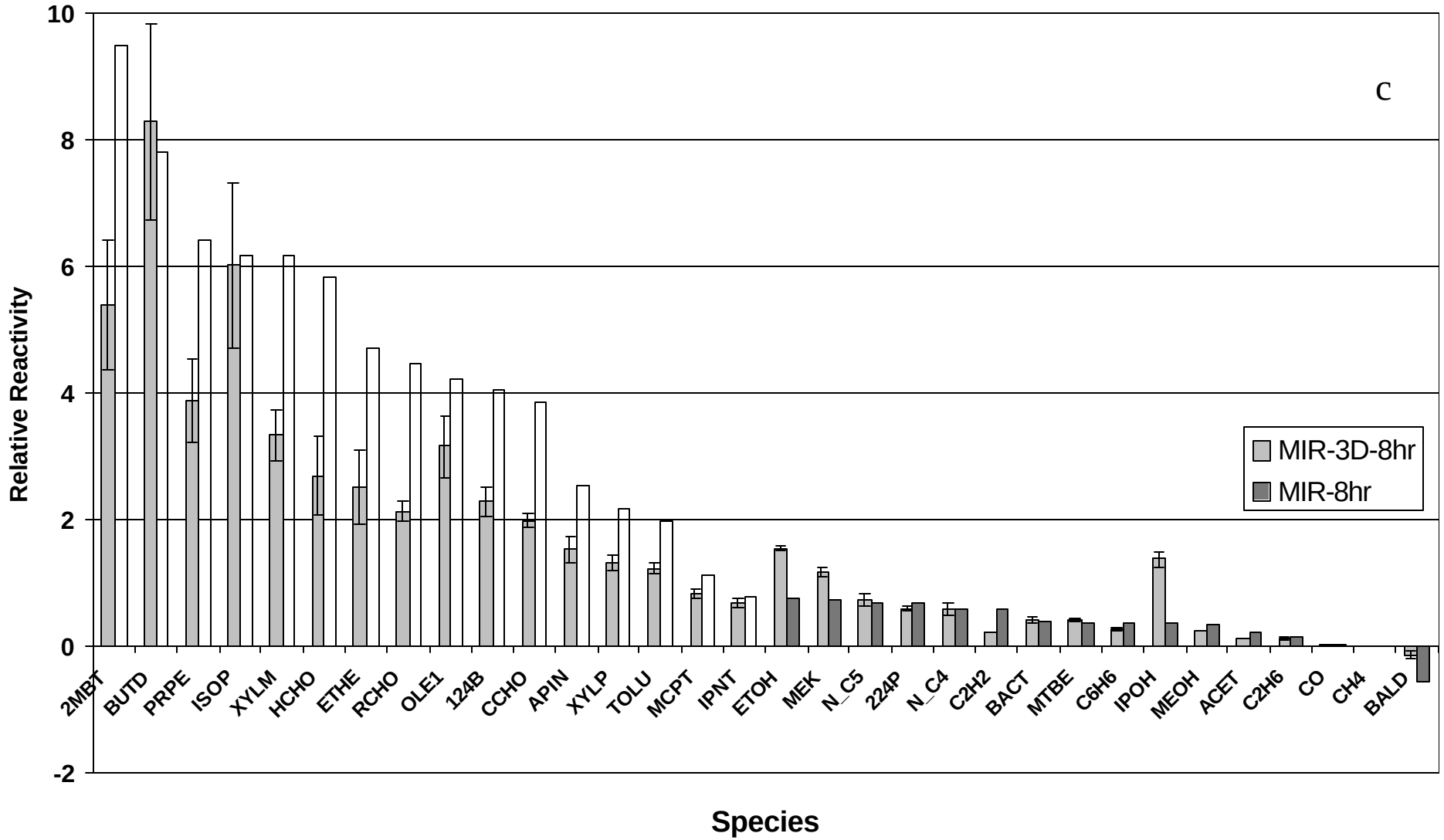

Figure 5.6c MIR-3D$_{8hr}$ metric. Error bars are 1-σ variability for 5 modeling days.

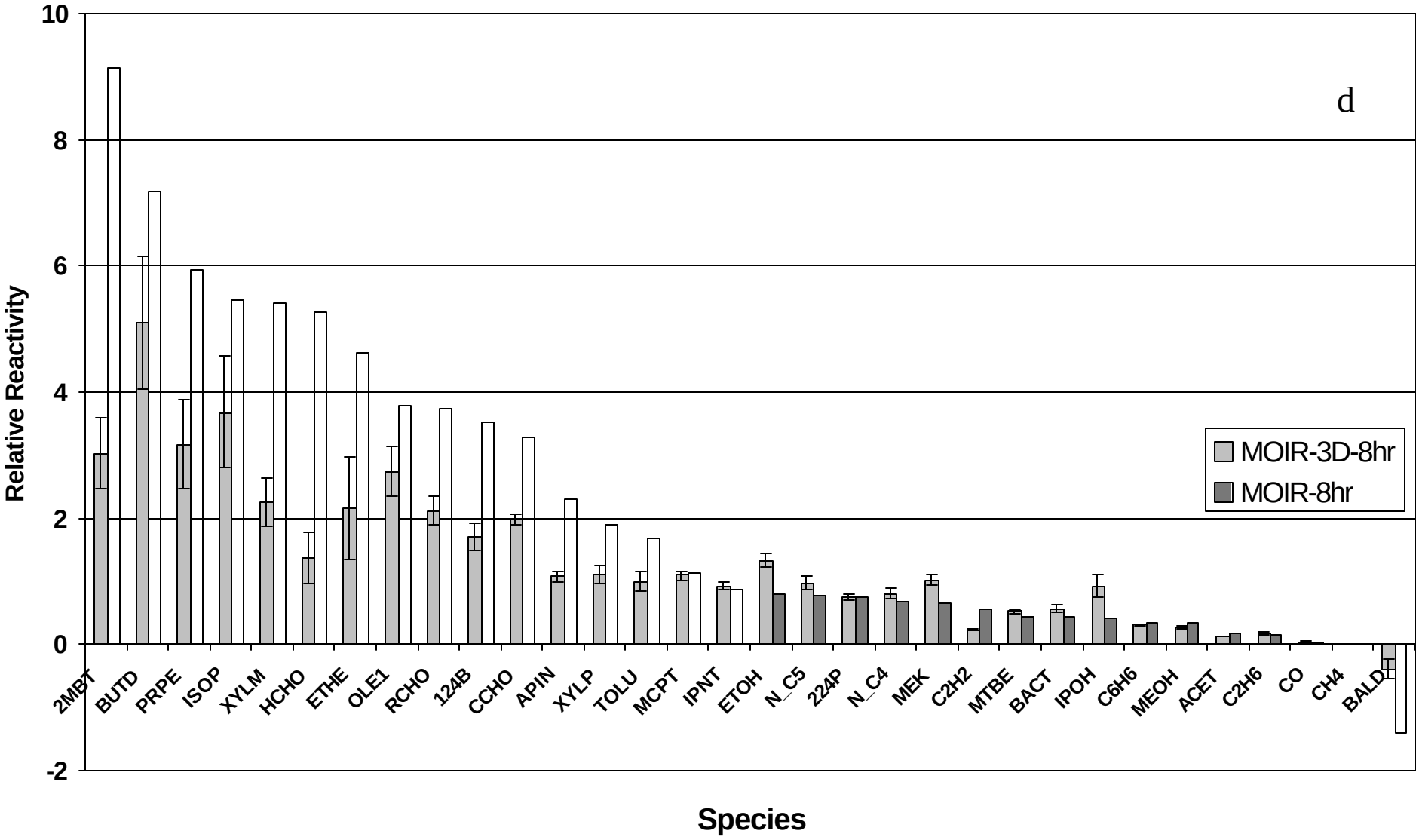

Figure 5.6d MOIR-3D$_{8hr}$ metric. Error bars are 1-σ variability for 5 modeling days.

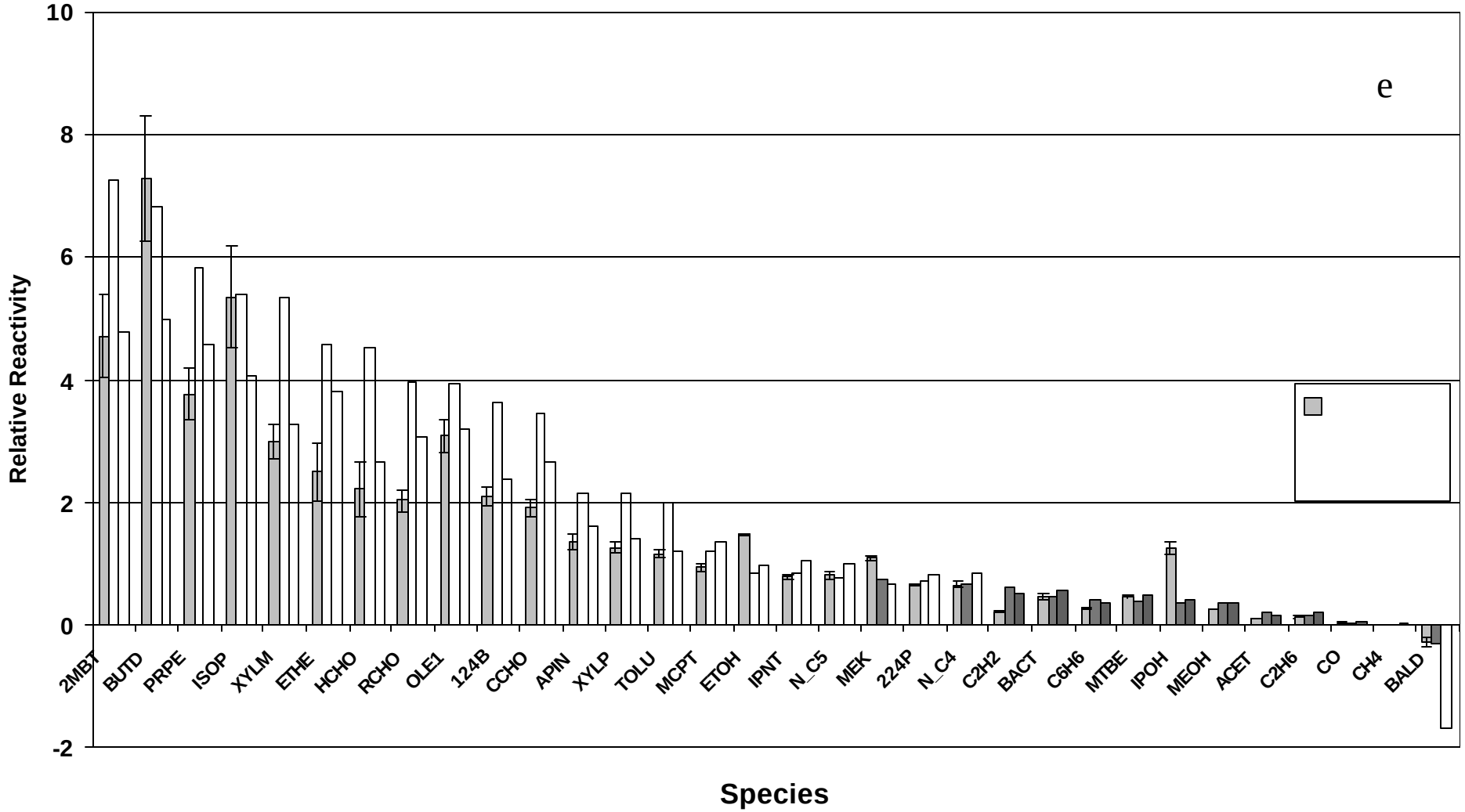

Figure 5.6e MIR-3D metric. Error bars are 1-σ variability for 5 modeling days. Exposure metric is calculated for 80 ppb ozone threshold.

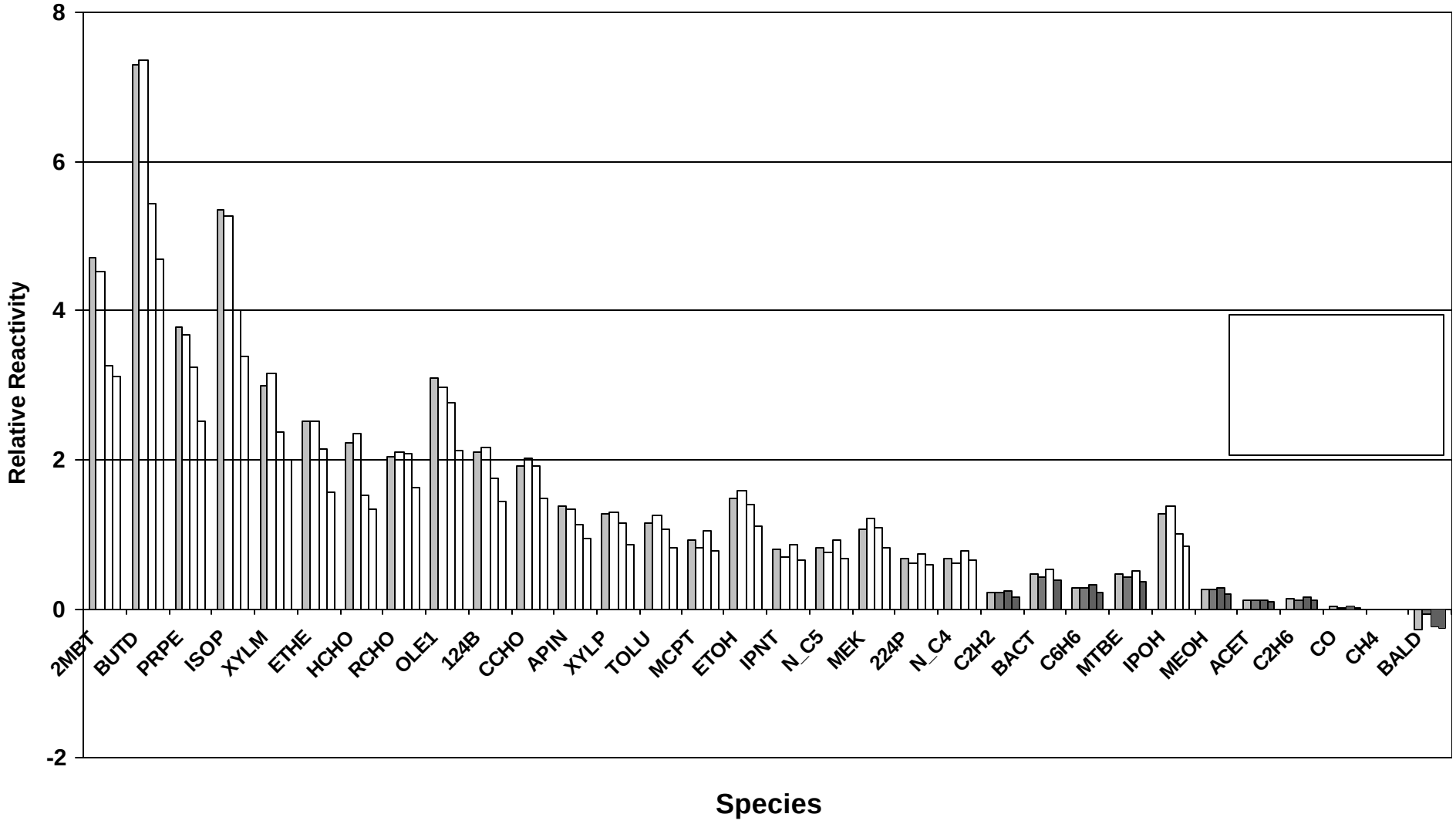

Figure 5.7 Comparison of different three-dimensional relative reactivity metrics.

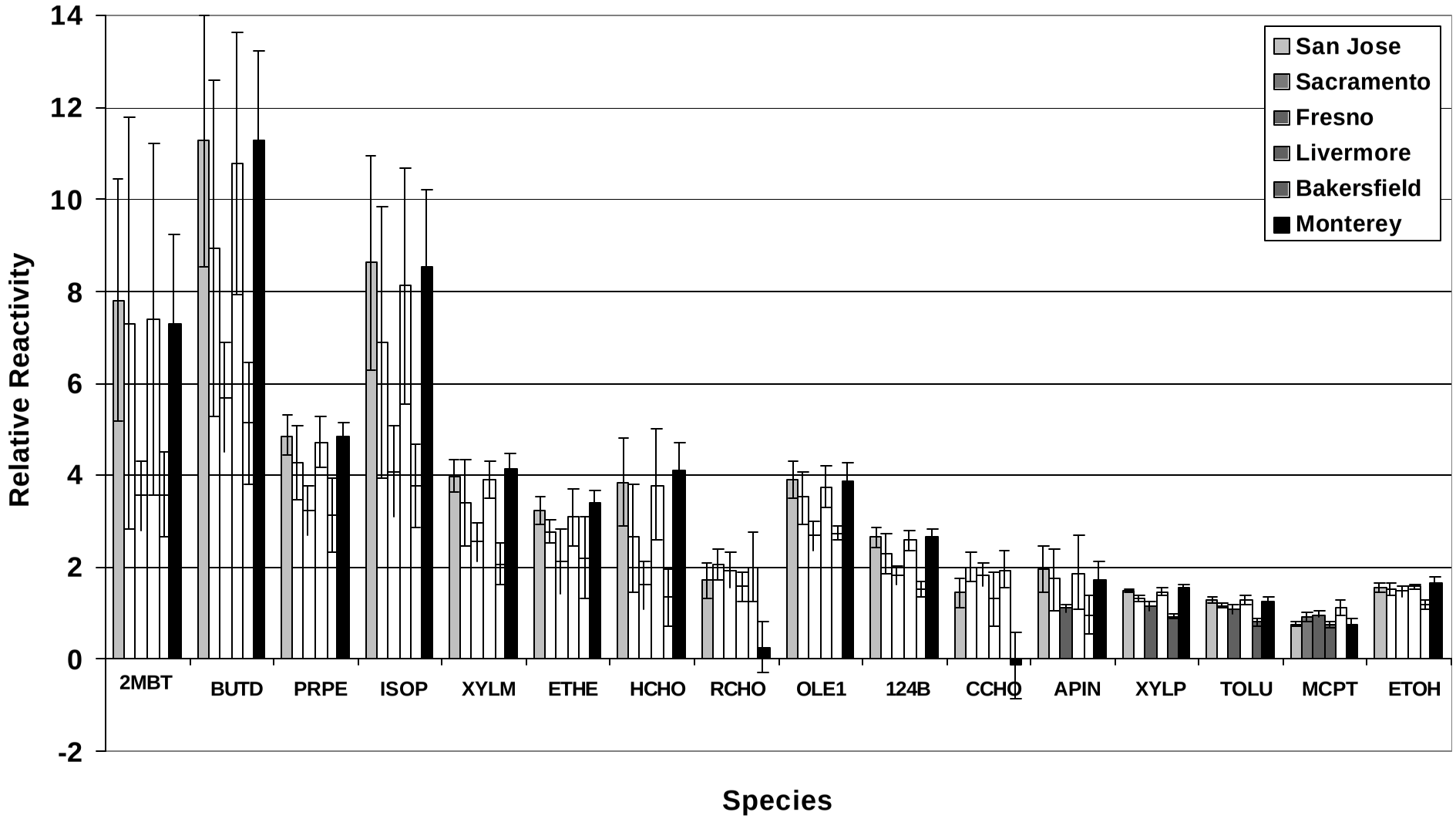

Figure 5.8a Local relative reactivities at the time of the maximum simulated ozone for more reactive species.

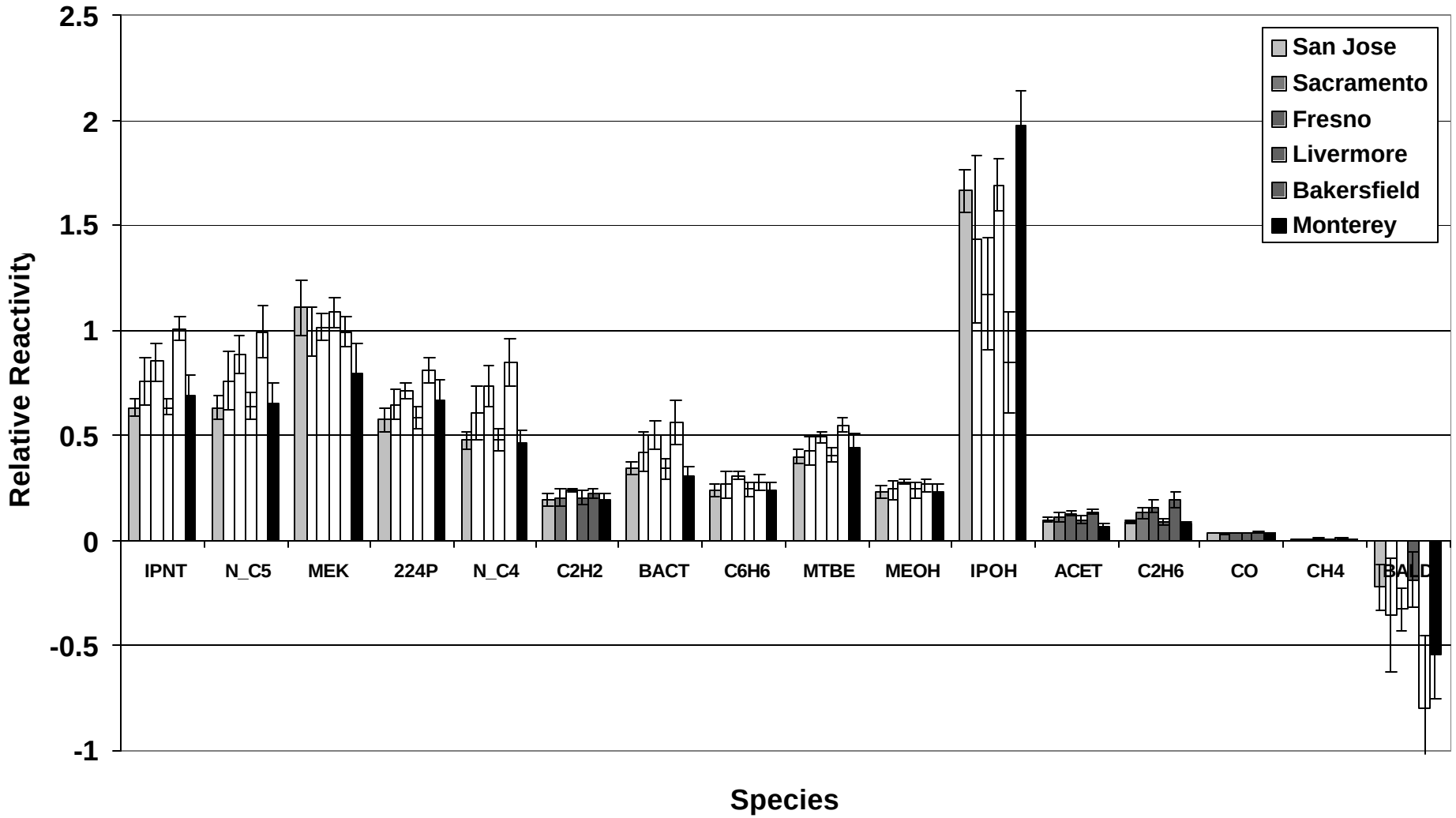

Figure 5.8b Local relative reactivities at the time of the maximum simulated ozone for less reactive species.

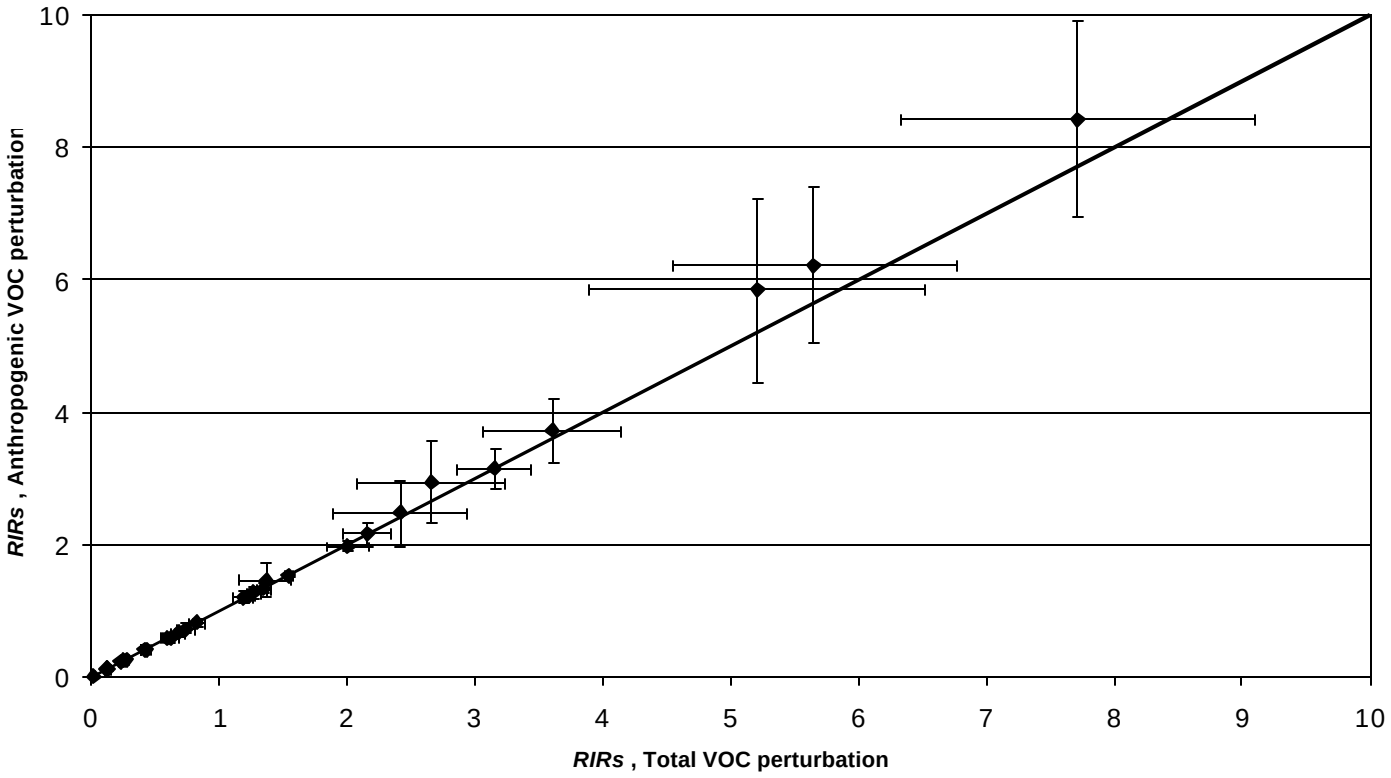

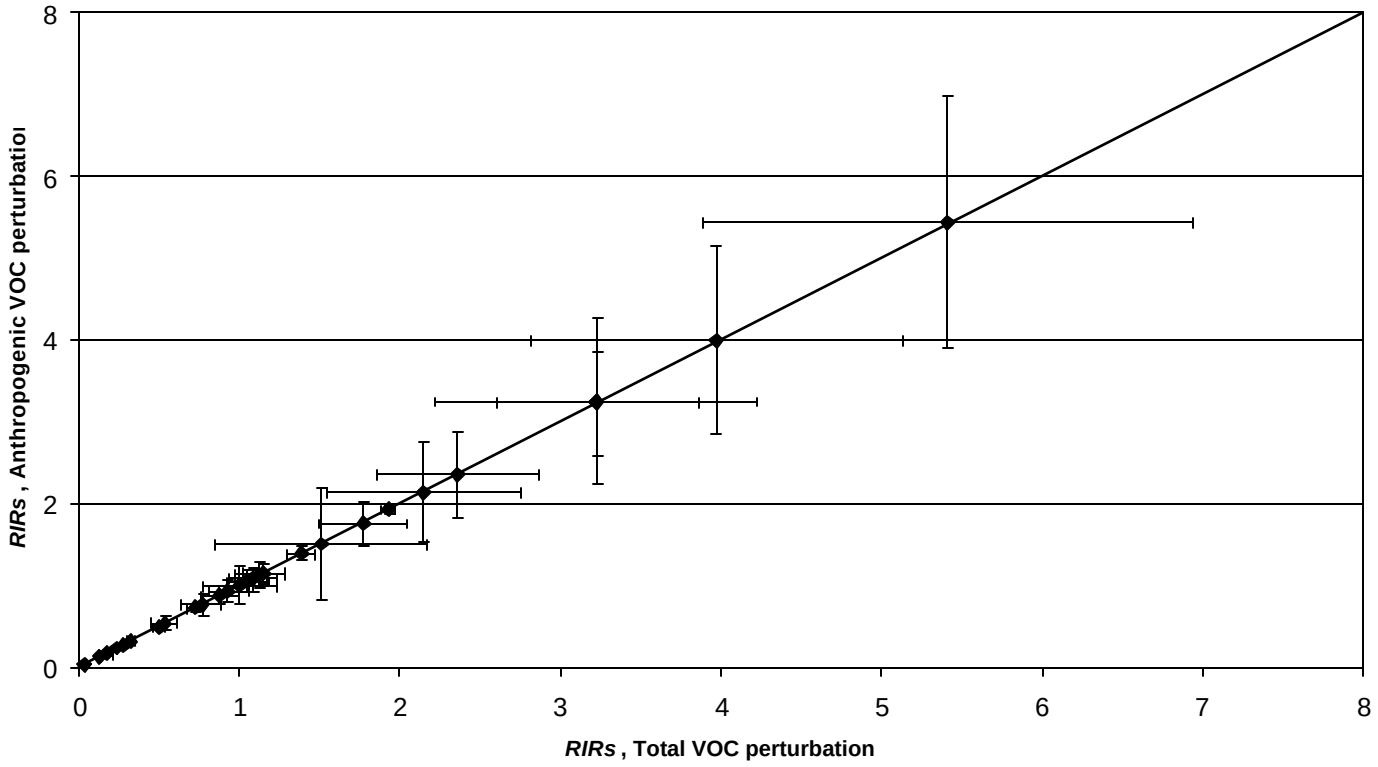

Figure 5.9 Comparison of a) MIR-3D, and b) MOIR-3D for total vs. total anthropogenic VOC emissions.

6. Conclusions and Recommendations

The incremental reactivity of carbon monoxide and 30 organic compounds has been assessed using 3-D photochemical air quality models with online sensitivity analysis. In our assessment, perturbations to the emissions of each compound follow the underlying, existing spatial and temporal distribution of VOC emissions. Hot summertime conditions that were conducive to high levels of photochemical smog formation were considered in the modeling, for both the South Coast Air Basin and Central California (including the San Francisco Bay Area, Sacramento and the San Joaquin Valley). The most important chemical and emissions uncertainties that affect ozone formation have been propagated through the analysis to quantify the magnitude of their contribution to uncertainties in reactivity.

We found that for most species examined in the present study, reactivity scales developed using 3-D modeling resulted in similar rankings of individual VOC when compared to reactivity scales developed by Carter using a 0-D box model. The 3-D modeling results support previous findings that there can be large differences among VOCs in terms of their reactivity with respect to ozone formation, and that these differences can be quantified.

The absolute reactivity of all VOC at locations along the upwind edge of the modeling regions was low, as expected because most of the VOC emissions occur downwind of these locations and do not influence ozone formation near the inflow boundary. Site-to-site differences can be large when absolute reactivity scales are considered. The variation in reactivity across sites is reduced when reactivity is measured on a relative rather than absolute scale. Differences in relative reactivity may still occur as a function of location, with differences likely to be magnified where absolute reactivities are low.

Biogenic VOC such as isoprene and α-pinene have a different spatial pattern of emissions from anthropogenic VOC. In the case of the South Coast Air Basin, because most of the isoprene and α-pinene emissions were located downwind of the eight urban monitoring sites that were considered, the incremental reactivity of biogenic VOC was

lower than the MIR scale would suggest when their emissions pattern was similar to the underlying biogenic emissions. This analysis was done using estimates of historical (circa 1990) anthropogenic emissions; the relative importance of biogenic VOC is expected to increase as anthropogenic VOC emissions are controlled.

Our results for central California are similar to those for the South Coast Air Basin. Absolute reactivities showed a great deal of spatial variability while relative reactivities were reasonably constant. We used a slightly different method of perturbation for central California, where all the VOCs are perturbed equally on a mass basis. This led to the relative reactivities of biogenic VOCs that were more consistent with other species, as well as with the box model scales. Thus, if a substitution between compounds is done within the same source, one can be much more confident that reactivity adjustments will provide the desired result.

For central California, the analysis mainly focused on domain-wide reactivity metrics. Three-dimensional MIR and MOIR (with different averaging times), as well as daily population exposure metrics were considered. Most VOCs behaved similarly in all metrics (including the box model scales), i.e. the relative ranking of the compounds was similar across metrics. We also found that the three-dimensional metrics were usually lower than the box model scales for the more reactive species. This is particularly true for the 8-hour MOIR-3D metric, where the reactivity response of different species is much less dynamic.

We found that the alkenes and some carbonyls (especially formaldehyde and acetaldehyde) exhibit greater site-to-site variability in reactivity than other classes of VOC. Specifically, the alkenes and formaldehyde were more reactive in upwind/near-source regions where ozone formation was strongly radical-limited. Alkenes and formaldehyde form HO_x radicals promptly and directly during photo-oxidation, which distinguishes them from many other VOC. At two sites (Hawthorne, at the upwind edge of the South Coast Air Basin, and Monterey on the coast south of the San Francisco Bay area) we found increasing acetaldehyde to have a locally negative effect on ozone

formation, because acetaldehyde's role in the formation of PAN competed with NO_2 photolysis that would otherwise have formed more ozone. This effect was not seen at other sites. Use of alkenes and aldehydes as reference compounds in development of relative reactivity scales may increase site-to-site variability in relative reactivity scales.

Uncertainties in incremental reactivity estimates were calculated using a vertically-resolved (1-D) photochemical trajectory model for eight representative organic compounds and four trajectory endpoints in the South Coast Air Basin. Uncertainties in relative incremental reactivities ranged from 8% (coefficient of variation) for propene at Anaheim and Azusa to 49% for CO at Riverside, with values for most of the compounds ranging from 20 to 35%. The parameters that contributed most to the uncertainty in the absolute incremental reactivity of the base mixture included photolyis rates for NO_2, HCHO and O_3, rate coefficients for the reactions HO + NO_2 and PAN decomposition, and NO_x emissions from stationary sources. The relative incremental reactivities (RIRs) of individual compounds are strongly influenced by uncertainties in the rate parameters of their primary oxidation reactions. In principle, uncertainties in reactivity scales can be reduced by research that defines better the values of relevant emissions and chemical rate parameters.

A. Extensions to SAPRC99 Chemical Mechanism

This appendix shows the reactions of volatile organic compounds (the organic species codes are defined in Table 2.1 and in the text on p. 11).

REACTIONS INPUT:	A (E_A B (IN PPM-MIN UNITS)
FAHV) HCHO + HV = #2 HO2. + CO	PHOT. = HCHO_R
FAVS) HCHO + HV = H2 + CO	PHOT. = HCHO_M
FAOH) HCHO + HO. = HO2. + CO + H2O	1.262E+04 -0.04 -1.000
FAH2) HCHO + HO2. = HOCOO.	1.424E+01 -1.24 -1.000
FAN3) HCHO + NO3 = HNO3 + HO2. + CO	2.936E+03 4.83 -1.000
AAOH) CCHO + HO. = CCO-O2. + H2O	8.220E+03 -0.62 -1.000
AAHV) CCHO + HV = CO + HO2. + C-O2.	PHOT. = CCHO_R
AAN3) CCHO + NO3 = HNO3 + CCO-O2.	2.055E+03 3.70 -1.000
PAOH) RCHO + HO. = #.034 RO2-R. + #.001 RO2-N. & + #.965 RCO-O2. + #.034 CO + #.034 CCHO + & #-0.003 XC	2.936E+04 0.00 -1.000
PAHV) RCHO + HV = CCHO + RO2-R. + CO + HO2.	PHOT. = C2CHO
PAN3) RCHO + NO3 = HNO3 + RCO-O2.	2.055E+03 3.52 -1.000
K3OH) ACET + HO. = HCHO + CCO-O2. + R2O2.	1.615E+03 1.03 -1.000
K3HV) ACET + HV = CCO-O2. + C-O2.	PHOT. = ACETONE
K4OH) MEK + HO. = #.37 RO2-R. + #.042 RO2-N. + & #.616 R2O2. + #.492 CCO-O2. + #.096 RCO-O2. & + #.115 HCHO + #.482 CCHO + #.37 RCHO + #.287 XC	1.908E+03 0.05 1.000
K4HV) MEK + HV + #.15 = CCO-O2. + CCHO + RO2-R.	PHOT. = KETONE
MeOH) MEOH + HO. = HCHO + HO2.	4.550E+03 0.71 1.000
BZOH) BALD + HO. = BZCO-O2.	1.894E+04 0.00 -1.000
BZHV) BALD + HV + #.05 = #7 XC	PHOT. = BZCHO
BZNT) BALD + NO3 = HNO3 + BZCO-O2.	2.055E+03 3.72 -1.000
c1OH) CH4 + HO. = H2O + C-O2.	3.156E+03 3.45 -1.000
etOH) ETHE + HO. = RO2-R. + #1.61 HCHO + #.195 CCHO	2.877E+03 -0.87 -1.000

REACTIONS INPUT:	A (IN PPM-MIN UNITS)	E_A	B
etO3) ETHE + O3 = #.12 HO. + #.12 HO2. + #.5 CO + & #.13 CO2 + HCHO + #.37 HCOOH	1.342E+01	5.13	-1.000
etN3) ETHE + NO3 = RO2-R. + RCHO + #-1 XC + XN	6.444E+02	4.54	1.000
etOA) ETHE + O3P = #.5 HO2. + #.2 RO2-R. + #.3 C-O2. & + #.491 CO + #.191 HCHO + #.25 CCHO + #.009 GLY & + #.5 XC	1.527E+04	1.57	-1.000
isOH) ISOP + HO. = #.907 RO2-R. + #.093 RO2-N. + & #.079 R2O2. + #.624 HCHO + #.23 METHACRO + & #.32 MVK + #.357 ISO-PROD + #-0.167 XC	3.670E+04	-0.81	-1.000
isO3) ISOP + O3 = #.266 HO. + #.066 RO2-R. + & #.008 RO2-N. + #.126 R2O2. + #.192 MA-RCO3. + & #.275 CO + #.122 CO2 + #.592 HCHO + #.1 PROD2 & + #.39 METHACRO + #.16 MVK + #.204 HCOOH + & #.15 RCO-OH + #-0.259 XC	1.154E+01	3.80	-1.000
isN3) ISOP + NO3 = #.187 NO2 + #.749 RO2-R. + & #.064 RO2-N. + #.187 R2O2. + #.936 ISO-PROD + & #-0.064 XC + #.813 XN	4.448E+03	0.89	-1.000
isOP) ISOP + O3P = #.01 RO2-N. + #.24 R2O2. + & #.25 C-O2. + #.24 MA-RCO3. + #.24 HCHO + & #.75 PROD2 + #-1.01 XC	5.284E+04	0.00	-1.000
t1OH) TRP1 + HO. = #.75 RO2-R. + #.25 RO2-N. + & #.5 R2O2. + #.276 HCHO + #.474 RCHO + & #.276 PROD2 + #5.146 XC	2.686E+04	-0.89	-1.000
t1O3) TRP1 + O3 = #.567 HO. + #.033 HO2. + & #.031 RO2-R. + #.18 RO2-N. + #.729 R2O2. + & #.123 CCO-O2. + #.201 RCO-O2. + #.157 CO + & #.037 CO2 + #.235 HCHO + #.205 RCHO + #.13 ACET & + #.276 PROD2 + #.001 GLY + #.031 BACL + & #.103 HCOOH + #.189 RCO-OH + #4.183 XC	1.585E+00	1.63	-1.000
t1N3) TRP1 + NO3 = #.474 NO2 + #.276 RO2-R. + & #.25 RO2-N. + #.75 R2O2. + #.474 RCHO + & #.276 RNO3 + #5.421 XC + #.25 XN	5.373E+03	-0.35	-1.000
t1OP) TRP1 + O3P = #.147 RCHO + #.853 PROD2 + #4.441 XC	4.800E+04	0.00	-1.000
a3OH) ALK1 + HO. = #.695 RO2-R. + #.07 RO2-N. + & #.559 R2O2. + #.236 TBU-O. + #.026 HCHO + & #.445 CCHO + #.122 RCHO + #.024 ACET + #.332 MEK & + #-0.05 XC	1.497E+04	0.86	-1.000

REACTIONS INPUT:	A (IN PPM-MIN UNITS)	E_A	B
a4OH) ALK2 + HO. = #.835 RO2-R. + #.143 RO2-N. + & #.936 R2O2. + #.011 C-O2. + #.011 CCO-O2. + & #.002 CO + #.024 HCHO + #.455 CCHO + #.244 RCHO & + #.452 ACET + #.11 MEK + #.125 PROD2 + #-0.105 XC	8.734E+03	0.18	-1.000
a5OH) ALK3 + HO. = #.653 RO2-R. + #.347 RO2-N. + & #.948 R2O2. + #.026 HCHO + #.099 CCHO + & #.204 RCHO + #.072 ACET + #.089 MEK + & #.417 PROD2 + #2.008 XC	1.629E+04	0.10	-1.000
b1OH) ARO1 + HO. = #.224 HO2. + #.765 RO2-R. + & #.011 RO2-N. + #.055 PROD2 + #.118 GLY + & #.119 MGLY + #.017 PHEN + #.207 CRES + & #.059 BALD + #.491 DCB1 + #.108 DCB2 + & #.051 DCB3 + #1.288 XC	2.657E+03	-0.70	-1.000
b2OH) ARO2 + HO. = #.187 HO2. + #.804 RO2-R. + & #.009 RO2-N. + #.097 GLY + #.287 MGLY + & #.087 BACL + #.187 CRES + #.05 BALD + #.561 DCB1 & + #.099 DCB2 + #.093 DCB3 + #1.68 XC	3.875E+04	0.00	-1.000
o1OH) OLE1 + HO. = #.91 RO2-R. + #.09 RO2-N. + & #.205 R2O2. + #.732 HCHO + #.294 CCHO + & #.497 RCHO + #.005 ACET + #.119 PROD2 + #.92 XC	1.042E+04	-0.90	-1.000
o1O3) OLE1 + O3 = #.155 HO. + #.056 HO2. + & #.022 RO2-R. + #.001 RO2-N. + #.076 C-O2. + & #.345 CO + #.086 CO2 + #.5 HCHO + #.154 CCHO + & #.363 RCHO + #.001 ACET + #.215 PROD2 + & #.185 HCOOH + #.05 CCO-OH + #.119 RCO-OH + & #.654 XC	3.846E+00	3.26	-1.000
o1N3) OLE1 + NO3 = #.824 RO2-R. + #.176 RO2-N. + & #.488 R2O2. + #.009 CCHO + #.037 RCHO + & #.024 ACET + #.511 RNO3 + #.677 XC + #.489 XN	6.532E+01	0.75	-1.000
o1OP) OLE1 + O3P = #.45 RCHO + #.437 MEK + & #.113 PROD2 + #1.224 XC	1.571E+04	0.47	-1.000
o2OH) OLE2 + HO. = #.918 RO2-R. + #.082 RO2-N. + & #.001 R2O2. + #.244 HCHO + #.732 CCHO + & #.511 RCHO + #.127 ACET + #.072 MEK + #.061 BALD & + #.025 METHACRO + #.025 ISO-PROD + #-.054 XC	2.554E+04	-0.76	-1.000
o2O3) OLE2 + O3 = #.378 HO. + #.003 HO2. + & #.033 RO2-R. + #.002 RO2-N. + #.137 R2O2. + & #.197 C-O2. + #.137 CCO-O2. + #.006 RCO-O2. + & #.265 CO + #.07 CO2 + #.269 HCHO + #.456 CCHO + & #.305 RCHO + #.045 ACET + #.026 MEK + & #.006 PROD2 + #.042 BALD + #.026 METHACRO + & #.073 HCOOH + #.129 CCO-OH + #.303 RCO-OH + & #.155 XC	7.369E-01	0.92	-1.000

REACTIONS INPUT:	A (IN PPM-MIN UNITS)	E_A	B
o2N3) OLE2 + NO3 = #.391 NO2 + #.442 RO2-R. + & #.136 RO2-N. + #.711 R2O2. + #.03 C-O2. + & #.079 HCHO + #.507 CCHO + #.151 RCHO + & #.102 ACET + #.001 MEK + #.015 BALD + #.048 MVK & + #.321 RNO3 + #.075 XC + #.288 XN	1.066E+03	0.00	-1.000
o2OP) OLE2 + O3P = #.013 HO2. + #.012 RO2-R. + & #.001 RO2-N. + #.012 CO + #.069 RCHO + #.659 MEK & + #.259 PROD2 + #.012 METHACRO + #.537 XC	3.068E+04	0.00	-1.000
PEOH) PRPE + HO. = #.984 RO2-R. + #.984 HCHO & + #.984 CCHO + #.016 RO2-N. + #-.048 XC	7.119E+03	-1.00	-1.000
PEO3) PRPE + O3 = #.5 HCHO + #.5 CCHO + #.185 HCOOH & + #.320 HO. + #.060 HO2. + #.510 CO & + #.135 CO2 + #.260 C-O2. & + #.17 CCO-OH + #.070 INERT + #.070 XC	8.088E+00	3.73	-1.000
PEN3) PRPE + NO3 = #.949 RO2-R. + #.051 RO2-N. & + #2.693 XC + XN	6.738E+02	2.30	-1.000
PEOA) PRPE + O3P = #.45 RCHO + #.55 MEK & + #-0.55 XC	1.732E+04	0.64	-1.000
BDOH) BUTD + HO. = #.961 RO2-R. + #.039 RO2-N. & + #.48 "HCHO + METHACRO + ISO-PROD" & + #-1.039 XC	2.172E+04	-0.89	-1.000
BDO3) BUTD + O3 = #.06 "HO2. + HO." & + #.25 CO + #.19 CO2 + #.5 " HCHO + METHACRO" & + #.125 PROD2 + #.375 MVK + #.185 HCOOH & + #-1.375 XC	1.967E+01	4.54	-1.000
BDN3) BUTD + NO3 = #.920 RO2-R. + #.08 RO2-N. & + #.92 MVK + #-.161 XC + XN	1.468E+02	0.00	-1.000
BDOA) BUTD + O3P = #.25 HO2. + #.02 RO2-N. & + #.23 "RO2-R. + CO + METHACRO" & + #.75 PROD2+ #-1.77 XC	2.906E+04	0.00	-1.000
MBOH) 2MBT + HO. = #.935 RO2-R. + #.065 RO2-N. & + #.935 CCHO + #.935 ACET + #-0.065 XC	2.818E+04	-0.89	-1.000
MBO3) 2MBT + O3 = #.7 R2O2. + #.156 C-O2. & + #.7 CCO-O2. + #.856 HO. + #.156 CO & + #.042 CO2 + #.7 HCHO + #.7 CCHO & + #.3 ACET + #.102 CCO-OH & + #.042 "INERT + XC"	4.213E+00	1.16	-1.000
MBN3) 2MBT + NO3 = #.935 "NO2 + R2O2. + CCHO + ACET" & + #.065 "RO2-N. + XN" + #-.065 XC	1.375E+04	0.00	-1.000
MBOA) 2MBT + O3P = MEK + XC	7.486E+04	0.00	-1.000

REACTIONS INPUT:	A (IN PPM-MIN UNITS)	E_A	B
C2H6) C2H6 + HO. = RO2-R. + CCHO	2.011E+03	0.99	1.000
AYOH) C2H2 + HO. = #.1 RO2-R. + #.297 HO2. & + #.603 HO. + #.393 CO + #.096 HCHO & + #.607 GLY + #.297 HCOOH	1.380E+04	1.39	-1.000
AYO3) C2H2 + O3 = #1.5 HO2. + #.5 HO. & + #1.5 CO + #.5 CO2	2.936E+01	8.74	-1.000
C3H8) C3H8 + HO. = #.965 RO2-R. + #.035 RO2-N. & + #0.000 R2O2. + #.261 RCHO + #.704 ACET & + #-.104 XC	2.055E+03	0.12	1.000
N-C4) N-C4 + HO. = #.079 RO2-N. + #.921 RO2-R. & + #.413 R2O2. + #.632 CCHO & + #.12 RCHO + #.485 MEK + #-0.038 XC	2.231E+03	-0.29	1.000
IPNT) IPNT + HO. = #.095 RO2-N. & + #.881 RO2-R. + #.902 R2O2. + #.780 CCHO & + #.762 ACET + #.101 RCHO + #.038 MEK & + #.094 XC + #.024 C-O2. + #.012 HCHO	5.431E+03	0.00	-1.000
N-C5) N-C5 + HO. = #.145 RO2-N. + #.855 RO2-R. & + #.650 R2O2. + #.147 CCHO & + #.220 RCHO + #.238 MEK + #-.157 XC & + #.397 PROD2	3.229E+03	-0.36	1.000
224P) 224P + HO. = #.227 RO2-N. + #.403 RO2-R. & + #.388 RCHO + #.133 MEK + #1.809 XC & + #1.961 R2O2. + #.370 TBU-O. + #.717 HCHO & + #.002 CCHO + #.380 ACET + #.027 PROD2	2.745E+03	-0.39	1.000
MCPT) MCPT + HO. = #.306 RO2-N. + #.453 RO2-R. & + #1.847 R2O2. + #.017 HCHO + #.689 RCHO & + #.000 MEK + #.023 CO + #1.556 XC & + #.239 CCO-O2. + #.003 RCO-O2. + #.003 PROD2	8.339E+03	0.00	-1.000
BAOH) HO. + BACT = #.675 RO2-R. + #.120 RO2-N. & + #.516 R2O2. + #.205 RCO-O2. + #.006 CO & + #.116 CCHO + #.211 CCO-OH & + #.172 RCHO + #.024 INERT & + #.252 MEK + #.251 PROD2 + #.950 XC	6.165E+03	0.00	-1.000
UNID) UNID + HO. = #.835 RO2-R. + #.143 RO2-N. + & #.936 R2O2. + #.011 C-O2. + #.011 CCO-O2. + & #.002 CO + #.024 HCHO + #.455 CCHO + #.244 RCHO & + #.452 ACET + #.11 MEK + #.125 PROD2 + #-0.105 XC	8.734E+03	0.18	-1.000
C6H6) C6H6 + HO. = #.236 PHEN + #.207 GLY & + #.764 DCB1 + #.764 RO2-R. + #.236 HO2. & + #1.114 XC	3.626E+03	0.41	-1.000

REACTIONS INPUT:	A (IN PPM-MIN UNITS)	E_A	B
TOLU) TOLU + HO. = #.085 BALD + #.234 CRES & + #.116 GLY + #.135 MGLY + #.460 DCB1 & + #.758 RO2-R. + #.234 HO2. + #1.178 XC & + #.156 DCB2 + #.057 DCB3 & + #.008 RO2-N.	2.657E+03	-0.70	-1.000
XYLM) XYLM + HO. = #.037 BALD + #.210 CRES & + #.107 GLY + #.335 MGLY + #.347 DCB1 & + #.782 RO2-R. + #.210 HO2. + #1.628 XC & + #.008 RO2-N. + #.290 DCB2 & + #.108 DCB3	3.464E+04	0.00	-1.000
XYLP) XYLP + HO. = #.083 BALD + #.188 CRES & + #.195 GLY + #.112 MGLY + #.709 DCB1 & + #.804 RO2-R. + #.188 HO2. + #2.432 XC & + #.008 RO2-N. + #.012 DCB3	2.099E+04	0.00	-1.000
124B) 124B + HO. = #.044 BALD + #.186 CRES & + #.364 MGLY + #.733 DCB1 + #.804 RO2-R. & + #.186 HO2. + #2.730 XC + #.010 RO2-N. & + #.063 GLY + #.079 BACL + #.027 DCB3	4.771E+04	0.00	-1.000
APOH) APIN + HO. = #.75 RO2-R. + #.25 RO2-N. & + #.75 RCHO + #6.5 XC + #.5 R2O2.	1.776E+04	-0.88	-1.000
APO3) APIN + O3 = #.081 RO2-R. + #.321 RO2-N. & + #1.375 R2O2. + #.298 RCO-O2. + #.7 HO. & + #.051 CO + #.339 HCHO + #.218 RCHO & + #.345 ACET + #.002 GLY + #.081 BACL & + #.3 RCO-OH + #3.875 XC	1.483E+00	1.46	-1.000
APN3) APIN + NO3 = #.75 "NO2 + R2O2. + RCHO" & + #.25 RO2-N. + #6.25 XC + #.25 XN	1.747E+03	-0.97	-1.000
APOA) APIN + O3P = PROD2 + #4 XC	4.697E+04	0.00	-1.000
MTBE) MTBE + HO. = #.078 RO2-N. + #.743 RO2-R. & + #.381 R2O2. + #.234 HCHO + #.719 MEK & + #.939 XC + #.162 C-O2. + #.016 TBU-O. & + #.024 ACET + #.007 PROD2 + #.155 INERT	8.646E+02	-0.96	1.000
ETOH) ETOH + HO. = #.05 RO2-R. + #.95 HO2. & + #.081 HCHO + #.960 CCHO	8.162E+02	-1.06	-1.000
POOH) IPOH + HO. = #.953 HO2. + #.046 HCHO & + #.046 CCHO + #.953 ACET + #.046 RO2-R. & + #.001 RO2-N. +#-.003 XC	9.527E+02	-1.25	-1.000

B. Supporting Tables and Figures

This appendix provides additional tables and figures supporting material presented in the main body of the report.

Table B.1. Relative incremental reactivity of all 31 species at the time of maximum ozone on 25 June 1987 at all sites. The R_MIR from Carter (2000b) is included for comparison. These data are plotted in Figure 3.7.

Species Names	Hawt.	Long Beach	Cent. L.A.	Anah.	Burk.	Azusa	Clar.	Rubx.	Carter R_MIR
methane	0.00	0.01	0.00	0.01	0.01	0.01	0.01	0.01	0.01
ethane	0.00	0.10	0.05	0.08	0.10	0.06	0.16	0.22	0.16
n-butane	0.56	1.45	0.43	0.64	0.63	0.61	0.80	0.81	0.67
n-propane	0.87	1.55	0.44	0.67	0.86	0.65	0.89	0.86	0.78
isopentane	0.86	0.55	0.47	0.64	0.86	0.59	0.87	1.07	0.85
methylcyclopentane	0.49	0.57	0.35	0.59	0.94	0.58	0.85	0.98	1.22
2,2,4-trimethylpentane	0.33	0.26	0.20	0.35	0.47	0.33	0.38	0.35	0.72
ethene	4.98	3.25	4.26	5.71	7.02	4.47	5.24	5.41	4.57
propene	9.32	4.45	6.50	8.08	8.06	5.61	5.29	5.53	5.83
2-methyl-2-butene	32.58	7.08	23.80	20.72	13.27	12.18	8.16	8.36	7.28
1,3-butadiene	15.76	8.22	17.65	18.79	13.64	11.82	9.48	9.10	6.84
isoprene	1.54	0.80	0.92	1.31	1.41	1.05	1.28	2.42	5.38
α–pinene	0.23	0.06	0.16	0.15	0.33	0.11	0.13	0.40	2.16
OLE1	6.00	2.93	4.04	4.90	4.47	3.38	3.21	3.21	3.92
benzene	0.32	0.21	0.17	0.28	0.38	0.23	0.29	0.26	0.41
toluene	0.67	1.04	1.30	1.59	1.97	1.50	1.43	1.15	2.00
m-xylene	5.57	3.14	5.87	6.28	6.04	5.14	4.09	3.75	5.34
p-xylene	1.85	1.23	1.42	1.91	2.35	1.59	1.44	1.15	2.14
1,2,4-trimethylbenzene	2.86	2.23	3.62	4.46	4.07	3.25	2.58	2.48	3.62
acetone	0.00	0.11	0.13	0.11	0.13	0.15	0.18	0.25	0.22
methylethylketone	1.16	0.82	2.24	1.34	1.18	2.24	1.95	1.97	0.75
formaldehyde	12.22	4.25	9.12	7.95	6.63	5.04	3.27	2.74	4.52
acetaldehyde	-1.89	1.47	2.43	1.80	1.34	2.13	2.03	2.81	3.44
propionaldehyde	0.00	1.82	3.87	2.60	2.55	2.48	1.95	2.41	3.97
benzaldehyde	-2.04	-0.27	-0.40	-0.35	-0.83	-0.17	-0.31	-0.59	-0.31
acetylene	0.28	0.18	0.21	0.29	0.49	0.26	0.33	0.35	0.63
ethanol	0.00	0.26	0.27	0.24	0.37	0.36	0.46	0.54	0.85
isopropanol	0.00	0.31	0.27	0.27	0.32	0.36	0.55	0.68	0.36
MTBE	0.00	0.46	0.34	0.46	0.72	0.41	0.53	0.68	0.39
n-butylacetate	0.00	0.33	0.18	0.16	0.25	0.33	0.44	0.36	0.45
CO	0.05	0.03	0.03	0.04	0.05	0.03	0.05	0.05	0.03

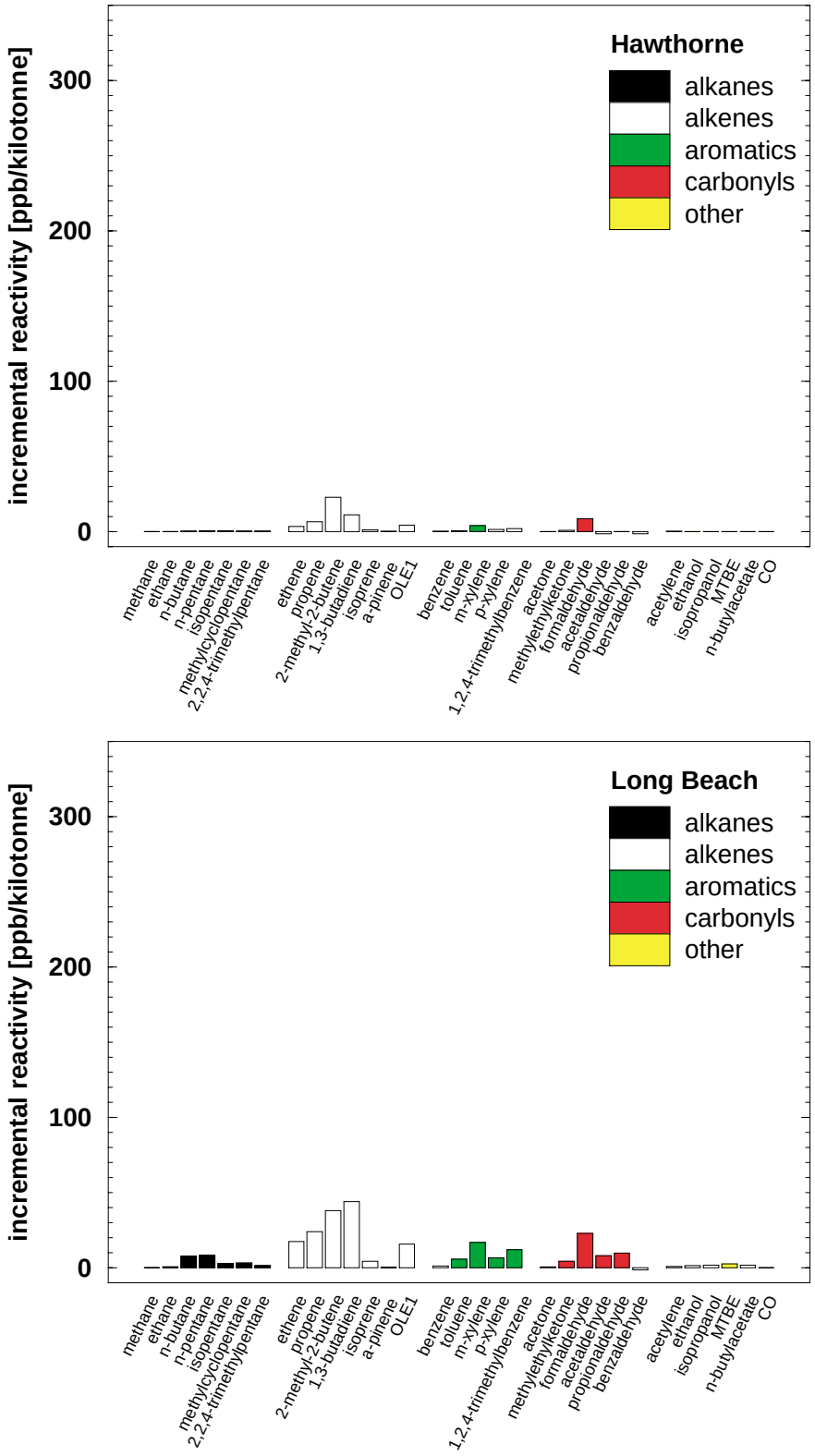

Figure B.1. Absolute incremental reactivity calculated at the time of maximum observed ozone on 25 June 1987 at coastal sites (a) Hawthorne and (b) Long Beach.

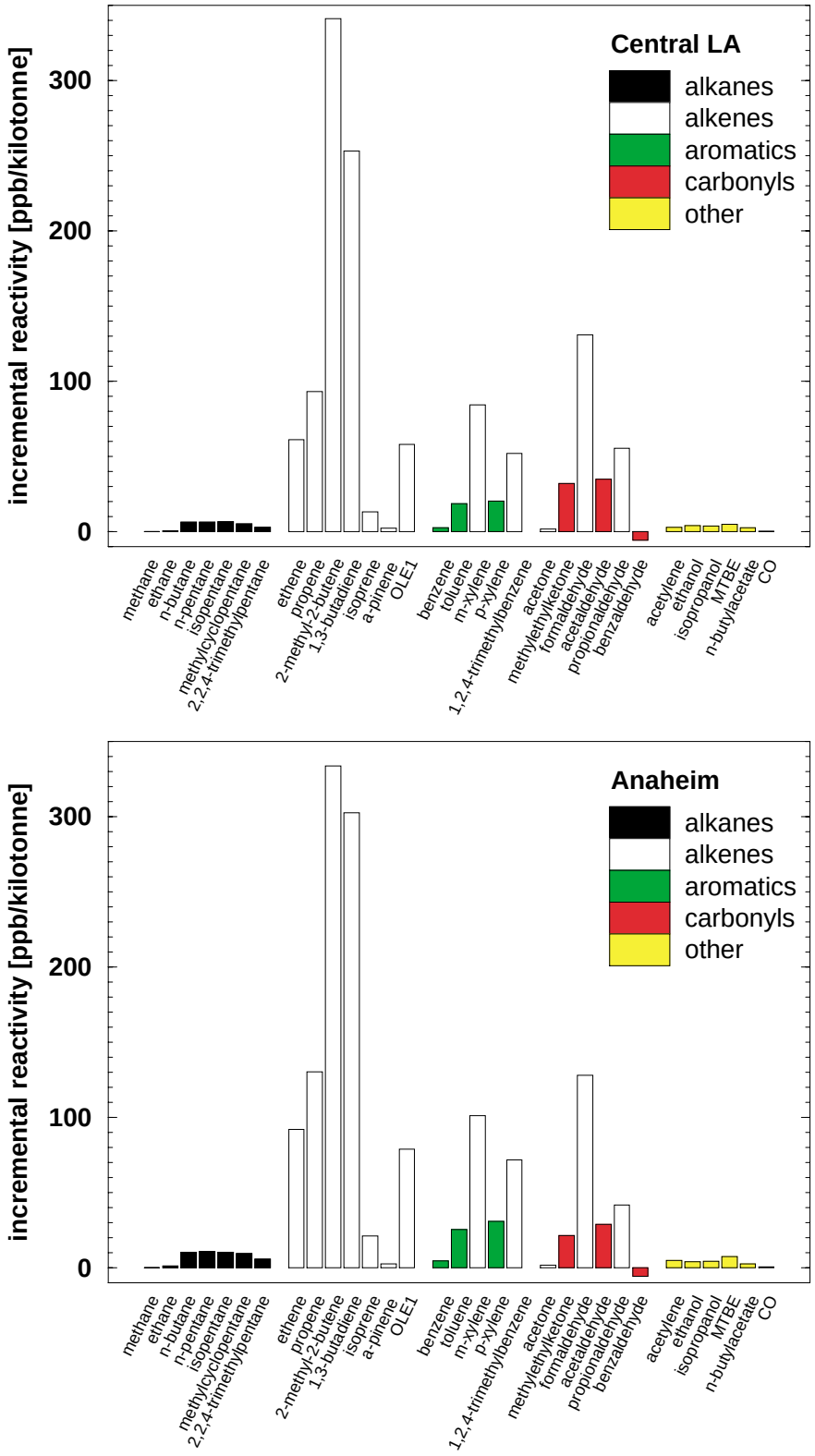

Figure B.1. Absolute incremental reactivity calculated at the time of maximum observed ozone on 25 June 1987 at central sites (c) Central Los Angles and (d) Anaheim.

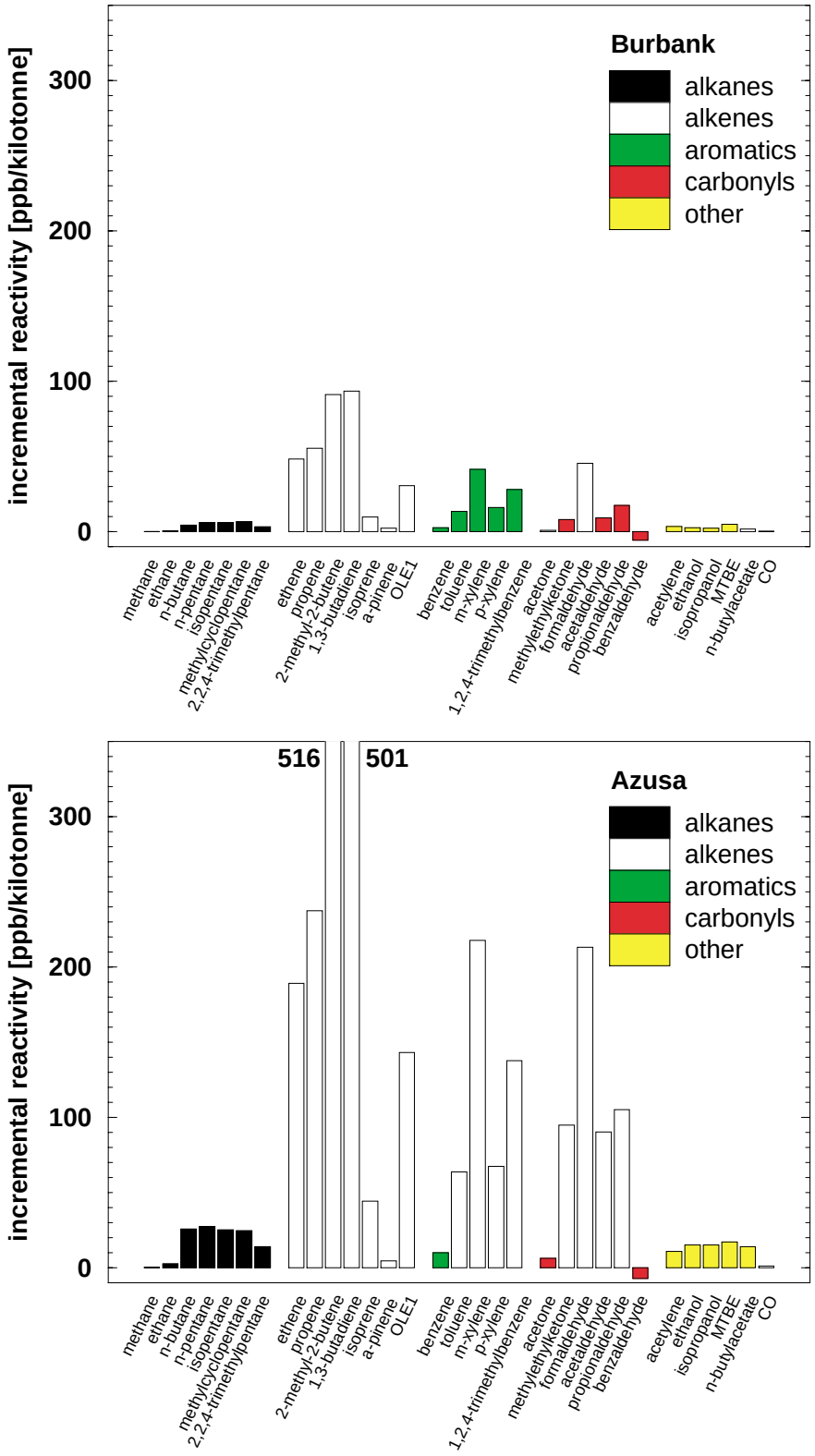

Figure B.1. Absolute incremental reactivity calculated at the time of maximum observed ozone on 25 June 1987 at inland sites (e) Burbank and (f) Azusa.

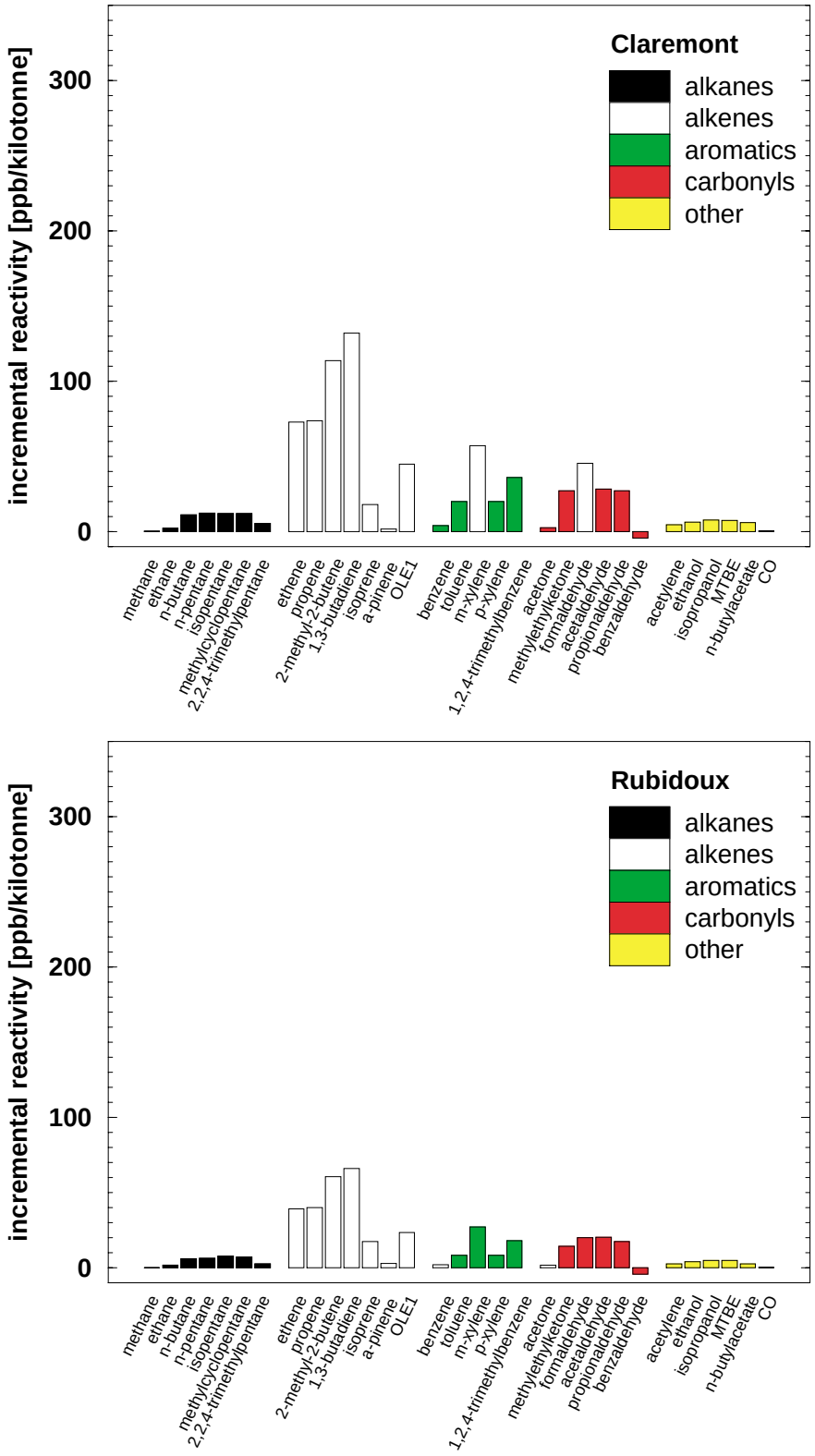

Figure B.1. Absolute incremental reactivity calculated at the time of maximum observed ozone on 25 June 1987 at inland sites (g) Claremont and (h) Rubidoux.

Table B.2. Data used to prepare Figure 4.1: Absolute incremental reactivities and associated uncertainties for selected compounds and the base mixture.

AIRs	Anaheim	Azusa	Claremont	Riverside
CO x 10	0.05±0.02	0.05±0.02	0.05±0.02	0.05±0.02
ETOH	0.03±0.01	0.06±0.02	0.07±0.03	0.07±0.03
HCHO	0.92±0.20	1.47±0.30	1.07±0.41	0.54±0.34
MEK	0.03±0.01	0.09±0.03	0.09±0.05	0.08±0.05
N-C4	0.06±0.02	0.04±0.01	0.05±0.02	0.03±0.01
PRPE	0.94±0.18	1.03±0.22	0.95±0.30	0.75±0.30
224P	0.09±0.03	0.08±0.03	0.09±0.02	0.08±0.03
XYLM	0.88±0.14	1.04±0.19	1.07±0.40	0.70±0.41
BASEMIX	0.11±0.02	0.13±0.03	0.13±0.04	0.10±0.04

Table B.3. Data used to prepare Figure 4.2: Relative incremental reactivities and associated uncertainties for selected compounds.

RIRs	Anaheim	Azusa	Claremont	Riverside
CO x 10	0.51±0.15	0.40±0.12	0.44±0.18	0.65±0.32
ETOH	0.29±0.07	0.48±0.11	0.55±0.15	0.73±0.25
HCHO	8.45±1.69	11.54±1.62	8.01±1.68	5.18±1.81
MEK	0.30±0.11	0.67±0.23	0.66±0.24	0.80±0.26
N-C4	0.53±0.10	0.31±0.06	0.42±0.11	0.33±0.08
PRPE	8.45±0.68	7.99±0.64	7.17±0.65	7.73±0.70
224P	0.80±0.14	0.60±0.13	0.74±0.22	0.91±0.24
XYLM	8.30±1.25	8.15±1.14	8.11±1.95	6.82±2.32

Table B.4. Data used to prepare Figures 5.6 and 5.7. Domain-wide 3-D reactivity metrics for central California, sorted by box model MIR.

Species	MIR-3D	MOIR-3D	MIR-3D (8 h)	MOIR-3D (8 h)	Exposure
2-me-2-Butene	4.53	3.25	5.40	3.03	4.72
1,3-Butadiene	7.36	5.44	8.29	5.10	7.29
Propene	3.68	3.23	3.88	3.16	3.78
Isoprene	5.28	4.00	6.01	3.69	5.35
m-Xylene	3.14	2.36	3.33	2.26	2.99
Ethene	2.51	2.14	2.68	1.38	2.50
Formaldehyde	2.35	1.51	2.52	2.16	2.23
Propionaldehyde	2.11	2.09	2.13	2.13	2.04
Lumped OLE1	2.97	2.77	3.15	2.75	3.09
1,2,4-tm-Benzene	2.17	1.76	2.28	1.71	2.10
Acetaldehyde	2.01	1.93	1.98	1.99	1.92
a-Pinene	1.34	1.13	1.52	1.07	1.36
p-Xylene	1.29	1.15	1.32	1.11	1.27
Toluene	1.26	1.08	1.24	1.01	1.16
me-Cyclopentane	0.84	1.05	0.84	1.09	0.94
Ethanol	1.58	1.39	0.69	0.93	1.47
Isopentane	0.69	0.88	1.54	1.33	0.79
n-Pentane	0.74	0.93	1.18	1.01	0.81
MEK	1.21	1.08	0.74	0.98	1.08
2,2,4-tm-Pentane	0.61	0.72	0.60	0.75	0.67
n-Butane	0.60	0.77	0.59	0.81	0.66
Acetylene	0.23	0.24	0.22	0.24	0.22
n-Butyl Acetate	0.42	0.53	0.42	0.56	0.46
Benzene	0.28	0.32	0.42	0.52	0.29
MTBE	0.43	0.50	0.27	0.32	0.46
Methanol	0.26	0.28	1.37	0.93	0.26
Isopropanol	1.37	1.00	0.25	0.28	1.26
Acetone	0.13	0.13	0.12	0.13	0.12
Ethane	0.12	0.17	0.12	0.19	0.14
CO	0.03	0.04	0.03	0.04	0.03
Methane	0.01	0.01	0.01	0.01	0.01
Benzaldehyde	–0.09	–0.24	–0.14	–0.38	–0.28

7. References

Allen, P.D. (1999). Modeling Emissions Data System (MEDS) data files for southern California in summer 1987. Personal communication. Planning and Technical Support Division, California Air Resources Board, Sacramento, CA, February 19, 1999.

Atkinson, R., Baulch, D.L., Cox, R.A., Hampson, R.F. Jr., Kerr, J.A., Troe, J. (1989). Evaluated kinetic and photochemical data for atmospheric chemistry: Supplement III. IUPAC Subcommittee on Gas Kinetic Data Evaluation for Atmospheric Chemistry. *J. Phys. Chem. Ref. Data*, **18**, 881-1097.

Bergin, M.S., Russell, A.G. and Milford, J.B. (1995). Quantification of individual VOC reactivity using a chemically detailed, three-dimensional photochemical model. *Environ. Sci. Technol.*, **29**, 3029-3037.

Bergin, M.S., Russell, A.G. and Milford, J.B. (1998). Effects of chemical mechanism uncertainties on the reactivity quantification of volatile organic compounds using a three-dimensional air quality model. *Environ. Sci. Technol.*, **32**, 694-703.

Bergin, M.S., Noblet, G.S., Petrini, K., Dhieux, J.R., Milford, J.B., Harley, R.A. (1999). Formal uncertainty analysis of a Lagranian photochemical air pollution model. *Environ. Sci. Technol.*, **33**, 1116-1126.

Carter, W.P.L. (1988). Documentation for the SAPRC atmospheric photochemical mechanism preparation and emissions processing programs for implementation in airshed models, Appendix C. Statewide Air Pollution Research Center, University of California, Riverside, CA, report to the California Air Resources Board.

Carter, W.P.L. (1990). A detailed mechanism for gas-phase atmospheric reactions of organic compounds. *Atmos. Environ.*, **24A**, 481-518.

Carter, W.P.L. (1994). Development of ozone reactivity scales for volatile organic compounds. *J. Air Waste Manage. Assoc.*, **44**, 881-899.

Carter, W.P.L. (1995). Computer modeling of environmental chamber studies of maximum incremental reactivities of volatile organic compounds. *Atmos. Environ.*, **29**, 2513-2527.

Carter, W.P.L. (1996). Development and application of an updated photochemical mechanism for VOC reactivity assessment. University of California, Riverside, CA. Quarterly report to the California Air Resources Board, Contract No. 92-329.

Carter, W.P.L., Luo, D. and Malkina, I.L. (1997). Environmental chamber studies for development of an updated photochemical mechanism for VOC reactivity assessment, Statewide Air Pollution Research Center, University of California, Riverside, CA, final report to the California Air Resources Board, the Coordinating Research Council, and the National Renewable Energy Laboratory.

Carter, W.P.L. (2000a). Documentation of the SAPRC99 chemical mechanism for VOC reactivity assessment. Final Report to California Air Resources Board, Contract No. 92-329, and (in part) 95-308.

Carter, W.P.L. (2000b). VOC Reactivity Data as of November 13, 2000. ftp.cert.ucr.edu/pub/carter/SAPRC99/r99tab.xls. Accessed August 2, 2001.

Colella, P.; Woodward, P.R. (1984). *J. Comp. Phys.* **54**, 174.

DaMassa, J.; Tanrikulu, S.; Magliano, K.; Ranzieri, A.J.; Niccum, L. (1996). Performance evaluation of SAQM in Central California and Attainment Demonstration for the August 3-6, 1990 Ozone Episode. Technical Support Division, California Air Resources Board, Sacramento, CA.

DeMore, W.B., Sander, S.P., Golden, D.M., Hampson, R.F., Kurylo, M.J., Howard, C.J., Ravishankara, A.R., Kolb, C.E., Molina, M.J. (1997). Chemical kinetics and photochemical data for use in stratospheric modelingm Evaluation No. 12. NASA Panel for Data Evaluation. Jet Propulsion Laboratory, Pasadena, CA. JPL Publication 97-4.

Dunker, A.M. (1984). The direct decoupled method for calculating sensitivity coefficients in chemical kinetics. *J. Chem. Phys.*, **81**, 2385-2393.

Goodin, W.R.; McRae, G.J.; Seinfeld, J.H (1979). A comparison of interpolation methods for sparse data: application to wind and concentration fields. *J. Appl. Meteorol.* **18**, 761-771.

Goodin, W.R.; McRae, G.J.; Seinfeld, J.H (1980). An objective analysis technique for constructing three-dimensional urban-scale wind fields. *J. Appl. Meteorol.* **19**, 98-108.

Harley, R.A.; Hannigan, M.P.; Cass, G.R. (1992). Respeciation of organic gas emissions and the detection of excess unburned gasoline in the atmosphere. *Environ. Sci. Technol.*, **26**, 2395-2408.

Harley, R.A.; Russell, A.G.; McRae, G.J.; Cass, G.R.; Seinfeld, J.H. (1993). Photochemical modeling of the Southern California Air Quality Study. *Environ. Sci. Technol.*, **27**, 378-388.

Harley, R.A.; Sawyer, R.F.; Milford, J.B. (1997). Updated photochemical modeling for California's South Coast Air Basin: comparison of chemical mechanisms and motor vehicle emission inventories. *Environ. Sci. Technol.*, **31**, 2829-2839.

Iman, R.L., Shortencarier, M.J. (1984). A FORTRAN77 program and user's guide for the generation of Latin hypercube and random samples for use with computer models. SAND83-2365, U.S. Department of Energy, Sandia National Laboratory, Albuquerque, NM.

Khan, M.; Yang, Y.-J.; Russell, A.G. (1999). Photochemical reactivities of common solvents: comparison between urban and regional domains. *Atmos. Environ.* **33**, 1085-1092.

Lawson, D. R. (1990). The Southern California Air Quality Study. *J. Air Waste Manage. Assoc.* **40**, 156-165.

Main, H.H.; Lurmann, F.W.; Roberts, P.T. (1990). Pollutant concentrations along the western boundary of the South Coast Air Basin. Part I: a review of existing data. Sonoma Technology Inc., Santa Rosa, CA. Report to the South Coast Air Quality Management District, October 1990.

McNair, L.A.; Russell, A.G.; Odman, M.T. (1992). Airshed calculation of the sensitivity of pollutant formation to organic compound classes and oxygenates associated with alternative fuels. *J. Air Waste Manage. Assoc.* **42**, 174-178.

McNair, L.A.; Harley, R.A.; Russell, A.G. (1996). Spatial inhomogeneity in pollutant concentrations and implications for air quality model evaluation. *Atmos. Environ.*, **30**, 4291-4301.

McRae, G.J.; Goodin, W.R.; Seinfeld, J.H. (1982). Numerical solution of the atmospheric diffusion equation for chemically reacting flows. *Journal of Computational Physics*, **45**, 1-42.

Odman, M.T.; Ingram, C. (1996). Multi-scale Air Quality Simulation Program (MAQSIP): Source Code Documentation and Validation. MCNC – North Carolina Supercomputing Center Report ENV-96TR002, Research Triangle Park, NC.

Odman, M.T.; Russell, A.G. (2000). Mass conservative coupling of non-hydrostatic meteorological models with air quality models. In *Air Pollution Modelling and Its Application XIII*, S.-E. Gryning and E. Batchvarova (eds.), Kluwer Academic/Plenum Publishers, New York, 651-660.

Ranzieri, A.J.; Thuillier, R.H. (1994). SJVAQS and AUSPEX: a collaborative air quality field measurement and modeling program. In *Planning and managing regional air quality modeling and measurement studies*. Lewis Publishers, Boca Raton, FL, pp. 1-36.

Russell, A.G.; McCue, K.F.; Cass, G.R. (1988). Mathematical modeling of the formation of nitrogen-containing air pollutants. 1. Evaluation of an Eulerian photochemical model. *Environ. Sci. Technol.,* **22**, 263-271.

Russell, A.G., Milford, J.B., Bergin, M.S., McBride, S., McNair, L., Yang, Y-J, Stockwell, W.R., Croes, B. (1995). Urban ozone control and atmospheric reactivity of organic gases. *Science*, **269**, 491-495.

Seinfeld, J.H.; Pandis, S.N. (1998). *Atmospheric Chemistry and Physics – From Air Pollution to Climate Change.* Wiley, New York, NY.

Sillman, S.; Odman, M.T.; Russell, A.G. (2000). Comment on "On the indicator-based approach to assess ozone sensitivities and emissions features" by Cheng-Hsuan Lu and Julius S. Chang. *J. Geophys. Res.* **106**, D18, 20,941.

Tesche, T. W.; Georgopoulos, P.; Seinfeld, J. H.; Cass, G. R.; Lurmann, F. W.; Roth, P. M. (1990). Improvement of procedures for evaluating photochemical models. Radian Corporation, Sacramento, CA. Report to the California Air Resources Board.

Wang, L., Milford, J.B., Carter, W.P.L. (2000). Reactivity estimates for aromatic compounds. Part 2. Uncertainty in incremental reactivities. *Atmos. Environ.*, **34**, 4349-4360.

Yang, Y.-J.; Stockwell, W.R.; Milford, J.B. (1995). Uncertainties in incremental reactivities of volatile organic compounds. *Environ. Sci. Technol.*, **29**, 1336-1345.

Yang, Y.-J.; Milford, J.B. (1996). Quantification of uncertainty in reactivity adjustment factors from reformulated gasolines and methanol fuels. *Environ. Sci. Technol.*, **30**, 196-203.

Yang, Y-J.; Stockwell, W.R.; Milford, J.B. (1996). Effect of chemical product yield uncertainties on reactivities of VOCs and emissions from reformulated gasolines and methanol fuels. *Environ. Sci. Technol.*, **30**, 1392-1397.

Yang, Y-J.; Wilkinson, J.G.; Russell, A.G. (1997). Fast, direct sensitivity analysis of multi-dimensional photochemical models. *Environ. Sci. Technol.*, **31**, 2859-2868.

Young, T.R.; Boris, J.P. (1977). A numerical technique for solving stiff ordinary differential equations associated with the chemical kinetics of reactive-flow problems. *J. Phys. Chem.* **81**, 2424-2427.